STRUCTURE-SWITCHING SIGNALING APTAMERS IN NANOMATERIALS: FROM UNDERSTANDING TO APPLICATIONS

STRUCTURE-SWITCHING SIGNALING APTAMERS IN NANOMATERIALS: FROM UNDERSTANDING TO APPLICATIONS

By

CHRISTY YUK SAN HUI, B.SC.

A Thesis Submitted to the School of Graduate Studies in Partial Fulfillment of the Requirements for the Degree Doctor of Philosophy

McMaster University

DOCTOR OF PHILOSOPHY (2017) McMaster University

(Chemical Biology) Hamilton, Ontario

TITLE: Structure-Switching Signaling Aptamers in Nanomaterials: From Understanding to Applications

AUTHOR: Christy Y. Hui, B.Sc. (University of Victoria)

SUPERVISOR: Dr. John D. Brennan

NUMBER OF PAGES: xix, 137

ABSTRACT

Functional nucleic acids (FNAs), which include both DNA/RNA aptamers and DNA enzymes, have emerged as promising biological recognition elements for biosensors. These species typically require immobilization on or within a solid support, which is usually interfaced to some kind of signal transducer and readout system when use in biosensor. Our group has successfully immobilized several functional nucleic acids in the past, including fluorescence-signalling DNA enzymes, DNA aptamers and RNA aptamers by entrapping them into porous silica or organosilica materials prepared by the sol-gel method using percursors such as sodium silicate (SS), diglyceryl silane (DGS), tetrametylorthosilicate (TMOS) and trimethoxymethysilane (MTMS).

While the earlier work established the ability of entrapped FNAs to retain binding and catalytic activity, only limited information was obtained on how different factors affect the performance of immobilized FNAs, and no information was obtained on the effects of aging and storage conditions on FNA performance. The initial objective of this thesis was to employ advanced fluorescence methods to better understand the nature of immobilized DNA and RNA aptamers, and in particular how entrapment in different sol-gel based materials affected FNA performance for detection of small molecule analytes. It was found that the ability of the entrapped aptamer reporters to remain fully hybridized was the most important factor in terms of signalling capability for both DNA and RNA aptamer reporters. It was also observed that more polar materials derived from SS were optimal for both types of aptamer reporters, since these allowed the entrapped aptamers to

remain hydridized to their complementary strands and still retain the dynamic motion needed to undergo structure switching, while providing a minimum degree of leaching.

The second objective of my research was to develop a paper-based biosensing device incorporating immobilized DNA and RNA aptamers that could be used in the fields of point-of-care diagnostics to further expand the utility of structure-switching aptamer reporters to real world application. A dual response (fluorescence / colorimetric) paper-based sensor utilized printed graphene oxide to immobilize both a RNA and a DNA aptamer in a recognition zone. Upon target addition, the aptamer desorbed and eluted to an amplification zone where rolling circle amplification was used to generate a colorimetric output. This sensor could function with clinical samples such as serum and stool, and allowed detection of key bacterial markers (ATP and glutamate dehydrogenase) at clinically relevant levels.

ACKNOWLEDGEMENTS

I would like to express my most sincere gratitude to my supervisor, Dr. John Brennan for his precious insightful guidance, numerous suggestions and constant support throughout my research work. Without his encouragement, motivation and assistance, completion of this document and work herein would have been exponentially more difficult. Having a well-known professor as my supervisor have brought me more than usual privilege in wisdom and knowledge from the scientific world. I truly appreciate the opportunities provided to me in attending conferences and delivering skills in paper writing. I would like to further direct my thanks to my committee members, Dr. Yingfu Li and Dr. Jose Moran-Mirabal for the valuable suggestions and support during our meetings. I would also like to thank Dr. Nancy McKenzie for insightful comments and encouragement throughout my study.

In addition, I would like to thank my fellow lab members, past and present for support and interesting discussions, specifically Anne Marie Smith, Carmen Carrasquilla, Tracy Wang and Roger Bialy.

On a more personal level, I would like to convey my appreciation to all my friends from HCAC, especially my brothers and sisters in Christ from Cephas and Daniel Fellowships, for steady encouragement, endless support and keeping me in prayers over the years. To auntie Christine and auntie Lyminh, for the unconditional support and feeding me all the time so that I don't have to worry about food. To Pastor Chia-en Liu, for the countless conversations, consistent affirmation, wise direction and encouragements, as well as the daily coffee.

My gratitude to my family and friends for their ongoing support cannot fully be expressed. To Richard, for all the editing you have done for me throughout the years and keeping me entertained when I am bored waiting for my next reactions. To my roommate and one of my best friends, Cindy, you have been beyond supportive and encouraging. Thank you for always believe in me, which has kept me motivated and the 'udon-time' has made truly stressful times more bearable.

And lastly, to my family, for being patience throughout my entire academic career. 感謝祖父母的養育和教導，感謝三姑姑與三姑丈的疼愛和鼓勵, 因為有你們的支持，讓我的生活未曾貧乏；因為有你們的愛，讓我能為夢想飛翔。

“ I can do all things through HIM who strengthens me.”

Philippians 4:13 ESV

TABLE OF CONTENTS

CHAPTER 3. INVESTIGATION OF RNA STRUCTURE-SWITCHING APTAMERS IN TUNABLE SOL-GEL-DERIVED MATERIALS

List of Figures

List of Tables

LIST OF ABBREVIATIONS

3-D	three-dimensional
μPAD	microfluidic paper-based analytical devive
ϕ29DP	phi 29 DNA polymerase
A	acceptor
ABTS	2,2'-azino-bis(3-ethylbenzthiazoline-6-sulphonic acid)
ATP	adenosine 5'-triphosphate
AuNPs	gold nanoparticles
BDNA	blocking DNA
BSA	bovine serum albumin
CTP	cytidine 5'-triphosphate
D	donor
Dabcyl	4-(dimethylaminoazo)benzene-4-carboxylic acid
DFA	DNAzyme feedback amplification
DGS	diglycerylsilane
DMSO	dimethyl sulfoxide
DNA	deoxyribonucleic acid
DNase	deoxyribonuclease
dNTPs	2'-deoxyribonucleoside 5'-triphosphates
dPAGE	denaturing polyacrylamide gel electrophoresis
dsDNA	double-stranded DNA
DTT	dithiothreitol
F-DNA	fluorophore-labelled DNA
FNAs	functional nucleic acids
FRET	fluorescence reasonance energy transfer
GDH	glutamate dehydrogenase
GO	graphene oxide
GOx	glucose oxidase
GTP	guanosine 5'-triphosphate
H_2O_2	hydrogen peroxide
HBV	Hepatits B virus
HDA	helicase dependant amplification
HDNA	helper DNA
HPLC	high-performance liquid chromatography
HRCA	hyperbranched rolling circle amplification
K_d	dissociation constant
LAMP	loop-medicated isothermal amplification
MB	molecular beacon
MTMS	trimethoxymethylsilane
MW	molecular weight
nPAGE	native polyacrylamide gel electrophoresis
nt	nucleotide
NTPs	nucleoside triphosphate

PAGE	polyacrylamide gel electrophoresis
PCR	polumerase chain reaction
Q-DNA	quencher-labelled DNA
RCA	rolling circle amplification
RCD	RNA cleaving DNAzyme
rGO	reduced graphene oxide
RNA	ribonucleic acid
RNase A	ribonuclease A
RNase H	ribonuclease H
RP	RCA products
RPA	recombinase polymerase amplification
SELEX	system evolution of ligands by exponential enrichment
SS	sodium silicate
ssDNA	single-stranded DNA
ssRNA	single-stranded RNA
T4 PNK	T4 polynucleotide kinase
tcdA	toxin A
tcdB	toxin B
TEOS	tetraethylorthosilicate
TMB	3,3',5,5'-tetramethylbenzidine
TMOS	tetramethylorthosilicate
TTP	thiamine purophosphate
UTP	uridine 5'-triphophate

CHAPTER 1. INTRODUCTION

1.1 Thesis Overview and Goals

Functional nucleic acids (FNAs), which include both DNA/RNA aptamers and DNA enzymes, have emerged as promising biological recognition elements for biosensor development owing to the ability to generate such species with high affinity and selectivity for a wide range of targets.[1-3] Aptamers and DNAzymes are single-stranded DNA oligomers that are engineered through an *in vitro* selection method called SELEX (systematic evolution of ligands by exponential enrichment)[4] and have the ability to fold into well-defined three-dimensional structures. Such species are able to either bind a target (aptamers) or catalyze a reaction (DNAzymes), and have been generated for targets that include small molecules, proteins, and whole cells.

For use in biosensors, aptamers and DNAzymes typically require immobilization on or within a solid support, which is usually interfaced to signal transducer and readout system. In the past, our group has successfully immobilized several functional nucleic acids, including fluorescence-signalling DNA enzymes[5], DNA aptamers[3, 6] and RNA aptamers[6, 7]. In this work, the signalling FNAs were entrapped into porous silica or organosilica materials prepared by the sol-gel method using percursors such as sodium silicate (SS), diglyceryl silane (DGS), tetrametylorthosilicate (TMOS) and trimethoxymethysilane (MTMS). When entrapped in these sol-gel-derived materials, the reporters were able to retain their ability to change conformation and produce an adequate fluorescence signal upon

target binding. These materials could also protect the DNA/RNA from degradation by nucleases.

While the earlier work established the ability of entrapped FNA to retain binding and catalytic activity, only limited information was obtained on the effects of different factors on the performance of immobilized FNAs, and no information was obtained on the effects of aging and storage conditions on FNA performance. The initial objective of this thesis was to employ advanced fluorescence methods to better understand the nature of immobilized DNA and RNA aptamers and, in particular, how entrapment in different sol-gel based materials affected FNA performance for the detection of small molecule analytes. The chosen signaling aptamers detect analytes by coupling the conformational change upon target binding with a dequenching mechanism to produce a fluorescent signal. Parameters studied included aptamer accessibility, aptamer dynamics, degree of leaching, long-term stability and thermal stability. The ultimate goal was to generate a full understanding of factors that affected entrapped structure-switching signaling aptamers and thereby produce optimized materials for entrapment of aptamers that can sense a variety of target analytes. This work was applied to both DNA aptamers (Ch. 2) and RNA aptamers (Ch. 3) to determine if there were any major differences in factors affecting these different types of aptamers.

The second objective of my research was to develop a paper-based biosensing device incorporating immobilized DNA and RNA aptamers that could be used in the fields of point-of-care diagnostics. Paper-based biosensors have been widely used for

point-of-care diagnostics and on-site environmental monitoring,[8, 9 10-13] and many of these devices have been developed using FNAs as recognition elements[14-16]. Immobilization of biomolecules onto paper using sol-gel materials has been reported previously by our group, but it was determined that printing of such materials onto paper was not possible owing to clogging of printer nozzles upon gelation of the sol-gel based materials.[17, 18] Hence, this part of the thesis made use of a different immobilization method, wherein the FNA species were adsorbed onto graphene oxide (GO), which was then printed onto a paper device to create a paper-based analytical device (μPAD). Both DNA and RNA aptamers were investigated, and the sensor was formatted to allow both fluorimetric and amplified colorimetric readouts. This μPAD was tested as a platform for detection of key clinical analytes.

1.2 Biosensors

Biosensors are small, analytical devices that convert a biological recognition response into a detectable signal, such as a change in colour or fluorescence or an electrical current. By integrating the sensitivity and specificity of biomolecules with physicochemical transducers, complex bioanalytical measurements can be delivered in simple and easy-to-use formats.[19-23] Numerous biosensors have been developed for food analysis[24-26], bioterrorism[27, 28], environmental[26, 29-36], human health monitoring and diagnostics[37-44]. Biosensors have reduced the need for complicated sample preparation and offer great potential for on-site analytical application with rapid and low-cost measurements. They are categorized into three groups based on their

mechanisms: the biocatalytic group comprising enzymes, the bioaffinity group including antibodies and nucleic acids, and whole cell sensors.[45]

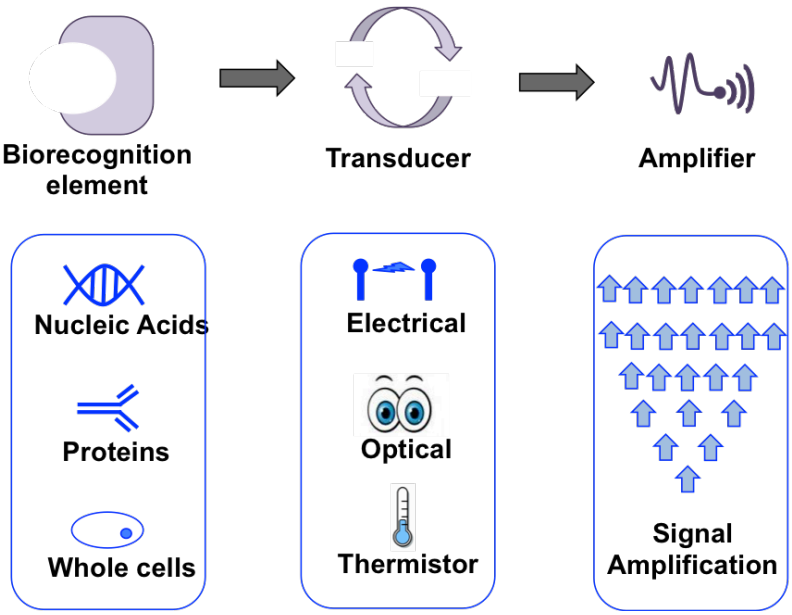

Figure 1-1. Design of biosensors. A biosensor is an analytical device that utilizes biological components to detect target molecules. It consists of a biorecognition element such as a protein (enzyme, antibody), nucleic acid (oligonucleotide, aptamer) or whole cell; and a transducer that translates the recognition event to an electrical, optical or thermometric signal. An amplification step is often added to reduce the signal-to-noise ratio and enhance the detection sensitivity.

The first color-based biodiagnostic test strips were developed in the late 1950's by Eli Lilly (glucose dipstick) and commercialized in 1961 under the tradename of Clinistix.[46] This paper test strip is specifically used for detection and rough quantitation of glucose in urine. The electrochemical biosensor was invented in 1962 by Leyland C. Clark while he immobilized glucose oxidase (GOx) on an electrode to measure the catalytic conversion of glucose to gluconic acid and hydrogen peroxide.[19] This technology was made commercially available by Yellow Springs Instrument Company in 1975 and glucose monitors for diabetes are now a

major commercial success. Another key diagnostic format is the lateral flow immunoassay, initially developed by Unilever and marketed as a simple pregnancy test for home use.[47] Such devices are simple and are based on flow of labelled antibodies along a nitrocellulose strip, with capture of the antibody in a sandwich structure if the analyte of interest is present. Such tests have more recently undergone a major resurgence and are now available for a range of targets, and in particular for infectious agents.[48] In more recent years, nucleic acids have been used in a wide range of biosensors due to their useful physical, chemical and biological properties.[49-52] Such nucleic acid-based biosensors utilized a single-stranded nucleic acid molecule to recognize and bind to its complementary strand specifically in a sample, allowing detection of genes or single nucleotide polymorphisms. Nucleic acid recognition elements have been integrated into a range of sensors (absorbance, fluorescence, electocemical, etc) and have also been used as components of lateral flow devices, but are typically limited to detection of nucleic acid-based analytes, limiting their versatility.[53, 54]

1.3 Nucleic Acids Aptamers

1.3.1 Overview of nucleic acids aptamers

Nucleic acid aptamers are single-stranded DNA or RNA molecules with that fold into specific three dimensional structures[55-58] that are able to specifically bind to a great diversity of targets from small molecules[59], antibodies[60] to proteins[61], viruses[62], and even cells,[63] moving nucleic acid recognition elements beyond simple detection of complementary DNA. Aptamers were first described in 1990 by three

different research groups[55, 56, 64] who independently reported on a method to develop aptamers artificially from a large random- sequence pool of RNA or DNA through a technique known as *in vitro* selection, which is dubbed "Systematic Evolution of Ligands by Exponential Enrichment" or SELEX.[4]

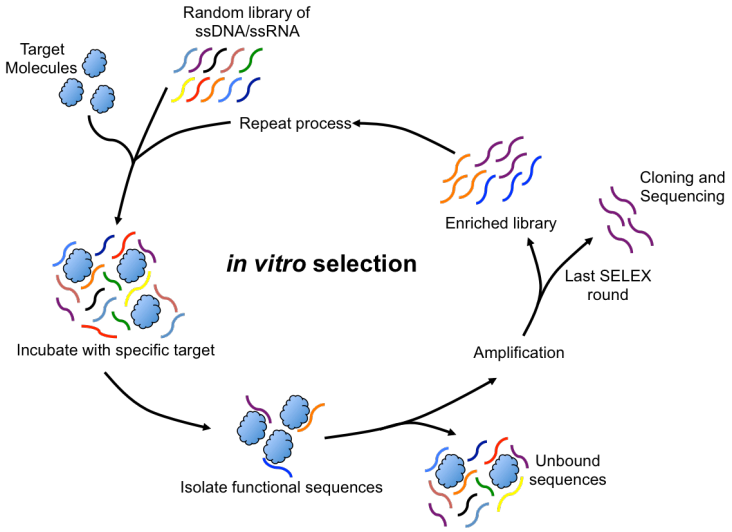

Figure 1-2. Schematic of Systematic Evolution of Ligands by Exponential Enrichment (SELEX). The typical procedure involves incubating a large library of nucleic acids with a target molecule, separating the bound from unbound sequences, and amplifying the bound nucleic acids sequences by polymerase chain reaction (PCR). This process is then repeated using the newly enriched library until the bound nucleic acids dominate the population. The dominant nucleic acids can then be cloned and sequenced. Generally, 8-15 rounds of SELEX are carried out to generate a pool of aptamers with sequences enabling the highest binding affinity for the target.

This process begins with a selection of sequences that are capable of binding with high affinity and specificity to target molecules from a large single-stranded DNA or RNA library, containing 10^{13} - 10^{16} unique molecules (Figure 1). Then, these functional sequences are partitioned from non-functional sequences by various methods, including column chromatography, magnetic bead separation, nitrocellulose membrane methods, gel electrophoresis or other biomolecular separation techniques

that are suitable for enrichment of any desired aptamer against a given target[4, 57, 58, 65-69]. The selection method is conceptually straightforward. Typically, the process begins with solid-phase synthesis of a long DNA oligonucleotide with a stretch of random nucleotides flanked by defined primer binding sites. It is assumed that there are only a few functional molecules with the correct properties or structures for ligand binding or catalytic activity in this large pool of random sequences; therefore, this random pool is then exposed to the target of interest so that the functional molecules can bind immobilized targets and be separated from the non-functional ones. The active molecules are then dissociated from the target and amplified by polymerase chain reaction (PCR) to enrich the pool with functional molecules for the next round of selection. In this way, by repeating the selection and amplification cycles, an exponential increase of the functional sequences occurs until they dominate the population. Once sufficient SELEX cycles are completed, the functional molecules are then sequenced and cloned.

By integrating with an effective counter-selection scheme (incubation of the library with negative controls to remove non-specifically binding oligonucleotides), this *in vitro* selection process allows generation of aptamers with high affinity and remarkable specificity that can differentiate variants, isoforms and enantiomers[70].

1.3.2 Fluorescence-based biosensors using structure-switching signaling aptamers

The development of *in vitro* selection techniques has led to the generation of DNA and RNA aptamers that bind to a wide variety of non-nucleic acid targets such

as proteins and metabolites as well as whole cells[71] or viruses[72]. The ability of post-selection modifications allows these aptamers can be exploited allow immobilization, tune affinity, or to produce signalling bio-recognition elements. One such method is the incorporation of fluorescently labelled nucleotides into the aptamer to allow for generation of fluorescence signals upon target binding.[73, 74] The first fluorescence-based aptamer sensor was developed in 1998 by Potyrailo *et al.*[75] to measure the binding of thrombin using the technique of fluorescence anisotropy. A fluorophore-labeled DNA aptamer was covalently bound to a glass microscope cover slip in this study. The interaction between the aptamer and the protein target slowed the rotation of the fluorophore, and hence increased the fluorescence anisotropy. Even though this fluorescence platform demonstrated high selectivity, a low K_d (47 nM), and a quick response time (10 min); however, it suffered from small change in signal.[76] Therefore, the researchers utilized the unique characteristics of aptamers undergo spontaneous conformational changes in response to binding of the target to design signaling platforms that operates in "on" or "off" states.

Another signaling version utilized the molecular beacon concept, which was initially described in 1996[77] as nucleic acid probe that possesses a stem-loop structure and is able to undergo a spontaneous conformational change following hybridization with a complementary nucleic acid target. Adapting this concept, the first molecular beacon-based signaling aptamer was reported in 2000 by Yamamoto et al.[78] This strategy used a fluorescence resonance energy transfer (FRET) mechanism, where a donor chromophore (F) in its electronic excited state can transfer energy to an non-

emitting acceptor chromophore (quencher, Q) through non-radiative dipole-dipole coupling when acceptor is in a sufficiently short distance (1-5 nm). Typically, the aptamer sequence is placed in a stem-loop hairpin structure through strand self-complementation and dual-labeled with a fluorophore and a quencher on either end. Binding of the target disrupts the stem hybridization, separates the fluorophore and the quencher and thus produces an increase in fluorescence[78, 79].

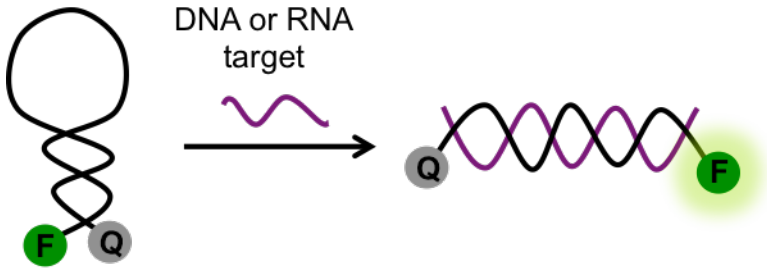

Figure 1-3. Schematic representation of molecular beacon aptamer signaling strategy (F = fluorescein tag and Q = dabcyl tag). One oligomer is designed to form a hairpin structure that contains a fluorophore (fluorescein) and quencher (DABCYL) at both ends. The fluorophore is quenched by energy transfer to the quencher owing to its close proximity. In the presence of a target, a duplex is formed between the molecular beacon and the target nucleic acid, resulting in breakage of the stem, separating the fluorophore from the quencher and leading to an increase in the fluorescence signal.

However, this design lacked wide applicability towards diverse aptamers; hence, Nutiu and Li[80] modified the aptamer-beacon scheme to create structure-switching signaling aptamers, that could easily be generalized[80]. This approach takes advantage of the ability of aptamers to form a strong aptamer-target complex and a weak DNA/DNA or DNA/RNA duplex with complementary sequences. Structure-switching aptamers consist of two schemes: in the tripartite scheme, a duplex composed of an extended primer region from the DNA or RNA aptamer strand hybridized to fluorophore-labelled complementary DNA strand (***F***-DNA), while a

quencher-labelled DNA strand (***Q***-DNA) hybridized to a region that stretches over from the aptamer to the primer, with the quencher next to the fluorophore ("off" mode), as shown in Figure 1-3. In the bipartite scheme, the fluorophore is covalently tethered to the primer sequence with use of a similar complementary quencher-labelled DNA strand. Addition of target facilitates formation of an aptamer-target complex for both schemes, where ***Q***-DNA is displaced and generates an increase in fluorescence intensity ("on" mode).

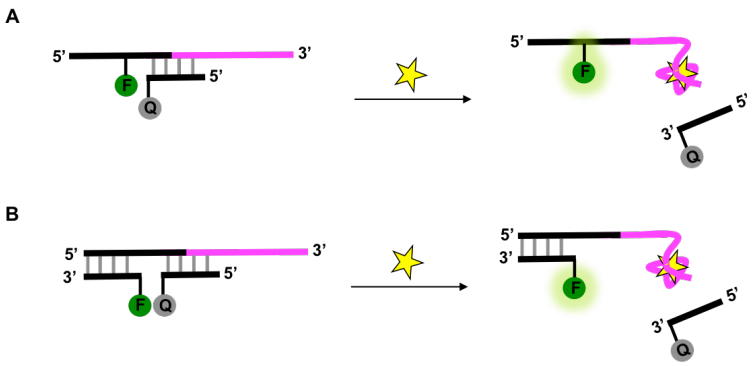

Figure 1-4. Various designs of structure-switching signaling aptamer reporters (F = fluorescein tag and Q = dabcyl tag). (A) Bipartite construct composed of a fluorophore-modified aptamer and a hybridized QDNA. (B) Tripartite complex composed of a two hybridized strands, a complimentary F-DNA and a complimentary Q-DNA strand bound to the aptamer. Upon target addition, the aptamer forms a hairpin loop, displaces the Q-DNA, and produces an increase in the fluorescence intensity.

The structure-switching approach has been exploited to design DNA aptamers to detect various targets such as NTPs[81, 82], mercury[83-85], and cocaine; with the anti-ATP[82] and anti-thrombin[86] aptamers being among the most widely used model systems for biosensor development. Similarly, structure-switching RNA aptamers have been developed that can recognize TPP[87], theophylline[88], and ATP.

1.3.3 DNAzyme-catalyzed colourimetric reaction

DNAzymes are single-stranded DNA molecules that exhibit catalytic activity. DNAzymes can be combined with aptamers to form aptazymes, wherein an aptamer binding event can trigger catalysis or it can be used separately with aptamers in a sensor. There are several advantages to using DNAzyme over conventional protein enzymes. First of all, unlike protein enzymes, DNAzymes are stable in a broad range of temperatures, even very high temperatures.[89, 90] DNAzymes can easily be prepared by chemical synthesis or PCR, whereas protein enzymes require tedious preparation and purification processes. Futhermore, DNAzyme can be combined with conventional DNA amplification methods to carry out signal amplification that is impossible with protein enzymes. One of the commonly used DNAzymes is denoted as PW17, which is a small DNAzyme with a G-quadruplex motif that can bind hemin and exhibit peroxidase-like activity. [91, 92].

A G-quadruplex comprises four G bases forming a square planar array called a G-quartet. G-quadruplexes are formed by stacking up square planar arrays that are joined by a phosphodiester backbone and stabilized by π-π stacking interactions of the stacked G-quartets. G-quadruplexes are formed by single-stranded oligonucleotides that can exhibit complex conformations such as parallel, hairpin, basket and chair motifs. Shangguan and coworkers[93] have found that the relationship between G-quadruplex and catalytic activity is related to its ability to bind hemin. Some structures such as the parallel structure are more favourable for binding hemin. This hemin-quadruplex complex can catalyze the hydrogen peroxide (H_2O_2)-mediated oxidation of substrates such as 2,2'-azino-bis(3-ethylbenzthiazoline-6-sulphonic acid)

(ABTS) or 3,3',5,5'-tetramethylbenzidine (TMB) and generate a coloured product[91, 94, 95]. This colourimetric change allows the development of assays for detecting metal ions[96, 97], aptamer-substrate complexes[98] and even proteins[99, 100].

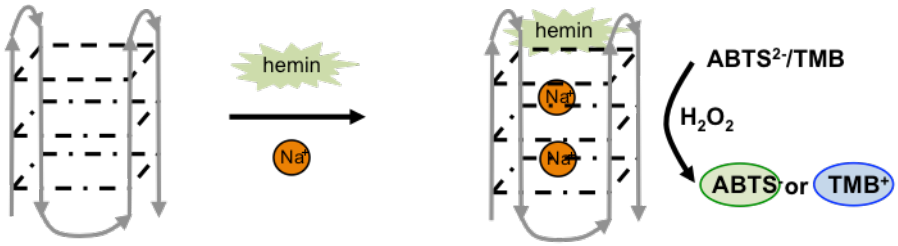

Figure 1-5. Schematic illustration of relationship between G-quadruplex and catalytic activity by binding to hemin. Hemin-quadruplex complex form a DNAzyme that can catalyze H_2O_2-mediated oxidation of ABTS and/or TMB to generate a colour product that is visible my eyes.

A series of papers by Liu *et al.*[101-103] coupled an aptamer to rolling circle amplification (RCA) to form multiple repeats of a G-quadruplex peroxidase DNAzyme units that catalyzed the oxidation of a chromogenic substrate to produce an easily visualized colour change. In the graphene displacement study[101], single-stranded DNA aptamer was adsorbed on reduced graphene oxide (rGO) nonspecifically. Upon addition of target, the aptamer underwent a target-induced conformational change that facilitated their release from the rGO surface. The released aptamer consisted of a primer domain that could perform RCA upon released. A biosensor engineering strategy is also presented by Liu *et al.*[102] by coupling ϕ29DP with structure-switching DNA aptamers. This design employed a DNA assembly made of a circular DNA template, a DNA aptamer and a pre-primer. The presence of the target triggered the structure-switching event and caused nucleolytic conversion of the pre-primer by ϕ29DP into a mature primer to facilitate

RCA. A massive DNA amplicon was then produced and enhanced detection sensitivity dramatically.

Another signal amplification strategy designed by same group named DNAzyme feedback amplification (DFA)[103] that took advantages of RCA and a RNA cleaving DNAzyme (RCD). In this DFA system, two special DNA complexes were employed. First complex was composed of a primer and a circular template containing the antisense sequence of an RCD, while the other complex was composed of the same circular template and an RNA-containing substrate for RCD. RCA was initiated at the first complex and produced RCD elements that cleaved the substrate in the second complex. This cleavage was then triggered the production of more complexes for RCA. As the reaction circuit continued, DNA amplified exponentially. The sensitivity using this system was improved 3-6 orders of magnitude over the conventional methods.

1.4 Immobilization of nucleic acid aptamers.

1.4.1 General overview

In order to utilize the full potential of structure-switching aptamers for applications such as biosensing, metabolite profiling, or affinity capture of specific analytes, it is necessary to immobilize the aptamer reporters on a suitable surface.[104-108] Typical methods for biomolecules immobilization include physical adsorption, covalent and affinity binding to the surface and entrapment into polymer microphores, hydrogels, semi-permeable membranes or porous inorganic materials.[109-117]

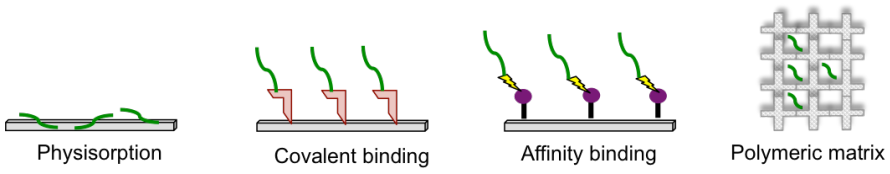

Figure 1-6. Different immobilization methods for DNA. Nucleic acid aptamers can be immobilized on a solid support via physical adsorption, covalent binding, affinity binding or entrapped within polymeric matrix.

Of particular relevance to this thesis are the methods of adsorption and physical entrapment. Adsorption is the simplest method to immobilize biomolecules onto a surface, which bind through non-specific interactions such as H-bonding, pi-stacking or vander Waal's interactions. This is the basis of immobilization of DNA onto graphene-based materials, which is described in more detail in the next section. The entrapment of biomolecules within sol-gel derived materials is an example of immobilization within a three-dimensional polymeric matrix. In this case, three-dimensional matrices can accommodate a greater number of biomolecules that is typically possible using affinity or covalent methods (which usually form monolayers), which improves the detection limits and sensitivity when used in sensor applications. In addition, with entrapment, biomolecules are not bound to the support surface but are retained through size-exclusion; and thus, they are orientated in a way that the active regions are accessible from all directions. Typical matrix entrapment generally includes water-soluble organic polymers such as acrylamide.[112, 113] However, the chemical processing conditions during encapsulation may lead to degradation of the biological species.[112, 113, 118] Furthermore, it is very difficult to control the pore size so that the entrapped biomolecules can retain conformation

mobility and accessibility to the analytes without leaching.[117] These problems can be addressed by entrapping the biomolecules in inorganic or organic/inorganic composite materials such as sol-gel derived silica.[117, 119, 120]

1.4.2 Immobilization using Sol-Gel entrapment

As mentioned above, many bio-immobilization methods result in monolayer coverage and thus can suffer from poor detection limits and sensitivity. Therefore, an emerging method for biomolecules entrapment involves the use of sol-gel processed materials as an entrapment matrix[119, 121-126]. The sol-gel processing method is a simple two-step process, which begins with the formation of an aqueous sol through acid or base catalyzed hydrolysis of a suitable silane precursor, typically tetraalkoxysilanes such as tetraethylorthosilicate (TEOS) or tetramethylorthosilicate (TMOS)[127]. The hydroxysilane is then mixed with a buffered aqueous solution containing the biomolecules as well as any additives for aiding biomolecular stability or modifying the properties of the final material. The change in pH along with the presence of salts leads to a large-scale polymerization, forming siloxane bonds and entrapping the biomolecules within the nanoscale pores of the cross-linking gel matrix. The speed of the condensation reaction depends on the pH and ionic strength of the sol as well as the types of additives present, resulting in gelation times of seconds to days. As the wet silica gel ages, polycondensation continues, releasing the entrapped alcohol and water and causing shrinkage and rigidity of the material.[120, 128]

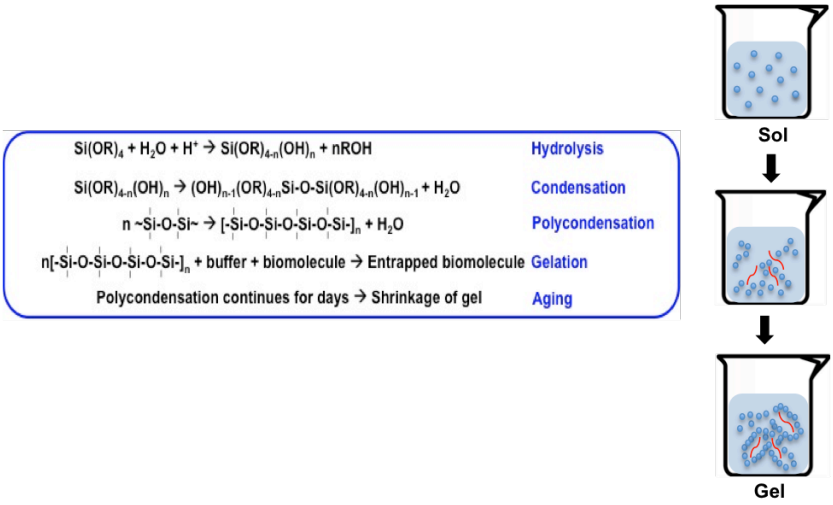

Figure 1-7. Sol-gel process method for entrapping biomolecules within silica materials using tetraalkoxysilanes as precursor. Biomolecules can be entrapped within various materials such as inorganic, organic or hybrid porous materials through this two-step sol-gel process of hydrolysis and condensation. Addition of biomolecules to the condensing sol become entrapped within the nanoscales pores network of gel matrix. The bonds to Si are denoting further Si-O bonds.

Initial studies on biomolecule entrapment via the sol-gel method focussed on TEOS and TMOS as precursors; however, these alkoxysilanes produce a large amount of alcohol that results in denaturation of the entrapped biomolecules, particularly proteins. Therefore, modified processes emerged, such as evaporation of residual alcohol[129] or using more biocompatible precursors like sodium silicate and diglyceryl silane[130]. As opposed to alkoxysilanes, which release alcohol during the sol-gel process, diglyceryl silane releases glycerol, which can act as bimolecular stabilizer and humectant[131].

Sol-gel materials have been used to entrap a wide variety of biological species, including proteins such as enzymes and antibodies, and even whole cells.[121,

[124, 125, 132, 133] However, this platform is not as widely used for entrapment of nucleic acid aptamers. To date, there are only a few reports in the literature describing the entrapment of nucleic acid aptamers in sol-gel derived materials. Rupcich *et al.*[78] was the first to report entrapment of a DNA aptamer within a sol-gel derived matrix. In this study, streptavidin was used to bind a biotinylated structure-switching signaling DNA aptamer for ATP to investigate the optimal signaling capability and response time of aptamers in solution and when entrapped in different sol-gel derived materials. It was demonstrated that the DNA aptamer entrapped in a sodium silicate derived material was able to retain its ability to change conformation and produce a fluorescence signal upon binding to ATP with sensitivity and selectivity comparable to solution. In addition, it was found that sol-gel derived materials were able to protect the entrapped DNA aptamer from degradation by nucleases. This property improved the long-term stability of the entrapped biomolecules and allowed them to be more useful for *in vivo* studies.

More recent studies by Brennan and coworkers have involved DNA aptamer co-entrapment with a protein enzyme as a reporter for enzyme activity in the solid-phase[134], sol-gel entrapment of a function deoxyribozyme for metal ion detection[5], surface immobilization of structure-switching DNA aptamers on sol-gel derived films for solid-phase biomolecular detection[135] and sol-gel entrapment of structure-switching RNA aptamer reporters[136].

The first successful immobilization of a structure-switching DNA aptamer was reported by Rupcich *et al.*[3] in 2005. Two different constructs of an ATP-binding

structure-switching DNA aptamer – bipartite and tripartite – were entrapped in various biocompatible sol-gel-derived materials such as sodium silicate (SS), diglycerylsilane (DGS), TEOS and 0.1% (v/v) (aminopropyl)-triethoxysilane (APTES) doped- SS and DGS hybrids. The structure-switching ability of both aptamer constructs was assessed after entrapment in these materials and it was shown that similar increases in florescence intensity were obtained relative to solution after entrapment in both SS- and DGS-derived. It also showed that the DNA aptamer was protected against degradation from nucleases by entrapment in silica materials.

Another study by Carrasquilla *et al.*[136] examined the immobilization of structure-switching RNA theophylline and TPP-binding aptamers in a variety of sol-gel processed composite materials (polar, anionic, cationic, hydrophobic). In this study, the signal generation ability, leaching, sensitivity, and long-term stability of entrapped RNA aptamers were assessed. RNA aptamers were also found to be resistant to nuclease degradation after entrapment in sol-gel-derived materials. However, interestingly, the results in this study showed that the optimal materials for entrapment of RNA aptamers were very different from those that stabilize proteins or DNA aptamers. RNA aptamers demonstrated the best performance when entrapped in alcohol-producing material prepared by 40% MTMS and 60% TMOS (v/v), whereas the alcohol liberated was found to cause problems to entrapped proteins.[120]

All these studies demonstrated the significant versatility and advantages of sol-gel derived materials for immobilization nucleic acid aptamers. However, there is no or limited information on the effects of different factors on the performance of

immobilized aptamers. In order to understand the underlying cause for the different performance of immobilized aptamers, it is necessary to understand the nature of immobilized aptamers, especially how entrapment in different sol-gel-derived materials affects aptamers performance for detection of analytes.

1.4.3 Paper-Based Biosensing Devices

Over the last decade, there has been a significant interest in developing on-site diagnostic analytical assays that are portable, affordable, sensitive, and deliver fast but accurate results in the areas of environmental monitoring, industrial control and healthcare, with a significant emphasis on paper-based biosensors.[15, 137-145] Paper is naturally abundant, inexpensive and biodegradable,[146] and various (bio)materials can easily be printed/coated on this porous substrate, which also can facilitate fluid movement by capillary action.[141, 143, 147]

The first microfluidic paper-based analytical devices (μPADs), developed by Martinez *et al.,*[148] utilized the capillary properties of paper to drive a liquid sample through channels that were created by producing hydrophobic barriers with a photoresist polymer. These flow channels allowed analyte to be transported to the detection zones, where colorimetric assays for glucose or proteins were performed using simple chemical reactions. Many of the μPAD studies in the early stages focused on creating hydrophobic barriers through technologies like photolithography, plasma treatment or screen-printing.[15, 140, 141] Later studies[149, 150] made use of an inkjet printer to print a 550 μm-wide channels with a hydrophobic polymer, which laid a

foundation of using inkjet printing as a method to create hydrophobic barriers. Since then, printing and subsequent heating of solid wax has become a dominant method to create microfluidic channels with hydrophobic barriers.[145, 151]

Paper is mainly composed of cellulose fibres, which contains few functional groups for chemical modification for biomolecule attachment.[137, 143, 144, 152-154] However, it was found that typical immobilization methods such as physical adsorption or covalent linking were not ideal when immobilizing aptamer molecules on paper.[153] Therefore, other strategies such as affinity-based immobilization or conjugation to larger colloidal particles were used to immobilize aptamers on paper.[25] Although entrapping aptamers within sol-gel-derived silica materials allows long-term stability and better performance[3, 136, 155], printing of the materials still remains challenging due to the clogging of printheads or cartridges due to polymerization of sol-gel occurs in cartridge or printheads.[18, 25]

The main methods for immobilizing aptamers on paper fall into four categories. The simplest is simple phyhsisorption of the functional nucleic acids on to paper zones that are demarcated with wax barriers to prevent the nucleic acids from leaving the reaction zone.[156-158] Several groups have bound aptamers to beads formed from polymers, microgels or other materials followed by deposition on paper.[159, 160] The large size of the bead prevents movement of the nucleic acid, but conjugation of the nucleic acid to the bead still requires a multi-step process. Another method is direct binding of biotin-modified nucleic acids to paper that is coated with avidin.[14, 157] Finally, our group recently reported the printing of RCA derived amplicons of

apltamers which were MDa in size directly onto unmodified paper surfaces. The large size of these amplicons allowed aptamers to be printed as patterns or text, with the abiity to undergo structure-switching to generate fluorescence signals.[161] While these methods all provide a means to immobilize aptamers, many are tedious and require several steps, or require extensive modification of the original aptamer (i.e., formation of an amplicon) to allow robust immobilization. Hence, an alternative method was sought for the work described in this thesis.

1.4.4 Immobilization using Graphene Oxide

Graphene, a single atomic layer consisting of sp^2-bonded carbons in a honeycomb lattice, has created an enormous interest in the scientific world owing to its specific 2D structure and unique electronic, optical, thermal and electrochemical properties.[162] Ever since its discovery, graphene has been used for a range of applications, including as scaffold materials, conductors for electronic devices and as a platform for bio/chemical sensors.

Graphene oxide (GO) is a key derivative of graphene which has been treated to generate a highly oxidized hydrophilic surface with a substantial number of hydroxyl and other oxygenated species such as expoxide and carboxylic groups.[163, 164] These surface functional groups provide reaction sites for anchoring biomolecules such as proteins, enzymes, or DNA without any further surface modification. A particularly important strategies for immobilization of nucleic acids is direct adsorption onto GO, which can strongly adsorb single-stranded DNA (ssDNA) while

having much less affinity for double-stranded DNA (dsDNA). This difference in affinity has been used to produce a platform to distinguish different DNA sequences.[165-168] GO also has the ability to produce extremely high (>99%) quenching of fluorescence when fluorophore-labelled ssDNA is adsorbed to the surface.[169-171] Hence, desorption of fluorophore labelled ssDNA upon binding to complementary DNA can produce a very large fluorescence signal. Other constructs, such as hairpin DNA and molecular beacon (MB) systems, have also been designed for homogenous DNA detection to take advantage of this mechanism.[172, 173]

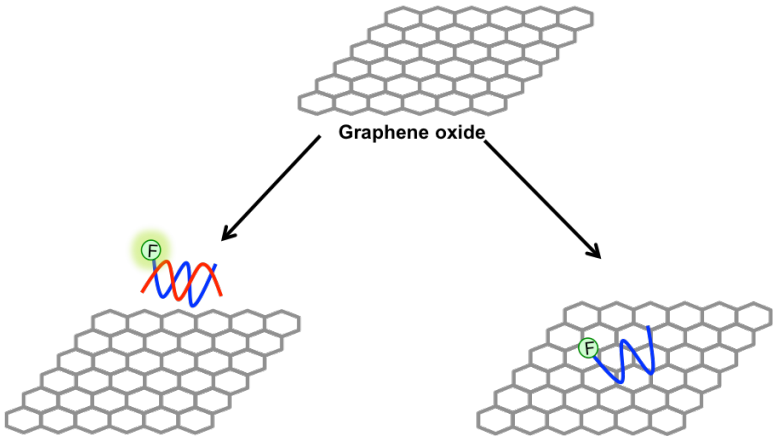

Figure 1-8. Fluorescent DNA detection based on the ssDNA/dsDNA discrimination ability of graphene oxide. ssDNA bind more strongly to graphene oxide than double-dsDNA. The difference in binding affinity between ssDNA and dsDNA allows graphene oxide to adopt as a platform to distinguish different DNA sequences.

The first reported GO-based fluorescent aptamer biosensor was made by Lu *et al.*[174] in 2009 using a fluorescent dye labelled DNA probe to detect HIV1 DNA or thrombin. This study demonstrated that fluorescence signal of the dye was quenched

when adsorbed on GO and was able to release from the GO when its corresponding DNA or protein target was introduced. Since then, researchers have shown great interest in utilizing GO as fluorescence-based biosensors. For instance, He *et al.*[175] reported a GO-based multicolour DNA sensing system that allowed detection of multiple DNA targets. This system consisted of three DNA probes, each labeled with different fluorescent dyes quenched on a large planar surface of GO, which led to a detection of multiple DNA targets in the same solution with a detection limit of 100 pM. They also demonstrated in the same study that a GO-based sensing platform was able to detect metal ions such as mercuric ion (Hg^{2+}) and small molecules like adenine by selecting appropriate aptamers.

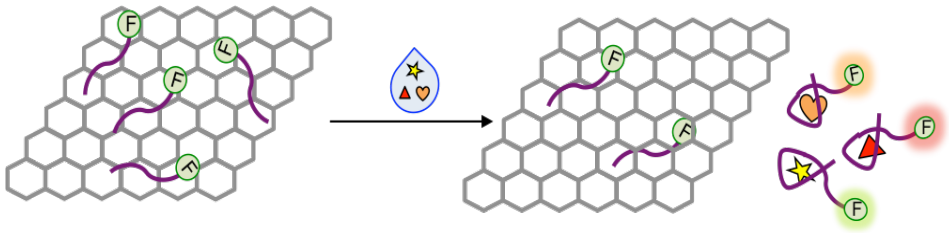

Figure 1-9. Schematic diagram for graphene oxide-based multicolour DNA analysis. Each DNA aptamer is labeled with different fluorescent probe and quenched on a large planar surface of GO. Upon addition of sample solution, which contains multiple targets, resulting in multi fluorescence signals.

The preferential adsorption of ssDNA over DNA target complex has created a great platform for broad applications to detect and quantitatively analyze meaningful target molecules such as DNA, RNA, proteins, and small molecules.[156, 172, 176-184] Unfortunately, the overall changes in fluorescence upon target binding can be relatively small, and detection limits can be compromised as the target must compete with the binding of the aptamer to the GO surface, which can reduce detection limits.

[101, 185] Therefore, signal amplification strategies may need to be used to improve the original FRET biosensors.

1.5 Rolling circle amplification on paper devices

To improve the sensitivity and lower the detection limits of bioassays, amplification techniques are often applied to the assays. Polymerase chain reaction (PCR) has been the most widespread amplification technology used for detecting low-abundance nucleic acids; however, it is somewhat restricted by its complexity, potential contamination, and cost. Thus, isothermal amplification techniques have become popular due to its rapid and efficient amplification of nucleic acids at a constant temperature without thermal cycling steps like PCR. Different research groups[186-188] also reported different types of enzymatic signal amplification, such as loop-mediated isothermal amplification (LAMP), recombinase polymerase amplification (RPA) and helicase dependant amplification (HDA) using the catalytic activity of polymerase to produce huge amounts of DNA duplex triggered by the strand displacement polymerization reaction and recycled short single strand DNA.

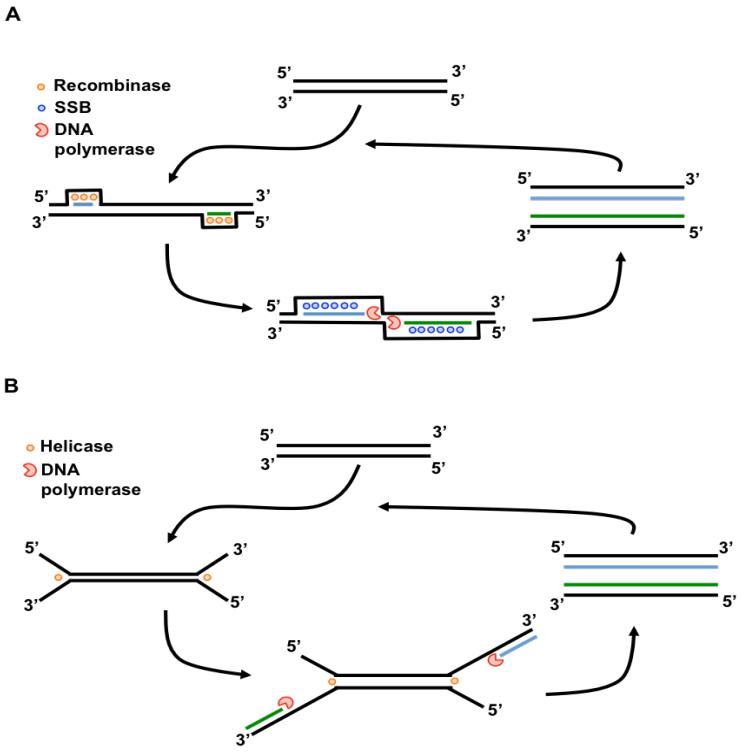

Figure 1-10. Schematic diagrams of example isothermal amplifications. (A) Recombinase Polymerase Amplification (RPA) – two oligonucleotide primers form a complex with the recombinase proteins (orange). The complex can invade the target DNA and direct the primer to homologous sequences. The amplification is then taken place at 38°C by strand-displacement synthesis that catalyzed by a DNA polymerase (red), while the single-strand binding proteins (SSB) (blue) is stabilizing the displaced strand. (B) Helicase Dependant Amplification (HAD) – Helicase separates the two strands of DNA duplex generating single-stranded templates. Two-sequence specific primers are then annealed to the 3'-end of each ssDNA template and exonclease-deficient DNA polymerase is then produce dsDNA by extending the primers annealed. Exponential amplification can be achieved when this process repeats at a single temperature.

Rolling circle amplification (RCA) is an isothermal enzymatic DNA replication process that uses DNA polymerases to generate long single-stranded DNA amplicons with tandem repeats of the complementary sequence of a circular DNA template.[189-191] The length of the newly synthesized RCA product is mainly dependent on the type of the polymerase used. Highly processive DNA polymerases such as phi29 DNA polymerase produce "longer" RCA products since it binds to the

circular DNA template longer as well as can displace newly synthesized DNA strands.[192-194] Several studies have demonstrated that RCA initiated by a specific target binding can amplify a single molecular recognition event to increase the sensitivities of the reporter system.[195-198]

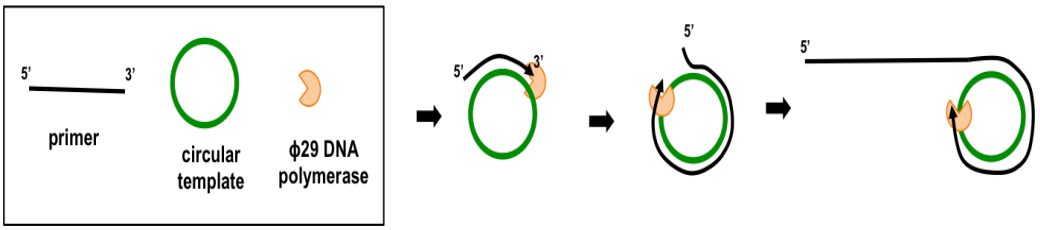

Figure 1-11. Schematic illustration of Rolling Circle Amplification (RCA) process. A circular DNA template is first hybridizes with a short primer sequence. This primer is then continuously extended as DNA polymerase adds nucleotides to the primer that are complimentary to the circular template. This isothermal enzymatic DNA replication process can generate long ssDNA with thousands of repeats.

Researchers have integrated these enzymatic signal amplification strategies to GO-based sensors since GO-based FRET cannot detect analyte levels below femtomolar concentrations. As an example, Cui *et al.*[199] developed a cyclic enzymatic amplification method for sensitive fluorescent miRNA detection in complex biological samples. The design used DNase for selective digestion of a DNA probe that hybridized with target miRNA, inducing the recycling of the miRNA and desorption of multiple probe strands from the GO surface. The sensor was able to reach the detection sensitivity of about three orders of magnitude higher than non-amplified system. In addition, enzyme mediated digestion of DNA probes was also employed by Wang *et al.*[200] for amplifying the electrochemical signals in GO-based biosensors. Liu *et al.*[101] also reported a highly sensitive enzymatic signal

amplification method in GO-based sensing system utilizing DNA probe consisting of target binding aptamer and polymerase recognizing primer to detect small molecules. The repeated sequence produced by RCA acted as a template to hybridize to MB to produce an intense fluorescence signal.

In addition to the typical method of hybridizing DNA probes with fluorescence dyes or AuNPs couples to the tandem-repeating units of RCA reaction products, RCA can also be used to produce a DNAzyme as the reaction output, and in the case of a hemin-binding DNAzyme, the reaction product can be used to catalyzed the peroxidase reaction with ABTS or TMB to create a highly sensitive colourimetric biosensor. One example is an aptamer-modified microchip developed by Lin *et al.*[201] that also combines rolling circle amplification (RCA) and G-quadruplex DNAzyme for thrombin detection. The system consists of an aptamer modified microchip and a reporter aptamer that contains a thrombin aptamer and a primer with a G-quadruplex circular template. Upon introducing thrombin, the thrombin is then captured by the thrombin aptamer immobilized on the chip and the reporter aptamer in a sandwich format. The reporter aptamer then acts as a primer for the RCA amplification process to generate repeating unit of G-quadruplex DNAzyme. Upon binding of hemin, a hemin-DNAzyme complex is formed and results in catalyzing a H_2O_2-mediated oxidation of ABTS to produce a green colour RCA product. RCA technology was used to improve the sensitivity by producing multiple G-quadruplex unit, improving the detection limit to 0.083 pg/mL. Another study by Liu et al.[157] mentioned

previously was able to detect 10 pM of HCV-1 DNA by coupling aptamer detection to RCA.

1.6 Thesis Outline

As noted earlier, the key objectives of the thesis are to examine the propertiese of DNA and RNA aptamers within sol-gel derived materials, and to then move to a more applied study involving the use of immobilized DNA and RNA aptamers for development of paper-based biosensors. The first research project (Chapter 2) characterizes the parameters that affect the function of DNA aptamer reporters when entrapped in a variety of silica and organosilicate materials using fluorescence techniques. These parameters include aptamer accessibility, aptamer dynamics, degree of leaching, long-term stability and thermal stability. The overall goal is to determine which factors affect the performance of entrapped aptamers and to further investigate how different materials might control these factors so as to allow optimization of aptamer performance.

In Chapter 3, the fluorescene methods were used to further evaluate RNA aptamers within sol-gel derived materials, with the key goal of determining if RNA aptamers behave differently and as such require alternative materials for entrapment.

The third research project (Chapter 4) investigated the fabrication of a paper-based sensor wherein GO was used for immobilization of both a RNA and a DNA aptamer, which could then undergo target induced desorption to generate a fluorescence signal. The ability to integrate the aptamer desorption with a

downstream RCA amplification reaction was also investigated to determine if a dual response (fluorescence / colorimetric) sensor could be produced. Key goals were to determine which response lead to the best analytical performance and to assess whether the overall method was sufficiently versatile to be used with both RNA and DNA aptamers.

The final chapter of the thesis (Chapter 5) summarizes the major achievements and conclusions drawn from the research projects outlined above and recommends future directions. References pertaining to specific research projects (Chapter 2-4) are found at the end of each section, respectively.

1.7 Cited References.

1. Brennan, J. D., *Applied Spectroscopy* **1999,** 53, (3), 106A-121A.
2. Navani, N. K.; Li, Y., *Current Opinion in Chemical Biology* **2006,** 10, (3), 272-281.
3. Rupcich, N.; Nutiu, R.; Li, Y.; Brennan, J. D., *Analytical Chemistry* **2005,** 77, (4), 4300-4307.
4. Klug, S. J.; Famulok, M., *Molecular Biology Reports* **1994,** 20, 97-107.
5. Shen, Y.; Mackey, G.; Rupcich, N.; Gloster, D.; Chiuman, W.; Li, Y.; Brennan, J. D., *Anal. Chem.* **2007,** 79, (9), 3494-3503.
6. Carrasquilla, C.; Li, Y.; Brennan, J. D., *Anal. Chem.* **2011,** 83, (3), 957-65.
7. Carrasquilla, C.; Lau, P. S.; Li, Y.; Brennan, J. D., *J. Am. Chem. Soc.* **2012,** 134, (26), 10998-1005.
8. Pelton, R., *Trends in Analytical Chemistry* **2009,** 28, (8).
9. Yetisen, A. K.; Akram, M. S.; R., L. C., *Lab on a Chip* **2013,** 12, 2210-2251.
10. Hossain, S. M. Z.; Luckham, R. E.; Smith, A. M.; Lebert, J. M.; Davies, L. M.; Pelton, R. H.; Filipe, C. D. M.; Brennan, J. D., *Anal. Chem.* **2009,** 81, 5474-5483.
11. Mazumdar, D.; Liu, J.; Lu, G.; Zhou, J.; Lu, Y., *Chem. Commun.* **2010,** 46, 1416-1418.
12. Martinez, A. W.; Philips, S. T.; Carrilho, E.; Thomas III, S. W.; Sindi, H.; Whitesides, G. M., *Anal. Chem.* **2008,** 80, 3699-3707.
13. Liu, J.; Mazumdar, D.; Lu, Y., *Angew. Chem. Int. Ed.* **2006,** 45, 7955-7959.
14. Liu, J.; Mazumdar, D.; Lu, Y., *Angew. Chem. Int. Ed* **2006,** 45, 7955-7959.
15. Liana, D. D.; Raguse, B.; Gooding, J. J.; Chow, E., *Sensors* **2012,** 12, (9), 11505-11526.
16. Liu, H.; Xiang, Y.; Lu, Y.; Crooks, R. M., *Angew. Chem. Int. Ed* **2012,** 51, (28), 6925-6928.
17. Wang, J.; Bowie, D.; Zhang, X.; Filipe, C.; Pelton, R.; Brennan, J. D., *Chemistry of Materials* **2014,** 25, (5), 1941-1947.
18. Hossain, S. M. Z.; Luckham, R. E.; Smith, A. M.; Lobert, J. M.; Davies, L. M.; Pelton, R. H.; Filipe, C. D. M.; Brennan, J. D., *Anal. Chem.* **2009,** 81, (13), 5474-5483.
19. Turner, A. P. F., *Chem. Soc. Rev.* **2013,** 42, 3184-3196.
20. Blonder, R.; Levi, S.; Tao, G.; Ben-Dov, I.; Willner, I., *J. Am. Chem. Soc* **1997,** 119, (43), 10467-10478.
21. Blonder, R.; Ben-Dov, I.; Dagan, A.; Willner, I.; Zisman, E., *Biosensors and Bioelectronics* **1997,** 12, (7), 627-644.
22. Drummond, T. G.; Hill, M. G.; Barton, J. K., *Nat. Biotechnol.* **2003,** 21, 1192-1199.
23. Berdat, D.; Marin, A.; Herrera, F.; Martin, A. M. G., *Sensor and Actuators B: Chemicals* **2006,** 118, (1-2), 53-59.
24. Eden-Firstenberg, R.; Schaertel, B. J., *J. of Food Protection* **1988,** 51, 811-820.
25. Hossain, S. M. Z.; Luckham, R. E.; McFadden, M. J.; Brennan, J. D., *Anal. Chem.* **2009,** 81, (21), 9055-9064.
26. Xu, X.; Ying, Y., *Food Reviews International* **2011,** 27, (3), 300-329.
27. Linder, D., *Lab on a Chip* **2001,** 1, 15N-19N.
28. Burkle, F. M., *Prehospital and Disaster Medicine* **2003,** 18, (3), 258-262.
29. Mascini, M., *Pure and Applied Chemistry* **2001,** 73, (1), 23-30.
30. Sicard, C.; Brennan, J. D., *MRS bulletin* **2013,** 38, (4), 331-334.
31. Hossain, S. M. Z.; Brennan, J. D., *Anal. Chem.* **2011,** 83, (22), 8772-8778.

32. Wang, J.; Rivas, G.; Cai, X.; Palecek, R.; Nielsen, P.; Shiraishi, H.; Dontha, N.; Luo, D.; Parrado, C.; Chicharro, M.; Faries, P. A. M.; Valera, F. S.; Grant, D. H.; Ozsoz, N.; Flair, M. N., *Analytica Chimica Acta* **1997,** 347, (1-2), 1-8.
33. Rodriguez-Mozaz, S.; Marco, M. P.; de Alda, M. J. L.; Barcelo, D., *Pure and Applied Chemistry* **2004,** 76, (4), 723-752.
34. Palchetti, I.; Marco, M., *Analyst* **2008,** 133, (7), 846-854.
35. Biswas, P.; Karn, A. K.; Blalasubramanian, P.; Kale, P. G., *Biosensors and Bioelectronics* **2017,** 94, 589-604.
36. Nguyen, V.-T.; Kwon, Y. S.; Gu, M. B., *Current Opinion in Chemical Biology* **2017,** 45, 15-23.
37. Kumar, S.; Kumar, S.; Ali, M. M.; Anand, P., *Biotechnol.* **2013,** 8, 1267-1279.
38. Malhotra, B. D.; Chaubey, A., *Sensor and Actuators B* **2003,** 91, 117-127.
39. Zhang, C.; Kim, J. P.; Creer, M.; Yang, J.; Liu, Z., *Biosensors and Bioelectronics* **2017,** 97, 164-168.
40. Scherf, K. A.; Ciccocioppo, R.; Pohanka, M.; Rimarova, K.; Opatrilova, R.; Rodrigo, L.; Kruzliak, P., *Mol. Biotechnol.* **2016,** 58, 381-392.
41. Moreira, F. T. C.; Moreira-Tavares, A. P.; Sales, M. G. F., *Current topics in medicinal Chemistry* **2015,** 15, (3), 245-255.
42. Jolly, P.; Formisano, N.; Estrela, P., *Chemical Papers* **2015,** 69, (1), 77-89.
43. Li, C.-z.; Vandenberg, K.; Prabhulkar, S.; Zhu, X.; Scheneper, L.; Methee, K.; Rosser, C. J.; Almeide, E., *Biosensors and Bioelectronics* **2911,** 26, (11), 4342-4348.
44. Hossain, S. M. Z.; Ozimok, C.; Sicard, C.; Aguirre, S. D.; Ali, M. M.; Li, Y.; Brennan, J. D., *Anal. Bioanal. Chem* **2012,** 403, (6), 1567-1576.
45. Mehrotra, P., *J. Oral. Biol. Craniofac. Res.* **2016,** 6, (2), 153-159.
46. Voswinckel, P., *Kidney International* **1994**, (supplement), S3-S7.
47. Jones, G.; Kraft, A., *Business History* **2004,** 46, (1), 100-122.
48. Cheng, C.-M.; Martinez, A. W.; Gong, J.; Mace, C. R.; Phillips, S. T.; Carrilho, E.; Mirica, K. A.; Whitesides, G. M., *Angew. Chem. Int. Ed* **2010,** 49, (28), 4771-4774.
49. Ellington, A. D.; Conrad, R. C., *Biotechnol. Annu Rev.* **1995,** 1, 185-214.
50. Jayasena, S. D., *Clinical Chemistry* **1999,** 45, (9), 1628-1650.
51. Brody, E. N.; Gold, L., *J. Biotechnol.* **2000,** 74, (1), 5-13.
52. Radom, F.; Jurek, P. M.; Mazurek, M. P.; Otlewski, J.; Jelen, F., *Biotechnol. Adv.* **2013,** 31, (8), 1260-1274.
53. Hu, R.; Liu, T.; Zhang, X.-B.; Huan, S.-Y.; Wu, C.; Fu, T.; Tan, W., *Anal. Chem.* **2014,** 86, (10), 5009-5016.
54. Bahadır, E. B.; Sezgintürk, M. K., *Trac-Trends in Analytical Chemistry* **2016,** 82, 286-306.
55. Ellington, A. D.; Szostak, J. W., *Nature* **1990,** 346, 818-822.
56. Tuerk, C.; Gold, L., *Science* **1990,** 249, 505-510.
57. Wilson, D. S.; Szostak, J. W., *Annu. Rev. Biochem* **1999,** 68, 611-647.
58. Breaker, R. R., *Current Opinion in Chemical Biology* **1997,** 1, 26-31.
59. Holeman, L. A.; Robinson, S. L.; Szostak, J. W.; Wilson, C., *Folding and Design* **1998,** 3, (6), 423-431.
60. Schurer, H.; Stembera, K.; Knoll, D.; Mayer, G.; Blind, M.; Forster, H.-H.; Famulok, M.; Welzel, P.; Hahn, U., *Bioorganic and Medicinal Chemistry* **2001,** 9, 2557-2563.
61. Lupold, S. E.; Hicke, B. J.; Lin, Y.; Coffey, D. S., *Cancer Research* **2002,** 62, 4029-4033.

62. Balogh, Z.; Lautner, G.; Bardoczy, V.; Komorowska, B.; Gyurcsanyi, R. E.; Meszaros, T., *The FASEB Journal* **2017,** 24, (11), 4187-4195.
63. Raddatz, M.-S. L.; Dolf, A.; Endl, E.; Knolle, P.; Famulok, M.; Mayer, G., *Angew. Chem. Int. Ed* **2008,** 47, 5190-5193.
64. Robertson, D. L.; Joyce, G. F., *Nature* **1990,** 344, 467-468.
65. Famulok, M.; Mayer, G.; Blind, M., *Accounts of Chemical Research* **2000,** 33, 591-599.
66. F., J. G., *Annu. Rev. Biochem.* **2004,** 73, 791-836.
67. Mendonsa, S. D.; Bowser, M. T., *J. Am. Chem. Soc* **2004,** 126, (1), 20-21.
68. Osborne, S. E.; Ellington, A. D., *Chem. Rev* **1997,** 97, 349-370.
69. Silverman, S. K., *Functional Nucleic Acids for Sensing and Other Analytical Applications*. Springer: New York, 2009.
70. Mairal, T.; Ozalp, V. C., *Anal. Bioanal. Chem* **2008,** 390, 989-1007.
71. Sefah, K.; Shangguan, D.; Xiong, X.; O'Donoghue, M. B.; Tan, W., *Nature Protocol* **2010,** 5, 1169-1185.
72. Allen, P.; Wprland, S.; Gold, L., *Virology* **1995,** 209, (2), 327-336.
73. Song, S.; Wang, L.; Li, J.; Zhao, J.; Fan, C., *Trends in Analytical Chemistry* **2008,** 27, 108-117.
74. Li, D.; Song, S.; Fan, C., *Accounts of Chemical Research* **2009,** 43, (5), 631-641.
75. Potyrailo, R. A.; Conrad, R. C.; Ellington, A. D.; Hieftje, G. M., *Anal. Chem.* **1998,** 70, 3419-3425.
76. McCauley, T. G.; Hamaguchi, N.; Stanton, M., *Anal. Biochem.* **2003,** 319, 244-250.
77. Tyagi, S.; Kramer, F. R., *Nature Biotechnology* **1996,** 14, 303-308.
78. Yamamoto, R.; Kumar, P. K. R., *Genes to Cells* **2000,** 5, 389-396.
79. Hamaguchi, N.; Ellington, A. D.; Stanton, M., *Analytical Biochemistry* **2001,** 294, 126-131.
80. Nutiu, R.; Li, Y., *J. Am. Chem. Soc* **2003,** 125, 4771-4778.
81. Nutiu, R.; Li, Y., *Angew. Chem. Int. Ed* **2005,** 44, (7), 1061-1065.
82. Huizenga, D. E.; Szostak, J. W., *Biochemistry* **1995,** 34, 656-665.
83. Wang, Z.; Lee, J. H.; Lu, Y., *Chem. Commun.* **2008**, (45), 6005-6007.
84. Wu, D.; Zhang, Q.; Chu, X.; Wang, H.; She, G.; Yu, R., *Biosensors and Bioelectronics* **2010,** 25, (5), 1025-1031.
85. Liu, J.; Lu, Y., *Angew. Chem. Int. Ed* **2005,** 45, (1), 90-94.
86. Bock, L. C.; Griffin, L. C.; Latham, J. A.; Vermaas, E. H.; Toole, J. J., *Nature* **1992,** 355, 564-566.
87. Lau, P. S.; Coombes, B. K.; Li, Y., *Angew. Chem. Int. Ed* **2010,** 49, 7938-7942.
88. Lee, J. F.; Hesselberth, J. R.; Meyers, L. A.; Ellington, A. D., *Nucleic Acids Research* **2004,** 32, D95-D100.
89. Li, H.; Zhang, Q.; Cai, Y.; Kong, D.-M.; Shen, H.-X., *Biosensors and Bioelectronics* **2012,** 34, (1), 159-164.
90. Nelson, K. E.; Bruesehoff, P. J.; Lu, Y., *Journal of Molecular Evolution* **2005,** 61, (2), 216-225.
91. Kosman, J.; Juskowiak, B., *Analytica Chimica Acta* **2011,** 707, 7-17.
92. Tian, Y.; He, Y.; Mao, C., *ChemBioChem* **2006,** 7, 1862-1864.
93. Cheng, X.; Liu, X.; Bing, T.; Cao, Z.; Shangguan, D., *Biochemistry* **2009,** 48, (33), 7817-7823.

94. Stefan, L.; Xu, H.-J.; Gros, C. P.; Denat, F.; Monchaud, D., *Chemistry - A European Journal* **2011,** 17, (39), 10857-10862.
95. Saito, K.; Tai, H.; Hemmi, H.; Kobayashi, N.; Yanamoto, Y., *Inorg. Chem.* **2012,** 51, 8168-8176.
96. Li, T.; Dong, S.; Wang, E., *Anal. Chem.* **2009,** 81, (6), 2144-2149.
97. Zhou, X.-H.; Kong, D.-M.; Shen, H.-X., *Analytica Chimica Acta* **2010,** 678, (1), 124-127.
98. Golub, E.; Freeman, R.; Niazov, A.; Willner, I., *Analyst* **2011,** 136, (21), 4397-4401.
99. Li, T.; Wang, E.; Dong, S., *Chemical Communications* **2008**, (31), 3653-3656.
100. Li, T.; Shi, L.; Wang, E.; Dong, S., *Chemistry - A European Journal* **2009,** 15, (4), 1036-1042.
101. Liu, M.; Song, J.; Shuang, S.; Dong, C.; Brennan, J. D.; Li, Y., *ACS Nano* **2014,** 8, (6), 5564-5573.
102. Liu, M.; Zhang, W.; ZHang, Q.; Brennan, J. D.; Li, Y., *Angew. Chem. Int. Ed* **2015,** 54, (9637-9641).
103. Liu, M.; Zhang, Q.; Chang, D.; Gu, J.; Brennan, J. D.; Li, Y., *Angew. Chem. Int. Ed* **2017,** 56, (22), 6142-6146.
104. Ostatma, V.; Vasiocherova, H.; Homola, J.; Hianik, T., *Anal. Bioanal. Chem* **2008,** 391, (5), 1861-1869.
105. Lee, M.; Walt, D. R., *Analytical Biochemistry* **2000,** 282, (1), 142-146.
106. Templin, M. F.; Stoll, D.; Schrenk, M.; Traub, P. C.; Vohringer, C. F.; Joos, T. O., *Trends Biotechnol* **2002,** 20, (4), 160-166.
107. Zhu, H.; Klemic, J. F.; Chang, S.; Bertone, P.; Casamayor, A.; Klemic, K. G.; Smith, D.; Gerstein, M.; Reed, M. A.; Snyder, M., *Nat. Genet.* **2000,** 26, (3), 283-289.
108. Zhu, H.; Snyder, M., *Current Opinion in Chemical Biology* **2003,** 7, (1), 55-63.
109. Ramsay, G., *Nat. Biotechnol.* **1998,** 16, (1), 40-44.
110. Andrade, J. D.; Hlady, V.; Wei, A. P., *Pure and Applied Chemistry* **1992,** 64, (11), 1777-1781.
111. Balamurugan, S.; Obubuafo, A.; Soper, S. A.; Spivak, D. A., *Anal. Bioanal. Chem* **2008,** 390, (4), 1009-1021.
112. Maleki, A.; Kjoniksen, A.-L.; Nystrom, B., *J. Phys. Chem. B.* **2005,** 109, (25), 12329-12336.
113. O'Driscoll, K. F., *Methods Enzymol.* **1976,** 44, 169-183.
114. Scouten, W. H., *Methods Enzymol.* **1987,** 135, 30-65.
115. Weetall, H., H., *Applied Biochemistry and Biotechnology* **1993,** 41, (3), 157-188.
116. Di Giusto, D. A.; King, G. C., *Topics in Current Chemistry* **2006,** 261, 131-168.
117. Rupcich, N.; Nutiu, R.; Shen, Y.; Li, Y.; Brennan, J. D., *The Use of Functional Nucleic Acids in Solid-Phase Fluorimetric Assays*. Springer: New York, 2009.
118. Livshits, M. A.; Mirzabekov, A. D., *Biophys J.* **1996,** 71, (5), 2795-2801.
119. Bhatia, R. B.; Brinker, C. J., *Chem. Mater* **2000,** 12, (8), 2434-2441.
120. Brennan, J. D., *Acc. Chem. Res.* **2007,** 40, (9), 827-835.
121. Avnir, D.; Braun, S.; Lev, O.; Ottolenghi, M., *Chem. Mater* **1994,** 6, (10), 1605-1614.
122. Avnir, D.; Coradin, T.; Lev, O.; Livage, J., *Journal of Materials Chemistry* **2006,** 16, 1013-1030.

123. Braun, S.; Rappoport, S.; Zusman, R.; Avnir, D.; Ottolenghi, M., *Materials Letters* **1990,** 10, (1-2), 1-5.
124. Jin, W.; Brennan, J. D., *Analytica Chimica Acta* **2002,** 461, (1), 1-36.
125. Pierre, A. C., *Biocatalysis and Biotransformation* **2004,** 22, (3), 145-170.
126. Ellerby, L. M.; Nishida, C. R.; Nishida, F.; Yamanaka, S. A.; Dunn, B.; Valentine, J. S.; Zink, J. I., *Science* **1992,** 255, (5048), 1113-1115.
127. Brinker, C. J.; Scherer, G. W., *Sol-Gel Science*. Academic Press: New York, 1990.
128. Brinker, C. J., *J. Non-cryst. Solids* **1988,** 100, 31-50.
129. Ferrer, M. L.; Del Monte, F.; Levy, D., *Chemistry of Materials* **2002,** 14, (9), 3619-3621.
130. Brook, M. A.; Chen, Y.; Guo, K.; Zhang, Z.; Jin, W.; Deisingh, A.; Cruz-Aguado, J.; Brennan, J. D., *Journal of Sol-Gel Science and Technology* **2004,** 31, (1-3), 343-348.
131. Cruz-Aguado, J.; Chen, Y.; Zhang, Z.; Elowe, N. H.; Brook, M. A.; Brennan, J. D., *J. Am. Chem. Soc* **2004,** 126, (22), 6878-6879.
132. Gill, I., *Chem. Mater* **2001,** 13, (10), 3404-3421.
133. Besanger, T. R.; Brennan, J. D., *Journal of Sol-Gel Science and Technology* **2006,** 40, 209-225.
134. Rupcich, N.; Nutiu, R.; Li, Y.; Brennan, J. D., *Angew. Chem. Int. Ed* **2006,** 45, (20), 3295-3299.
135. Carrasquilla, C.; Li, Y.; Brennan, J. D., *Anal. Chem.* **2011,** 83, 957-965.
136. Carrasquilla, C.; Lau, P. S.; Li, Y.; Brennan, J. D., *J. Am. Chem. Soc* **2012,** 134, (26), 10998-11005.
137. Pelton, R., *Trac-Trends in Analytical Chemistry* **2009,** 28, (8), 925-942.
138. Hu, J.; Wang, S.; Wang, L.; Li, F.; Pingguan-Murphy, B.; Lu, T. J.; Xu, F., *Biosensors and Bioelectronics* **2014,** 54, 585-597.
139. Pollock, N. R.; Colby, D.; Rolland, J. P., *Clinical Gastroenterology and Hepatology* **2013,** 11, (5), 478-482.
140. Yetisen, A. K.; Akram, M. S.; Lowe, C. R., *Lab on a Chip* **2013,** 13, (12), 2210-2251.
141. Martinez, A. W.; Phillips, S. T.; Whitesides, G. M.; Carrilho, E., *Anal. Chem.* **2010,** 82, (1), 3-10.
142. Meredith, N. A.; Casey, Q.; Cate, D. M.; Reilly, T. H.; Volckens, J.; Henry, C. S., *Analyst* **2016,** 141, (6), 1874-1887.
143. Then, W. L.; Garnier, G., *Reviews in Analytical Chemistry* **2013,** 32, (4), 269-294.
144. Mahadeva, S. K.; Walus, K.; Stoeber, B., *ACS Applied Materials and Interfaces* **2015,** 7, (16), 8345-8362.
145. Yang, Y. Y.; Noviana, E.; Nguyen, M. P.; Gesis, B. J.; Dandy, D. S.; Henry, C. S., *Anal. Chem.* **2017,** 89, (1), 71-91.
146. Boehm, A.; Biesalski, M., *MRS bulletin* **2017,** 42, (5), 356-364.
147. Ballerini, D. R.; Li, X.; Shen, W., *Microfluidics and Nanofluidics* **2012,** 13, (5), 769-787.
148. Martinez, A. W.; Philips, S. T.; Butte, M. J.; Whitesides, G. M., *Angew. Chem. Int. Ed* **2007,** 46, (8), 1318-1320.
149. Abe, K.; Suzuki, K.; Citterio, D., *Anal. Chem.* **2008,** 80, (18), 6928-6934.
150. Abe, K.; Kotera, K.; Suzuki, K.; Citterio, D., *Anal. Bioanal. Chem* **2010,** 398, (2), 885-893.
151. Carrilho, E.; Martinez, A. W.; Whitesides, G. M., *Anal. Chem.* **2009,** 81, (16), 7091-7095.

152. Araujo, A. C.; song, Y.; Lundeberg, J.; Stahl, P., L.; Brumer, H., *Anal. Chem.* **2012,** 84, (3311-3317), 11676-11676.
153. Su, S.; Nutiu, R.; Filipe, C. D. M.; Li, Y.; Pelton, R., *Langmuir* **2007,** 23, (3), 1300-1302.
154. Yu, A.; Shang, J.; Cheng, F.; Paik, B. A.; Kaplan, J. M.; Andrade, R. B.; Ratner, D. M., *Langmuir* **2012,** 28, (30), 11265-11273.
155. Hui, C. Y.; Li, Y.; Brennan, J. D., *Chem. Mater* **2014,** 26, (5), 1896-1904.
156. Liu, M.; Zhao, H.; Chen, S.; Yu, H.; Quan, X., *ACS Nano* **2012,** 6, (4), 3142-3151.
157. Liu, M.; Hui, C. Y.; Zhang, Q.; Gu, J.; Kannan, B.; Jahanshahi-Anbuhi, S.; Filipe, C. D. M.; Brennan, J. D.; Li, Y., *Angew. Chem. Int. Ed* **2016,** 55, 2709-2713.
158. Ali, M. M.; Brown, C. L.; Jahanshahi-Anbuhi, S.; Kannan, B.; Li, Y.; Filipe, C. D. M.; Brennan, J. D., *Scientific Reports* **2017,** 7, 12335.
159. Zhao, W.; Ali, M. M.; Aguirre, S. D.; Brook, M. A.; Li, Y., *Anal. Chem.* **2008,** 80, (22), 8431-8437.
160. Zhao, W.; Brook, M. A.; Li, Y., *ChemBioChem* **2008,** 9, (15), 2363-2371.
161. Carrasquilla, C.; Kapteyn, E.; Li, Y.; Brennan, J. D., *Angew. Chem. Int. Ed* **2017,** 56, (36), 10686-10690.
162. Allen, M. J.; Tung, V. C.; Kaner, R. B., *Chemical Reviews* **2010,** 110, (1), 132-145.
163. Yoo, J. M.; Kang, J. H.; Hong, B. H., *Chemical Society Revews* **2015,** 44, (14), 4835-4852.
164. Huang, X.; Yin, Z.; Wu, S.; Qi, X.; He, Q.; Zhang, Q.; Yan, Q.; Boey, F.; Zhang, H., *Small* **2011,** 7, (14), 1876-1902.
165. Liu, B.; Sun, Z.; Zhang, X.; Liu, J., *Anal. Chem.* **2013,** 85, 7987-7993.
166. Zhang, H.; Jia, S.; Lv, M.; Shi, J.; Zuo, X.; Su, S.; Wang, L.; Huang, W.; Fan, C.; Huang, Q., *Anal. Chem.* **2014,** 86, 4047-4051.
167. Lee, J.; Yim, Y.; Kim, S.; Choi, M.-H.; Choi, B.-S.; Lee, Y.; Min, D.-H., *Carbon* **2016,** 97, 92-98.
168. Wu, M.; Kempaiah, R.; Huang, P.-J. j.; Maheshwari, V.; Liu, J., *Langmuir* **2011,** 27, 2731-2738.
169. Liu, M.; Zhang, W.; Chang, D.; Zhang, Q.; Brennan, J. D.; Li, Y., *Trends in Analytical Chemistry* **2015,** 74, 120-129.
170. Xie, L.; Ling, X.; Fang, Y.; Zhang, J.; Liu, Z., *J. Am. Chem. Soc* **2009,** 131, (29), 9890-9891.
171. Swathi, R. S.; Sebastian, K. L., *Journal of Chemical Physics* **2008,** 129, (5), 4703.
172. Li, F.; Huang, Y.; Yang, Q.; Zhong, Z.; Li, D.; Wang, L.; Song, S.; Fan, C., *Nanoscale* **2010,** 2, (1021-1026).
173. Lu, C.-H.; Li, J.; Liu, J.-J.; Yang, H.-H.; Chen, X.; Chen, G.-N., *Chem. Eur. J.* **2010,** 16, 4889-4894.
174. Lu, C. H.; Yang, H. H.; Zhu, C. L.; Chen, X.; Chen, G. N., *Angew. Chem. Int. Ed* **2009,** 48, (26), 4785-4787.
175. He, S.; Song, B.; Li, D.; Zhu, C.; Qi, W.; Wen, Y.; Wang, L.; Song, S.; Fang, H.; Fan, C., *Adv. Funct. Mater.* **2010,** 20, (453-459).
176. Mao, Y.; Chen, Y.; Li, S.; Lin, S.; Juiang, Y., *Sensors* **2015,** 15, (11), 28244-28256.
177. Yi, J. W.; Park, J.; Singh, N. J.; Lee, I. J.; Kim, K. S.; Kim, B. H., *Bioorganic and Medicinal Chemistry Letters* **2011,** 21, 704-706.
178. Dong, H.; Zhang, J.; Ju, H.; Lu, H.; Wang, S.; Jin, S.; Hao, K.; Du, H.; Zhang, X., *Anal. Chem.* **2012,** 84, 4587-4593.

179. Cao, L.; Cheng, L.; Zhang, Z.; Wang, Y.; Zhang, X.; Chen, H.; Liu, B.; Zhang, S.; LKong, J., *Lab on a Chip* **2012,** 12, 4864-4869.
180. Chang, H.; Tang, L.; Wang, Y.; Jiang, J.; Li, J., *Anal. Chem.* **2010,** 82, 2341-2346.
181. Wen, Y.; Xing, F.; He, S.; Song, S.; Wang, L.; Long, Y.; Li, D.; Fan, C., *Chem. Commun.* **2010,** 46, 2596-2598.
182. He, Y.; Wang, Z.-G.; Tang, H.-W.; Pang, D.-W., *Biosensors and Bioelectronics* **2011,** 29, 76-81.
183. Pei, H.; Li, J.; Lv, M.; Wang, J.; Gao, J.; Lu, J.; Li, Y.; Huang, Q.; Hu, J.; Fan, C., *J. Am. Chem. Soc* **2012,** 134, 13843-13849.
184. Lu, Z.; Zhang, L.; Deng, Y.; Li, S.; He, N., *Nanoscale* **2012,** 4, 5840-5842.
185. Morales-Naraez, E.; Merkoci, A., *Adv. Mater.* **2012,** 24, (25), 3298-3308.
186. Li, Z.; Zhu, W.; Zhang, J.; Jiang, J.; Shen, G.; Yu, R., *Analyst* **2013,** 138, 3616-3620.
187. Hu, K.; Liu, J.; Chen, J.; Huang, Y.; Zhao, S.; Tian, J.; Zhang, G., *Biosensors and Bioelectronics* **2013,** 42, 598-602.
188. Liu, H.; Li, L.; Wang, Q.; Duan, L.; Tang, B., *Anal. Chem.* **2014,** 86, (5487-5493).
189. Liu, D.; Daubendiek, S. L.; Zillman, M. A.; Ryan, K.; Kool, E. T., *J. Am. Chem. Soc* **1996,** 118, 1587-1594.
190. Fire, A.; Xu, S.-Q., *Proc. Natl. Acad. Sci. USA* **1995,** 92, 4641-4645.
191. Zhao, W.; Ali, M. M.; Brook, M. A.; Li, Y., *Angew. Chem. Int. Ed* **2008,** 47, (34), 6330-6337.
192. Rodriguez, I.; Lazaro, J. M.; Blanco, L.; Kamtekar, S.; Berman, A. J.; Wang, J. M.; Steitz, T. A.; Salas, M.; de Vega, M., *Proc. Natl. Acad. Sci. USA* **2005,** 102, (6407-6412).
193. Blanco, L.; Berman, A. J.; Lazaro, J. M.; Martin, G.; Garmendia, C.; Salas, M., *J. Biol. Chem.* **1989,** 264, 8935-8940.
194. Esteban, A.; Salas, M.; Bianco, L., *J. Biol. Chem.* **1993,** 268, (4), 2719-2726.
195. Cho, E. J.; Yang, L.; Levy, M.; Ellington, A. D., *J. Am. Chem. Soc* **2005,** 127, (7), 2022-2023.
196. Di Giusto, D. A.; Wlassoff, W. A.; Gooding, J. J.; Messerle, B. A.; King, G. C., *Nucleic Acids Research* **2005,** 33, (6), e64.
197. Lizardi, P. M.; Huang, X.; Zhu, Z.; Bray-Ward, P.; Thomas, D. C.; Ward, D. C., *Nature Genetics* **1998,** 19, (3), 225-232.
198. Yang, L.; Fung, C. W.; Cho, E. J.; Ellington, A. D., *Anal. Chem.* **2007,** 79, 3320-3329.
199. Cui, L.; Lin, X.; Lin, N.; Song, Y.; Zhu, Z.; Chen, X.; Yang, C. J., *Chem. Commun.* **2012,** 48, 194-196.
200. Wang, T.; Zhang, Z.; Li, Y.; Xie, G., *Sensors and Actuators B* **2015,** 221, 148-154.
201. Lin, X.; Chen, Q.; Liu, W.; Li, H.; Lin, J.-M., *Biosensors and Bioelectronics* **2014,** 56, 71-76.

CHAPTER 2.

FLUORESCENCE ANALYSIS OF THE PROPERTIES OF STRUCTURE-SWITCHING DNA APTAMERS ENTRAPPED IN SOL-GEL-DERIVED SILICA MATERIALS

Author's Preface:

The following chapter was published in the journal *Chemistry of Materials* under the citation:

Hui, CY, Li, Y and Brennan JD. Fluorescence Analysis of the Properties of Structure-Switching DNA Aptamers Entrapped in Sol-Gel-Derived Silica Materials. *Chem. Mater.* **2014** 26: 1896-1904.

I was responsible for all the experimental designs, performance of said experiments, data analysis and interpretation included in this chapter. I wrote the first draft of the manuscript and Dr. Brennan and Dr. Li provided editorial input to generate the final draft for final submission. This article has been printed with permission from ACS Publications ©.

2.1 ABSTRACT

The entrapment of structure-switching, fluorescence-signaling DNA aptamers into sol-gel derived materials has recently been reported as a promising platform for solid-phase aptamer-based biosensors. However, there has not yet been a detailed study of the properties of such functional nucleic acids within different sol-gel based materials. Herein, we utilize a range of fluorescence based assays, which were previously used to assess the properties of entrapped proteins, to evaluate the factors that affect the function of structure-switching DNA aptamers upon entrapment within polar and non-polar sol-gel derived materials, using both bipartite and tripartite constructs of fluorescein-labelled, ATP-binding structure-switching aptamers as model systems. Steady-state and time-resolved aptamer dynamics, thermal and long-term stability, accessibility of entrapped aptamers to quenchers, the degree of aptamer leaching, and the overall target-binding and signaling capabilities of these entrapped aptamers were assessed relative to solution. These studies demonstrate that the ability of the aptamer complex to remain fully hybridized to its complementary dabcyl-labelled quencher strand (***Q***-DNA) upon entrapment is the most important factor in terms of signalling capability. It was also observed that more polar (anionic) materials derived from sodium silicate were optimal for DNA aptamers, since these allowed the entrapped aptamer to remain hybridized to its complementary strands, and retained the dynamic motion needed to undergo structure-switching while providing a minimum degree of leaching. Furthermore, such materials improve the thermal melting temperature of the ***Q***-DNA strand, and improve the long-term stability of entrapped DNA aptamers.

2.2 INTRODUCTION

Sol-gel entrapment of biomolecules within sol-gel derived silica and composite materials has been widely utilized over the past two decades, with the vast majority of studies focusing on entrapment of proteins for the development of biosensors, separation media or bioreactors.[1-6] As a result of this activity, numerous reports have appeared that describe the properties of entrapped proteins as a function of the entrapping material, including conformational dynamics, accessibility, degree of leaching, reaction kinetics, and thermal and long-term stability.[7-37] Such studies proved to be critical in understanding how proteins were affected upon entrapment, and led to the development of a range of biofriendly materials and processing methods using glycerol producing silane precursors[38, 39] or species such as sodium silicate, which do not liberate alcohol.[40]

More recently, there have been several reports on the entrapment of functional nucleic acids (FNAs),[1, 41-44] including DNA and RNA aptamers and DNA enzymes, into a variety of sol-gel derived materials, with the primary goal of using these as recognition elements in analytical and diagnostic applications.[45, 46] The most widely used FNA species is structure-switching signaling DNA aptamers, which are comprised of an aptamer with a primer extension bearing either a covalently bound fluorophore (bipartite construct) or a fluorescently-labeled strand (***F***-DNA) hybridized to the primer (tripartite construct), and a hybridized quencher strand (***Q***-DNA) that spans the primer and part of the aptamer, placing the ***F*** and ***Q*** in close proximity and quenching fluorescence. This species undergoes a large conformational change upon binding of analyte, displacing the ***Q***-DNA and enhancing fluorescence. This species was studied in several materials, and

was observed to be most active in polar materials derived from sodium silicate, though reasons for this finding were not reported.[42]

There are several factors that can influence the signal capability of an entrapped aptamer: (1) the aptamer complex needs to remain fully hybridized upon entrapment; (2) the aptamer should not leach from the matrix; (3) the aptamer needs to be accessible to the added target added; (4) the aptamer needs to retain sufficient conformational flexibility to undergo structure-switching upon target addition; and, (5) the ***Q***-DNA strand needs to be able to move sufficiently far enough to generate an adequate fluorescence signal enhancement. A key point to note when entrapping FNA species is that they have substantial differences relative to proteins. FNAs are highly charged polyanions, they are generally much smaller than proteins, and they often require highly specific buffers and metal ion co-factors to function. Hence, the optimal environment to maintain activity may be quite different than that required for proteins. As a starting point to better understand the properties of entrapped FNAs, we have undertaken a fluorescence-based study of the properties of bipartite and tripartite DNA aptamers in materials derived from sodium silicate, tetramethylorthosilicate (TMOS), and mixtures of 20% or 40% methyltrimethoxysilane (MTMS) in TMOS. These materials allow us to probe the effects of alcohol generation and polarity on the properties of the entrapped aptamers after entrapment.

In this report, steady-state and time-resolved fluorescence studies were used to provide information on rotational dynamics, accessibility to quenchers, leaching, thermal stability and long-term stability of entrapped ATP-binding, structure-switching DNA

aptamers in the above materials and in solution. The sensitivity and signaling capabilities of the entrapped aptamers were also evaluated relative to solution, and correlated to the properties of the entrapped aptamers. The data from these studies provide an overall picture of the behavior of structure-switching DNA aptamers upon entrapment and provide clear insights into the role that different materials play in controlling the stability and activity of the entrapped aptamers.

2.3 EXPERIMENTAL SECTION

2.3.1 Chemicals

All DNA oligonucleotides were chemically synthesized by Integrated DNA Technologies (Coralville, IA) and purified by HPLC prior to use. Adenosine 5'-triphosphate (ATP) was purchased from Fermantas Life Sciences (Burlington, ON). Tetramethylorthosilicate (TMOS), methyltrimethoxysilane (MTMS) and Dowex 50 x 8-100 cation-exchange resin were obtained from Sigma (Oakville, ON, Canada). Sodium silicate solution (SS, technical grade, 9% Na_2O, 29% silica, 62% water) was purchased from Fisher Scientific (Pittsburgh, PA). Water was purified with a Milli-Q synthesis A10 water purification system. All other chemicals and solvents used were of analytical grade and were used without further purification.

2.3.2 Preparation of Bipartite and Tripartite ATP DNA Aptamers

Both bipartite and tripartite structure-switching aptamers utilized identical aptamer sequences but had different primer regions. The bipartite aptamer construct

contained a covalently bound fluorescein label (***F***) on the primer (bound to the terminal thymidine), and no ***F***-DNA binding regions, whereas the tripartite aptamer utilized a primer that was complementary to a fluorescently labeled DNA strand (***F***-DNA). Both constructs used an identical sequence to bind a complementary dabcyl-labeled DNA strand (***Q***-DNA), placing the ***Q*** directly adjacent to the ***F*** in both constructs.[47-49] The specific DNA sequences used in this work were as follows.

Tripartite aptamer: 5'-

CCTGCCACGCTCCGCT*CACTGACCT**GGG**GGA*GT**A**TTGC**G**

GAGGAAGGT-3'

F-DNA: 5'-F**GCGGAGCGTGGCAGG**-3'

Q-DNA: 5'-*CCCAGGTCAGTG*-dabcyl-3'

Bipartite aptamer: 5'-

TTTTTTTTT***F***T*CACTGACCT**GGG**GGA*GTATTGC**GGAGGA**AG

GT-3'

The bold nucleotides refer to the ***F***-DNA binding region and the italicized nucleotides designate the ***Q***-DNA binding region. The bold and underline nucleotides indicate the ATP binding site.[48,50]

2.3.3 Preparation of DNA Aptamer Complexes

To create a bipartite complex, the fluorescently labeled aptamer and the quencher strand (***Q***-DNA) were combined in a 1:3 molar ratio in 20 mM Tris buffer at pH 7.80 (containing 100 mM NaCl and 5 mM $MgCl_2$). In the tripartite scheme, ***F-***DNA, aptamer

and ***Q***-DNA were combined in a 1:2:3 molar ratio in an identical buffer system. These ratios have previously been shown to be optimal for signaling,[51] and ensure that there is a minimal amount of free ***F***-DNA, and that all aptamers have a bound ***Q***-DNA. For both constructs the solutions were incubated for at least 15 min to ensure annealing and quenching.

2.3.4 Entrapment of DNA Aptamers within Sol-Gel Derived Materials

Precursor sols were prepared using sodium silicate (SS), TMOS and MTMS. Sodium silicate sols were prepared by diluting 2.6 g of stock sodium silicate in 10 mL of ddH_2O and immediately mixing with 5.5 g of Dowex resin. The mixture was then stirred for 2 minutes and then vacuum filtered through a Buckner funnel. The filtrate was then filtered through a 0.2 μm membrane syringe filter to remove any particulates in the solution. The final pH of SS solution was ~4. The TMOS sols were prepared by mixing 700 μL of water, 50 μL of HCl (0.1 N) and 2.25 mL of TMOS and then sonicating the mixture in ice-cold water for 20 min as described elsewhere.[41] The TMOS/MTMS hybrids were prepared by proportionally diving the 2.25 mL of silane using volume percentages of 20 or 40% MTMS in TMOS, mixing with water and acid and co-hydrolyzing in a sonicator as above. In all cases, the buffered DNA sample solution was mixed in a 1:1 (v/v) ratio with a freshly prepared silica sol at room temperature. The aptamer-sol mixtures were deposited into 96-well microliter plates at a volume of 50 μL per well or into polymethacrylate (PMMA) fluorimeter cuvettes (1 cm pathlength) at a volume of 2 mL per cuvette and allowed to gel. All samples were aged at room

temperature for 3x of the gelation time of each sol. Microwells containing the various sol-gel derived materials were then incubated with 100 μL of 1x assay buffer (20 mM Tris·HCl with 100 mM NaCl and 5 mM $MgCl_2$ at pH 7.5) for at least 1 h at room temperature. Upon removal of the supernatant, the materials were again washed with 100 μL of 1x assay buffer two more times to remove any leachable aptamers. The supernatant was used to calculate the amount of aptamer that leached as described below.

2.3.5 Leaching of Aptamers

Leaching of entrapped aptamers in different sols was determined using a TECAN M1000 plate reader operated in bottom-read fluorescence mode at 25 °C in 96-well plates. The aptamers were prepared and entrapped in different precursor sols as described above and then incubated with 100 μL of 1x assay buffer for 1 h. The total fluorescence emission of the sample was first taken, using excitation at 490 nm and emission at 520 nm (5 nm bandpasses), followed by the removal of the supernatant and measurement of the fluorescence intensity of both the supernatant and silica gel. This procedure was repeated two more times with 5 min incubation times for each wash. The percentage of aptamers that had leached from the gels was determined by comparing the total fluorescence intensity of the silica monolith prior to any washing to that of washed materials, as well as the total fluorescence intensity of the three supernatant samples, as described elsewhere.[42, 44]

2.3.6 Target-Binding Measurements

All measurements were performed in 96-well microplates at 25 °C using a TECAN M1000 plate reader operated in bottom-read fluorescence mode using the settings described above. Initial baseline fluorescence was measured every 15 s for 15 min for samples that had 100 μL of assay buffer overlaying the monolithic materials. Following this, 2 μL of a concentrated ATP solution was added to obtain a final concentration of 2 mM in the well, and fluorescence emission was again measured every 15 s for a total of 80 min. The emission intensity of undoped materials and solutions without aptamers present were also collected, and the intensity values were subtracted from those of aptamer samples to correct for background emission. All fluorescence measurements are reported as fluorescence enhancement or F/F_0 where F is the end point fluorescence intensity and F_0 is the initial fluorescence intensity prior to target addition.

2.3.7 Steady-State and Time-Resolved Fluorescence Anisotropy

Steady-state fluorescence anisotropy measurements were obtained using a TECAN M1000 plate reader, with instrumental calibration using 1 nM of fluorescein in 0.1 M NaOH. Samples were excited at 490 nm and emission was collected at 520 nm using a 5 nm bandpasses for both excitation and emission. The instrumental G factor was measured to account for any polarization bias in the monochromators and used to correct the anisotropy values. The values reported represent the average of five measurements. Time-resolved fluorescence intensity and anisotropy decay data were obtained using an IBH 5000U time-correlated single-photon-counting (TCSPC) fluorimeter (Glasgow, UK),

as described elsewhere.[36, 52] Fluorescein labeled aptamer samples were excited at 495 nm with a Nano-LED source, at a rate of 750 kHz, and emission was detected at 532 nm using a 32 nm bandpass in both excitation and emission paths. A 500 nm short-pass interference filter (Andover Corporation) was used in excitation path and a 515 nm long-pass filter (Andover Corporation) was used in emission path to minimized scattering of excitation light into the detector. Intensity and anisotropy decays of 1 μM aptamer entrapped in various materials were collected into 2,048 channels over a range of 200 ns (97.66 ps per channel) until 10,000 counts were obtained in the peak channel, or undint the difference in peak intensity between parallel and perpendicularly polarized outputs reached 10,000 counts. The instrument response profile was determined using Rayleigh scattering of the excitation source from a Ludox solution to minimize convolution artifacts.

The anisotropy decays were analyzed using the IBH DAN analysis software package, which generated two decay curves, the sum, *S(t)* and the difference, *D(t)*

$$S(t) = I_{VV}(t) + 2GI_{VH}(t) \qquad [1]$$

$$D(t) = I_{VV}(t) - GI_{VH}(t) \qquad [2]$$

The anisotropy decay *r(t)* is defined as

$$r(t) = \frac{D(t)}{S(t)} = \frac{I_{VV}(t) - GI_{VH}(t)}{I_{VV}(t) - 2GI_{VH}(t)} \qquad [3]$$

where $I_{VV}(t)$ and $I_{VH}(t)$ are the time dependent intensity values obtained with vertically polarized excitation and vertically or horizontally polarized emission, respectively. All anisotropy values were corrected for the instrumental G-factor to account for polarization

bias in the monochromator and PMT. The anisotropy decays were then fit to a two-component hindered rotor model,

$$r(t) = f_1 r_0 \exp(-t / \phi_1) + f_2 r_0 \exp(-t / \phi_2) + g r_0 \qquad [4]$$

where ϕ_1, and ϕ_2 are the rapid and progressively slower rotational correlation times, respectively; f_1 (reflects the local motion of fluorophore) and f_2 (reflects global motion of DNA aptamer) are the fractional contributions of ϕ_1 and ϕ_2 to *r(t)*; *g* is the fraction of fluorescence due to probes that rotate more slowly than can be measured during the probe emission lifetime and r_0 is the limiting anisotropy. The residual anisotropy, r_∞, reflects the anisotropy at times which greatly exceed the lifetime of the fluorescent probe, and is determined by $r_\infty = g r_0$. The fits were considered acceptable when the reduced chi-squared (χ^2) values were close to 1.[36, 52]

2.3.8 Accessibility of Entrapped Aptamers

Iodide quenching studies were done for aptamers entrapped in various silanes (SS, TMOS and MTMS/TMOS hybrids) and in solution in the absence of ***Q***-DNA. All studies were performed in 96-well plates using a TECAN Evolution plate reader operating in bottom-read mode. For solution studies, each sample well in 96-microwell plates contained 50 µL of 200 nM of either the bipartite or tripartite aptamer and 50 µL of different concentrations of potassium iodide up to 6.0 M were then added to individual sample wells giving a final concentration of aptamer of 100 nM and varying concentrations of quencher up to 3.0 M. The plates were placed on a plate shaker and shaken at 500 rpm for 3 min, after which the fluorescence intensity of each well was

collected. For studies of entrapped aptamers, each sample well contained a 50 μL monolith sample which was incubated with 50 μL of varying concentrations of potassium iodide for 20 min or 60 min. The fluorescence intensity of each well was then collected. The data obtained from different quencher concentrations were combined to yield quenching curves. All quenching data were analyzed using the following equation[36, 42, 53]:

$$\frac{F_0}{\Delta F} = \frac{1}{f_a K_a [Q]} + \frac{1}{f_a} \qquad [5]$$

where F_0 is the fluorescence intensity in the absence of the quencher, ΔF is the difference in fluorescence intensity at a given molar concentration of quencher [Q] relative to F_0, f_a is the fraction of accessible fluorophore, and K_a is the Stern-Volmer quenching constant (M^{-1}) for the accessible fluorophore. A plot of $F_0/\Delta F$ versus 1/[Q] yields $1/f_a$ as the y intercept and $1/f_a K_a$ as the slope.

2.3.9 Thermal Stability Studies

Fluorescence emission was measured as a function of temperature to generate melting curves and determine melting temperatures (T_m) of both the bipartite and tripartite aptamers in solution and when entrapped in various materials as described previously[8, 36, 54] using a Cary Eclipse fluorimeter with a computer controlled temperature controller. All samples were prepared in cuvettes. The temperature was raised in ca. 2 °C increments starting at 20 °C and going to 80 °C, with equilibration at each temperature for 10 min prior to measurement of fluorescence intensity. Samples without aptamers present were also tested to perform background correction. Fluorescence intensity of the

F-DNA strand alone was also collected to correct for temperature dependent changes in quantum yield. As such, the changes in emission intensity reflect the dehybridization of the ***Q***-DNA strand (which is shorter than the ***F***-DNA strand and should dissociate first). The T_m was determined from the mid-point of a melting curve where the complex is 50% dissociated, and it is determined from the maximum in the first derivative of the melting profile as described elsewhere.[55]

2.3.10 Long Term Stability of Aptamers

Bipartite and tripartite aptamer samples in 96-well microliter plates were prepared and aged as described above. 100 µL of 1x assay buffer was then added to top of each gel and the microwell plates were covered with lids and wrapped with Parafilm™ to prevent evaporation upon storage. Plates were stored for 1 day, 1 week or 1 month at 4 °C prior to target-binding measurements. Solution sample containing either bipartite and tripartite aptamer complexes were also prepared in microcentrifuge tubes and stored for up to 1 month at 4 °C prior to target-binding measurements to allow comparison to entrapped samples. Samples did not contain nuclease inhibitors.

2.4 RESULTS AND DISCUSSION

2.4.1 Target-Binding Fluorescence Measurements

In order to compare the signaling capabilities of bipartite and tripartite constructs, the degree of signal enhancement upon target addition was assessed for both free and entrapped aptamers. In this study, all sol-gel derived materials were first washed to remove leachable aptamers (% leached is reported later), followed by addition of 2 mM ATP (note that the aptamer will also bind adenosine, cyclic AMP, AMP and ADP, but not CTP, GTP or UTP)[48, 51] Figure 2-1 shows the fluorescence signal enhancements and rates of signal development upon target binding for both bipartite and tripartite constructs of ATP-binding DNA aptamers in solution and when entrapped in the different sol-gel-derived materials. Consistent with the previous findings,[42] the tripartite complex, which has a smaller ***Q-F*** distance and thus higher quenching, shows a higher degree of signal enhancement than the bipartite complex.

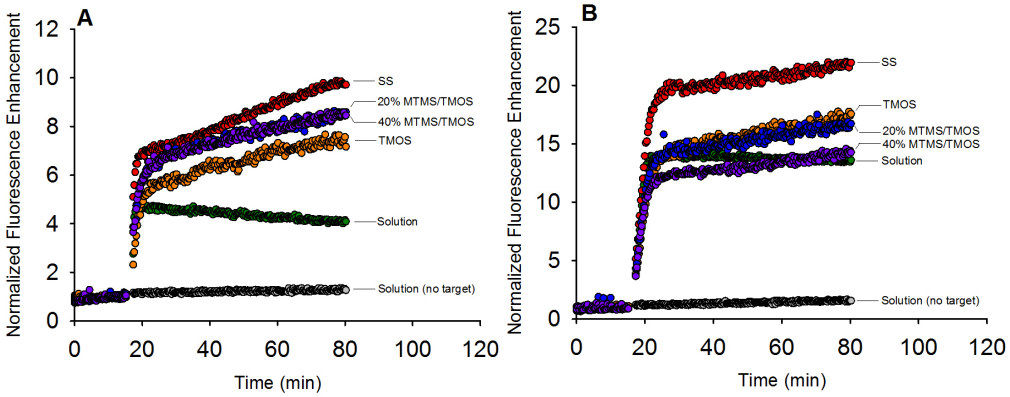

Figure 2-1. Fluorescence signaling ability of ATP-binding structure-switching DNA aptamers in solution and in various sol-gel-derived materials. (A) Bipartite construct. (B) Tripartite construct. The target-induced fluorescence signals were normalized to the fluorescence signals obtained from a baseline incubation of 15 min.

For both constructs the aptamer entrapped in the sodium silicate derived material produced a higher signal enhancement (~10 fold for bipartite construct and ~20 fold for tripartite constructs) than any of the alcohol-producing materials (~7 to 8.5 fold for bipartite construct and ~14 to 17 fold for tripartite construct). Interestingly, all materials produced signal enhancements at least as large as in solution, and the initial signaling rate was almost as high as in solution. Given that the samples had been washed to remove leachable aptamers, the rapid rise is not likely due to aptamer that had leached. A second feature is that all entrapped samples show a slower increase in signal after the initially rapid rise (particularly obvious for bipartite aptamers), which may be due to a subset of aptamers in a second, less accessible environment, or a slower secondary conformational change that alters the environment around the fluorophore. The inclusion of MTMS had a relatively minor effect on signaling; the more significant effect was related to whether the precursor generated alcohol.

2.4.2 Leaching of Aptamers from Sol-Gel Derived Materials

The extent of leaching of both bipartite and tripartite constructs entrapped in each material was investigated (Supplementary Information: Figure S2-1). Leaching of entrapped aptamers ranged from ~54% in the SS material to ~80% in composite materials containing up to 40% MTMS for both bipartite and tripartite aptamers. The degree of leaching did not depend on the nature of the aptamer, suggesting that leaching of dehybridized ***F***-DNA from tripartite aptamers was not a significant factor. The trend of increased leaching with increasing hydrophobicity and pore size is consistent with

previous findings.[44] However, the previous studies[42, 44] showed a lower degree of leaching in all materials, as the materials had been aged for a longer period of time, producing pore shrinkage and thus retaining more aptamer within the pores. Also, previous studies used shorter incubation times for washing steps and did not utilize shaking to promote leaching. Hence, the leaching test reported here is more rigorous and better represents the maximum leaching that is likely to occur. This data suggests that SS materials have the smallest pores and are best suited to entrapping the maximum amount of aptamer.

2.4.3 Dynamics of Entrapped DNA Aptamers

Figures S2-2 and S2-3 and Tables S2-1 and S2-2 (Appendix - Supporting Information) show detailed steady-state and time-resolved anisotropy data for both bipartite and tripartite ATP-binding aptamer constructs in solution and when entrapped. Focusing first on the steady-state anisotropy data, it was observed that entrapment of either aptamer caused an increase in anisotropy, and hence a decrease in rotational mobility in the region of the reporter probe, when compared to solution values. The decrease in mobility has been widely observed for other biomolecules, and is consistent with the higher viscosity of entrapped solvents relative to solution.[36] In general the tripartite aptamers have higher anisotropy values that the bipartite aptamers, as these have the additional ***F***-DNA strand that both increases overall size and rigidifies segmental motion in the region of the fluorescein probe. It is important to note that all tripartite

constructs show higher anisotropy than in solution, indicating that the ***F***-DNA species remains hybridized after entrapment in all materials.

The steady-state anisotropy values are highest for TMOS-derived materials for both constructs, followed by the composite materials of MTMS/TMOS, and finally sodium silicate-derived materials. Previous studies[44] have shown that TMOS-derived materials generally have the smallest mesopores among all the materials studied here, which reveals the mobility of entrapped DNA aptamer is highly restricted within a dense cross-linked material (we note that all anisotropy measurements were done after 3 solvent exchanges, so the effects of residual methanol on solvent viscosity should be negligible). The higher mobility of aptamers entrapped in the composite materials is likely due to the more open pore structure of these matrices, which increases with an increase in the concentration of MTMS.[44, 56-58] Furthermore, such materials will have fewer hydroxyl groups on the silica surface and thus may reduce the degree of hydrogen bonding between the DNA aptamer and the pore surface.[56, 57, 59, 60]

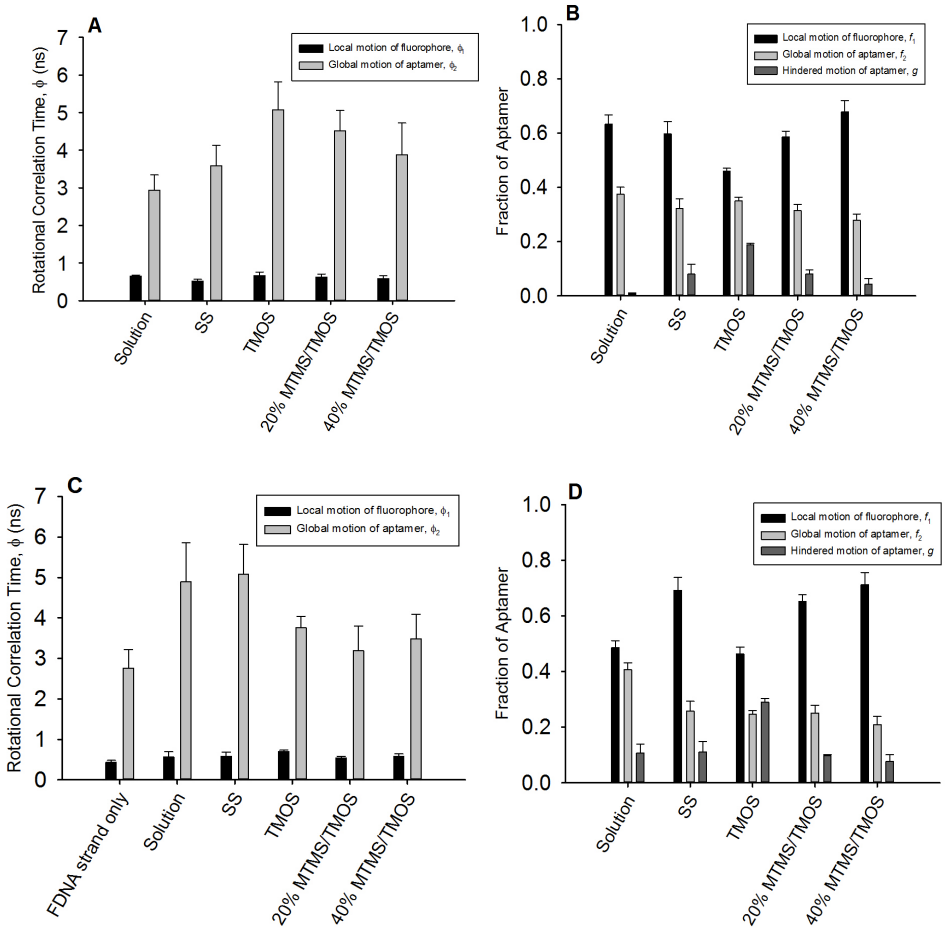

Figure 2-2. (A) Rotational correlation times of the bipartite aptamer and (B) the fractions of which correspond to local, global and hindered motions when free in solution and entrapped in various silica materials. (C) Rotational correlation times of the tripartite aptamer and (D) the fractions of which correspond to local, global and hindered motions when free in solution and entrapped in various silica materials. All samples were excited at 490 nm and emission was collected at 532 nm using a 32 nm bandpasses in both excitation and emission paths. All samples were tested in triplicate. Only the aptamer strand was used in case of bipartite construct, and the ***F***-DNA/aptamer complex was used in the case of the tripartite construct.

To gain further insight into the factors that influence the mobility of DNA aptamers, time-resolved anisotropy decay was examined. Figures S2-1 and S2-2 show the decay traces for the two constructs in solution and each of the four materials. Figure 2-2 shows the rotational correlation times (Φ_1, Φ_2) and fractional contributions from the local

(f_1), global (f_2) and hindered (g) motions of both the bipartite and tripartite constructs in solution and when entrapped in various sol-gel-derived materials (see also Tables S2-1 and S2-2). Focusing first on the bipartite aptamer, there are several key features that merit attention. First, the global rotational correlational time of the entrapped aptamers always increased upon entrapment, regardless of material, but is highest (i.e., slowest motion) in TMOS derived materials, in agreement with the highest steady-state anisotropy in this material. Secondly, the residual anisotropy and associated "g" term (fractional contribution from hindered motion) increase significantly upon entrapment, though in this case the extent of the increase depends on the material, being highest in TMOS derived materials and lowest in materials containing 40% MTMS. Thirdly, the faster rotational correlation time corresponding to local motion is not affected upon entrapment, showing that entrapment does not tend to cause direct alterations of the probe mobility (i.e., the probe does not interact directly with silica). Taken together, the data show that segmental motion in the region of the fluorophore is reduced, and that some of the aptamer is located in regions of very low mobility. Generally, aptamers within sodium silicate materials had dynamics that were closest to those in solution, while aptamers in TMOS derived materials had significantly less mobility, again consistent with the smaller mesopores in such materials.[44]

In the case of the tripartite construct of aptamer, the changes in mobility were somewhat different than those observed for the bipartite aptamer. In this case, the entrapped aptamers appeared to show more rapid global motion when entrapped in alcohol-producing materials, and often showed an increase in the fraction of local

dynamic motion (f_1), suggesting that a fraction of ***F***-DNA may have dehybridized. However, entrapment also led to a substantial increase in the fraction of non-mobile probe (increase in *g* value), which provides the rationale for the overall increase in the steady-state anisotropy values even though the global rotational correlation time was often smaller for the entrapped tripartite aptamer. Importantly, the fact that there was a large increase in fluorescence intensity upon introduction of ATP for all entrapped aptamers (Figure 1) indicated that the fraction of ***F***-DNA that may have dehybridized was small, but could be a factor in the observed reduction in fold-enhancement for alcohol-producing materials relative to SS.

A key conclusion from the anisotropy data is that the entrapped aptamers retain substantial mobility, which is important for these species to have structure-switching capability. The hindered motion indicates that there is a subset of aptamers that have an inability to undergo local or global motion during the lifetime of the probe ($\phi > 15\ \tau$, or ~60 ns), though this does not cause a major decrease in aptamer signaling ability. From a materials perspective, the dynamics were the least solution-like in TMOS derived materials, became more solution-like when MTMS was added to the material, and were relatively similar to solution in SS materials. Hence, alcohol-based processing methods are least compatible with retaining the function of structure-switching aptamers, even though relatively hydrophobic materials containing up to 40% MTMS did provide an environment that was conducive to retention of aptamer dynamics and function, which is not the case for most proteins.

2.4.4 Accessibility of Entrapped Aptamers

As noted above, signalling requires that the analyte reach the entrapped aptamer to bind and cause structure switching. Aptamers within interior pores that have no connection to the surface of the material cannot bind analyte. Furthermore, given that ATP is a trianion, it may also be electrostatically repelled from the anionic silica matrix and not reach the aptamer. To evaluate accessibility, we examined the ability of the anionic species iodide to access and thus quench the emission intensity of the fluorescein bound to the entrapped aptamer. Figure S2-4 shows Stern-Volmer plots and Figure 2-3 shows the fraction of accessible aptamers for both free and entrapped aptamers. In general, the fractional accessibility increased with time, and with the amount of MTMS present in the material. This suggests that inclusion of hydrophobic silane precursors helps to reduce the negative charge on the matrix,[56, 57, 59, 60] making the entrapped aptamer more accessible to the anionic iodide quencher by reducing electrostatic repulsion.

A second point to note is that the quenching constants (k_q) and accessibility constants (K_a) tended to increase with time (as did the accessible fraction), demonstrating that diffusion through the matrix is slow, and providing evidence that there is likely a subset of aptamers in environments that are poorly accessible, but not completely inaccessible, to analytes. This may explain the two-stage response shown in Figure 1, where the fast initial response reflects fully accessible aptamers and the slower secondary response reflects partially accessible aptamers.

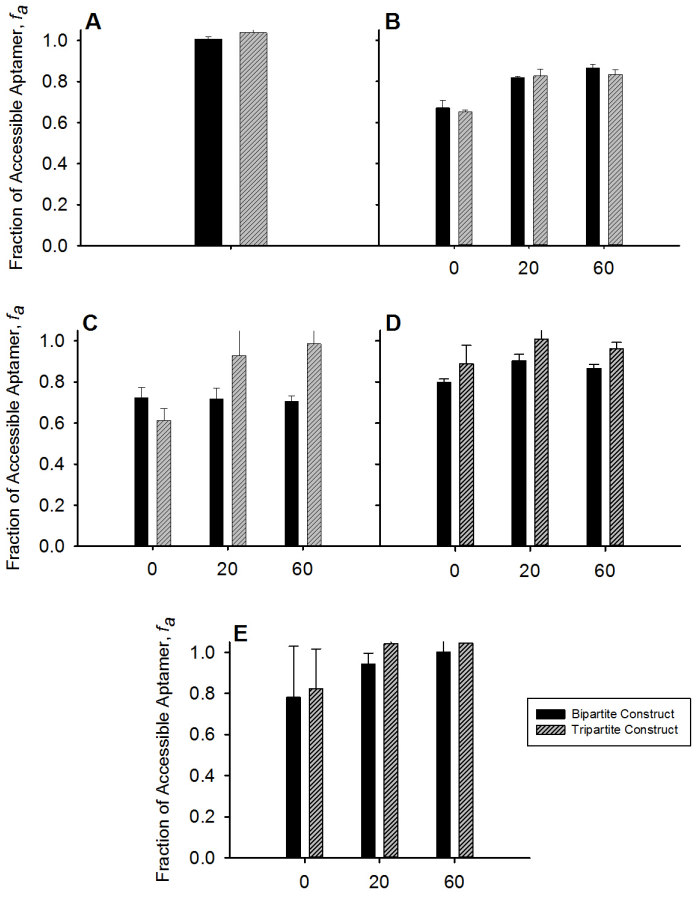

Figure 2-3. Fractional accessibility of the entrapped bipartite and tripartite constructs of ATP-binding DNA aptamers (A) free in solution and entrapped in: (B) SS (C) TMOS (D) 20% MTMS/TMOS (E) 40% MTMS/TMOS.

2.4.5 Thermal Stability

In order to determine how stable the entrapped aptamers were upon entrapment in the materials, the melting temperatures (T_m) of both constructs of aptamers were determined in solution and in each material. Figure 2-4 shows the changes in the relative fluorescence intensity of solution-based and entrapped DNA aptamers as a function of temperature. In this study, the ***Q***-DNA strand, being the shorter of the two hybridized strands, is expected to dehybridize first when the temperature increased, resulting in an

increase in fluorescence intensity, followed by dehybridization of ***F***-DNA when studying the tripartite construct. It was observed that the T_m of aptamer complex in SS was slightly higher than that in solution for the bipartite construct, while the tripartite DNA complex entrapped in SS showed a larger increase in T_m compared to that in free solution. In both complexes, aptamers entrapped in alcohol-producing materials demonstrated a lower T_m than those in free solution or entrapped in SS. The specific reason for this finding is unclear, as most of the methanol produced during the sol-gel process should have been removed during washing. Previous studies have shown that the T_m of DNA decreases as the concentration of methanol increases, owing to destabilization of the DNA double-helix, which in our case should facilitate dehybridization of ***Q***-DNA (see Figure S2-5).[61] This may indicate that three wash cycles were insufficient to remove all of the alcohol, or may relate to destabilization of the ***Q***-DNA hybridization in more hydrophobic materials containing MTMS. The first derivative of the melting profile for tripartite aptamers entrapped in alcohol-producing materials showed two maxima, which corresponded to the dehybridization of the shorter ***Q***-DNA complementary strand (1^{st} T_m) and then the longer ***F***-DNA complementary strand (2^{nd} T_m). Overall, the results indicated that the SS-derived material allowed the entrapped aptamer to be more stable than in other sol-gel-derived materials. On the other hand, it is possible that the lower T_m for the aptamers in hydrophobic or alcohol producing materials may actually be beneficial, as the Q-DNA will more easily dehybridize upon target binding, making it easier to produce signal enhancements. Clearly, a balance exists where a low T_m value can aid in sensitivity, but

could also produce poorer signaling if a substantial amount of ***Q***-DNA is dissociated in the absence of target.

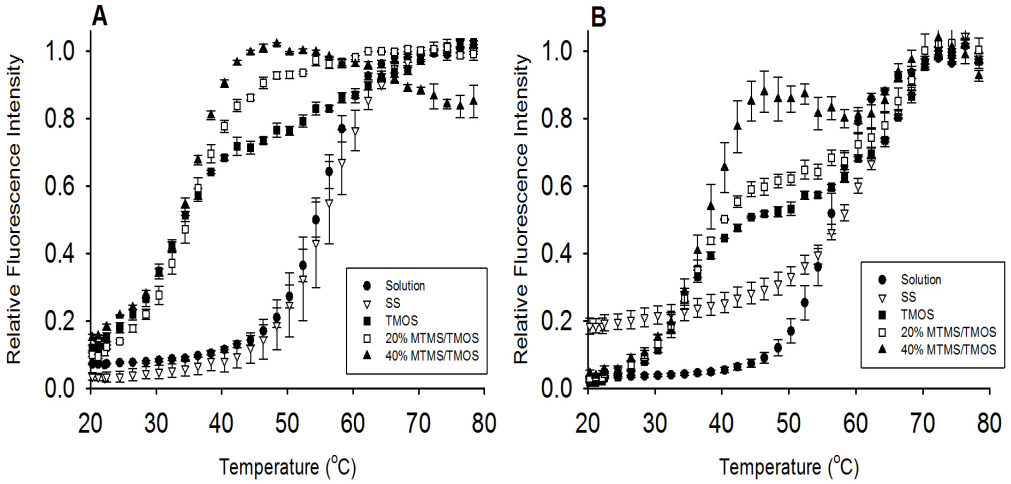

Figure 2-4. Fluorescence signal enhancement caused by dehybridization of quencher strand as a function of temperature. The quencher strand is considered to be dehybridized at a temperature corresponding to 50% of the maximum enhancement. (A) Bipartite construct: Solution: 56.3 ± 0.3 °C; SS: 57.6 ± 1.3 °C; TMOS: 34.9 ± 0.7 °C; 20% MTMS/TMOS: 36.2 ± 1.5 °C; and 40% MTMS/TMOS: 36.2 ± 1.8 °C. (B) Tripartite construct: Solution: 56.8 ± 0.8 °C; SS: 64.7 ± 1.8 °C; TMOS: 35 ± 0.5 °C and 70.1 ± 0.4 °C; 20% MTMS/TMOS: 37.5 ± 1.9 °C and 70.1 ± 1.9 °C; and 40% MTMS/TMOS: 38.2 ± 0.5 °C and 69.4 ± 3.0 °C. All samples were tested in triplicate.

2.4.6 Long-Term Stability

Figure 2-5 shows that the aptamers entrapped in hydrophobic or alcohol-producing materials demonstrate a decrease in fluorescence signal enhancement, ranging from 7 or 8-fold for the bipartite construct and 11 to 15-fold for tripartite construct when fresh, to 3 to 5-fold for the bipartite construct and 5 to 9-fold for the tripartite construct upon 1 month of storage. The observed loss of activity is due to the release of the quencher strand as the DNA degraded, which is evident based on the overall increase in F_0. On the other hand, aptamers entrapped in SS-derived materials showed no degradation in fluorescence enhancement within error even after 1 month of storage,

indicating that aptamers entrapped in SS were able to maintain an acceptable signaling ability over an extended storage time.

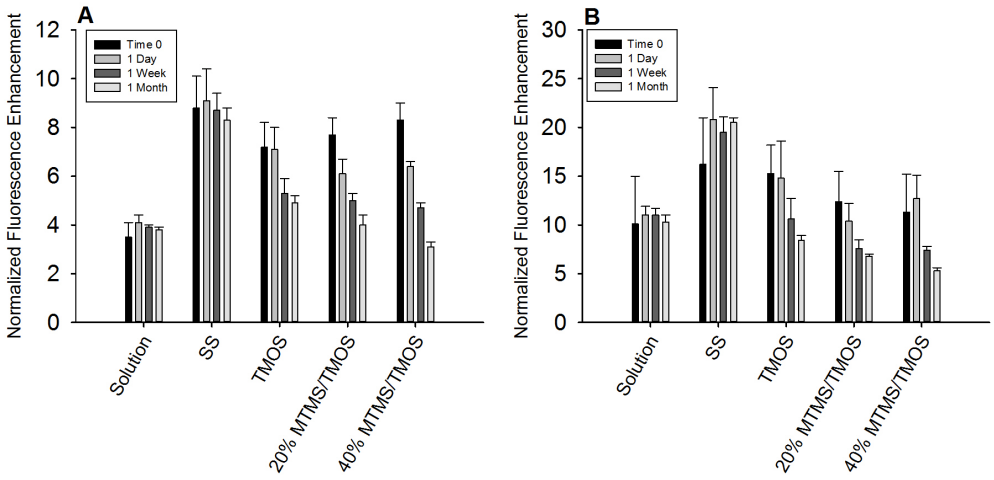

Figure 2-5. Structure-switching and signaling ability of (A) the bipartite construct and (B) the tripartite construct of ATP-binding DNA aptamer as a function of storage time. The data was obtained by adding 2 mM ATP to the entrapped aptamer after increasing storage time at 4 °C up to 1 month.

2.4.7 Performance of Aptamers in Optimal Material

The studies above identified sodium silicate based materials as being optimal for entrapment of structure-switching DNA aptamers for ATP detection. To further evaluate the performance of the aptamers in the SS materials, concentration-response curves were generated for both the bipartite and tripartite aptamers in solution and when entrapped. Figure 6 shows the fluorescence response of aptamers to addition of varying levels of ATP in free solution and when entrapped in sodium silicate. Interestingly, both aptamer constructs demonstrated higher sensitivity (i.e., almost double the initial slope) and approximately a 4-fold better detection limit when entrapped in SS derived materials. Detection limits (3 S/N) were 69 μM for the bipartite and 28 μM for the tripartite aptamer

when entrapped, as compared to 288 μM for the bipartite and 106 μM for the tripartite aptamer in solution. Previous reports[51] have shown that the tripartite reporter was able to detect ATP at concentrations as low as 10 μM, showing that entrapment leads to a poorer detection limit. This is most likely due to mass transfer limitations when using low concentrations of ATP, which would restrict the access of the ATP to the interior of the silica material. These data demonstrate that the entrapped aptamer has substantially better performance than the free aptamer, and show that sol-gel entrapment could be a very useful platform for development of highly sensitive solid-phase biosensors.

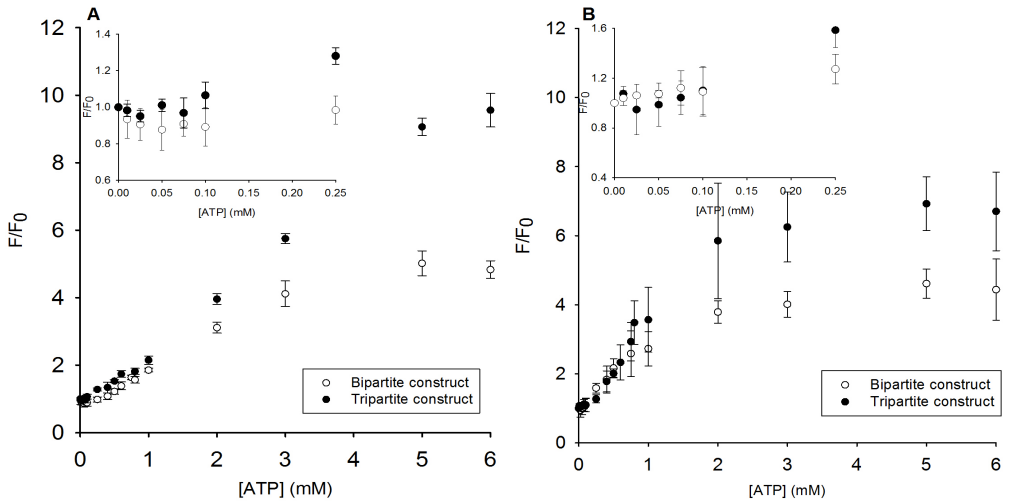

Figure 2-6. Concentration-response curves of ATP-binding DNA aptamers and detection limits in (A) free solution – bipartite construct: 288 μM, tripartite construct: 106 μM and (B) entrapped in SS-derived material - bipartite construct: 69 μM, tripartite construct: 28 μM at 25 °C with different concentrations of ATP. The data were normalized as F/F_0 ratios, where F is the fluorescence intensity upon addition of different concentrations of ATP and F_0 is the initial reading for the aptamer reporter in the absence of ATP. All samples were tested in triplicate.

2.4.8 A Model for the Behaviour of Entrapped Aptamers

Based on the data outlined above, a model can be developed for the effects of materials on entrapped structure-switching DNA aptamers, as summarized in Table 2-1. The alcohol-producing and highly cross-linked[44] TMOS-based material was the least suitable for aptamer entrapment. This material caused a dramatic loss in dynamic motion of entrapped aptamers, including a substantial increase in the fraction of aptamers showing hindered motion. The decreased mobility likely affected the ability of aptamers to structure-switch, decreasing the overall signal enhancement. The TMOS derived materials also showed the lowest fraction of accessible aptamers, the lowest thermal stability, and evidence for dehybridization of both ***Q***-DNA and ***F***-DNA after entrapment. This material also showed poor long-term stability, and is clearly not suited for entrapment of aptamers.

More hydrophobic alcohol producing materials containing MTMS have a smaller number of hydroxyl groups on their surface, are less anionic and tend to have larger pores.[44] These materials show increased mobility of entrapped aptamers relative to TMOS based materials, presumably owing to fewer biomolecule-surface interactions. Hence, the fraction of aptamers that were able to undergo structure-switching increased, leading to a higher signal enhancement. However, the larger pores in these materials lead to a higher degree of leaching, making such materials less suited for entrapment of DNA aptamers. Aptamers entrapped in composite materials also had substantially lower thermal and long-term stability relative to solution, reducing the efficacy of the material as a platform for solid-phase assays.

Aptamers entrapped in SS-derived materials produced the highest signal enhancement, had the lowest leaching, highest fractional accessibility and best thermal and long-term stability. The dynamics data suggested that bipartite aptamers were somewhat less mobile, but had less hindered motion than aptamers in TMOS derived materials. The retention of substantial mobility, along with the increased thermal stability, made this system the most robust for producing analyte-induced structure switching and signalling.

Overall, it appears that the ability of aptamers to remain fully hybridized to their complementary strands is a key issue in maintaining good performance, and that retention of dynamics is a secondary issue. Leaching does not play a major role in the initial signaling performance, as signal changes are relative (based on F/F_0). However, leaching may well play a significant role in determining long-term stability, as the aptamers may leach slowly during storage and ultimately become degraded. The potential for dehybridization of the complementary ***F***-DNA strand, particularly in alcohol-producing materials, suggests that bipartite constructs are better suited for entrapment, even though these show slightly lower overall signal enhancements. A potentially problematic issue with entrapped aptamers is the time-dependent changes in accessibility, which are likely responsible for the observed two-stage response to analyte addition (fast initial response and slower secondary response). Further optimization of sol-gel derived materials will likely be needed to overcome this issue.

Table 2-1. Factors that affect aptamer performance upon entrapment in various sol-gel derived silica materials.

	Parameters						
Materials	Pore Size	Mobility	Accessibility	Leaching	Thermal Stability	Remain hybridized?	Long term stability
TMOS	Medium	Poor	Poor	High	Poor	No	Poor
SS	Small	Good	Good	Low	Good	Yes	Excellent
MTMS/TMOS hybrids	Large	Good	Good	High	Poor	No	Poor

2.5 CONCLUSIONS

The current study shows that aptamer performance and properties can be significantly altered upon entrapment, and show that the structure-switching DNA aptamers examined herein performed best in sodium silicate materials. Based on the parameters studied, the most important factor determining the overall performance and stability of entrapped aptamers was the ability of the aptamer to remain fully hybridized to both the ***F***-DNA (tripartite) and ***Q***-DNA strands (both aptamers) upon entrapment. When entrapped in the sodium silicate derived material, both the bipartite and tripartite aptamers were able to remain fully hybridized. However, use of alcohol-producing precursors led to a much lower melting temperature for entrapped aptamers, leading to partial dehybridization, which presumably caused leaching of the small ***Q***-DNA strand, a higher background signal, and a lower overall signal enhancement. Sodium silicate based materials were also able to retain aptamers in a state where they could undergo dynamic motions that were similar to those in solution, which is a critical feature for retention of structure-switching ability, and also showed a lower degree of leaching that other materials. Thermal stability studies clearly demonstrated that entrapment of aptamers in sodium

silicate materials did not produce a loss in stability, but equally importantly did not significantly increase melting temperatures, which would have increased dehybridization of ***Q***-DNA and produced poorer signaling. Finally, the sodium silicate-derived material also provided the best long-term stability for the entrapped aptamers, and produced significant enhancements in stability relative to solution. Taken together, the data show that sol-gel entrapment into sol-gel derived materials is a viable platform for development of solid-phase assays, and that avoidance of alcohol during the production of materials is a key criteria for successfully entrapping DNA aptamers. Future studies will examine other functional nucleic acids including RNA aptamers and DNA enzymes, both of which have been reported to tolerate alcohol during entrapment, to determine how these FNA differ from structure-switching DNA aptamers.

2.6 ACKNOWLEDGMENTS

We thank the Natural Sciences and Engineering Research Council of Canada (NSERC), the SENTINEL Bioactive Paper Network, and Pro-Lab Developments for funding this work. We also thank the Canada Foundation for Innovation and the Ministry of Research and Innovation Ontario) for support of this work. Y.L. holds the Canada Research Chair in Directed Evolution of Nucleic Acids. J.D.B. holds the Canada Research Chair in Bioanalytical Chemistry and Biointerfaces.

2.7 REFERENCES

1. Gill, I., *Chem. Mater.* **2001,** 13, 3404-3421.
2. Jin, W.; Brennan, J. D., *Anal. Chim. Acta.* **2002,** 461, 1-36.
3. Avnir, D.; Coradin, T.; Lev, O.; Livage, J., *J. Mater. Chem.* **2006,** 16, (11), 1013.
4. Pierre, A. C., *Biocatal. Biotransfor.* **2004,** 22, (3), 145-170.
5. Coradin, T.; Boissiere, M.; Livage, J., *Curr. Med. Chem.* **2006,** 13, 99-108.
6. Besanger, T. R.; Brennan, J. D., *J. Sol-Gel Sci. Tech.* **2006,** 40, (2-3), 209-225.
7. Zheng, L.; Reid, W. R.; Brennan, J. D., *Anal. Chem.* **1997,** 69, 3940-3949.
8. Zheng, L.; Brennan, J. D., *Analyst* **1998,** 123, 1735-1744.
9. Edmiston, P. L.; Wambolt, C. L.; Smith, M. K.; Saavedra, S. S., *J. Colloid Interf. Sci.* **1994,** 163, 395-406.
10. Jordan, J. D.; Dunbar, R. A.; Bright, F. V., *Anal. Chem.* **1995,** 67, (14), 2436-2443.
11. Gottfried, D. S.; Kagan, A.; Hoffman, B. M.; M, F. J., *J. Phys. Chem. B* **1999,** 103, 2803-2807.
12. Doody, M. A.; Baker, G. A.; Pandey, S.; Bright, F. V., *Chem. Mater.* **2000,** 12, 1142-1147.
13. Wambolt, C. L.; Saavedra, S. S., *J. Sol-Gel Sci. Tech.* **1996,** 7, 53-57.
14. Shen, C.; Kostic, N. M., *Journal of American Chemical Society* **1997,** 119, 1304-1312.
15. Braun, S.; Shtelzer, S.; Rappoport, S.; Avnir, D.; Ottolenghi, M., *J. Non-Cryst. Solids* **1992,** 147-148, 739-743.
16. Avnir, D.; Braun, S.; Lev, O.; Ottolenghi, M., *Chem. Mater.* **1994,** 6, 1605-1614.
17. Wang, R.; Narang, U.; Prasad, P. N.; Bright, F. V., *Anal. Chem.* **1993,** 65, 2671-2675.
18. Ellerby, L. M.; Nishida, C. R.; Nishida, F.; Yamanake, S. A.; Dunn, B.; Valentine, J. S.; Zink, J. I., *Science* **1992,** 255, (5038), 1113-1115.
19. Wu, S.; Ellerby, L. M.; Cohan, J. S.; Dunn, B.; El-Sayed, M. A.; Valentine, J. S.; Zink, J. I., *Chem. Mater.* **1993,** 5, 115-120.
20. Dave, B. C.; Soyez, H.; Miller, J. M.; Dunn, B.; Valentine, J. S.; Zink, J. I., *Chem. Mater.* **1998,** 7, 1431-1434.
21. Yamanake, S. A.; Nishida, F.; Ellerby, L. M.; Nishida, C. R.; Dunn, B.; Valentine, J. S.; Zink, J. I., *Chem. Mater.* **1992,** 4, 497-500.
22. Dave, B. C.; Dunn, B.; Valentine, J. S.; Zink, J. I., *Anal. Chem.* **1994,** 66, (22), 1120-1127.
23. Blyth, D. J.; Aylott, J. W.; Richardson, D. J.; Russell, D. A., *Analyst* **1995,** 120, 27725-27730.
24. Aylott, J. W.; Richardson, D. J.; Russell, D. A., *Analyst* **1997,** 122, 77-80.
25. Williams, A. K.; Hupp, J. T., *J. Am. Chem. Soc.* **1998,** 120, 4366-4371.
26. Braun, S.; Rappoport, S.; Zusman, R.; Avnir, D.; Ottolenghi, M., *Mater. Lett.* **1990,** 10, (1- 2), 1-5.
27. Reetz, M. T.; Zonta, A.; Simpelkamp, J.; Werner, K., *Chem. Commun.* **1996**, 1397-1398.

28. Narang, U.; Prasad, P. N.; Bright, F. V., *Chem. Mater.* **1994,** 6, 1596-1598.
29. Narang, U.; Prasad, P. N.; Bright, F. V., *Anal. Chem.* **1994,** 66, 3139-3144.
30. Barbadillo, M.; Casero, E.; Petit-Domínguez, M. D.; Pariente, F.; Lorenzo, E.; Vázquez, L., *J. Sol-Gel Sci. Tech.* **2011,** 58, (2), 452-462.
31. Ju, H.; Zhang, X.; Wang, J., **2011**, 305-332.
32. Esquembre, R.; Poveda, J. A.; Mateo, C. R., *J. Phys. Chem. B* **2009,** 113, 7534-7540.
33. Pastor, I.; Prieto, M.; Mateo, C. R., *J. Phys. Chem. B* **2008,** 112, 15021-15028.
34. Pastor, I.; Ferrer, M. L.; Lillo, M. P.; Gomez, J.; Mateo, C. R., *J. Phys. Chem. B* **2007,** 111, 11603-11610.
35. Gadre, S. Y.; Gouma, P. I., *J. Am. Ceram. Soc.* **2006,** 89, (10), 2987-3002.
36. Siu, X.; Cruz-Aguado, J. A.; Chen, Y.; Zhang, Z.; Brook, M. A.; Brennan, J. D., *Chem. Mater.* **2005,** 17, 1174-1182.
37. Goring, G. L. G.; Brennan, J. D., *J. Mater. Chem.* **2002,** 12, (12), 3400-3406.
38. Gill, I.; Ballesteros, A., *J. Am. Chem. Soc.* **1998,** 120, 8587-8598.
39. Brook, M. A.; Chen, Y.; Guo, K.; Zhang, Z.; Jin, W.; Deisingh, A.; Cruz-Aguado, J.; Brennan, J. D., *J. Sol-Gel Sci. Tech.* **2004,** 31, 343-348.
40. Bhatia, R. B.; Brinker, C. J., *Chem. Mater.* **2000,** 12, 2434-2441.
41. Shen, Y.; Mackey, G.; Rupcich, N.; Gloster, D.; Chiuman, W.; Li, Y.; Brennan, J. D., *Anal. Chem.* **2007,** 79, 3494-3503.
42. Rupcich, N.; Nutiu, R.; Li, Y.; Brennan, J. D., *Anal. Chem.* **2005,** 77, 4300-4307.
43. Carrasquilla, C.; Li, Y.; Brennan, J. D., *Anal. Chem.* **2011,** 83, (3), 957-65.
44. Carrasquilla, C.; Lau, P. S.; Li, Y.; Brennan, J. D., *J. Am. Chem. Soc.* **2012,** 134, (26), 10998-1005.
45. Clark, S. L.; Remcho, V. T., *Electrophoresis* **2003,** 23, 1335-1340.
46. Song, S.; Wang, L.; Li, J.; Fan, C.; Zhao, J., *TrAC* **2008,** 27, (2), 108-117.
47. Nutiu, R.; Mei, S.; Liu, Z.; Li, Y., *Pure Appl. Chem.* **2004,** 76, (7-8), 1547-1561.
48. Huizenga, D. E.; Szostak, J. W., *Biochemistry* **1995,** 34, 656-665.
49. Klug, S. J.; Famulok, M., *Mol. Biol. Rep.* **1994,** 20, 97-107.
50. Nutiu, R.; Li, Y., *Angew. Chem. Int. Edit.* **2005,** 44, 1061-1065.
51. Nutiu, R.; Li, Y., *J. Am. Chem. Soc.* **2003,** 125, 4771-4778.
52. Eleftheriou, N. M.; Brennan, J. D., *J. Sol-Gel Sci. Tech.* **2009,** 50, (2), 184-193.
53. Rupcich, N.; Chiuman, W.; Razvan, N.; Mei, S.; Flora, K. K.; Li, Y.; Brennan, J. D., *J. Am. Chem. Soc.* **2006,** 128, 780-790.
54. Flora, K. K.; Brennan, J. D., *Chem. Mater.* **2001,** 13, 4170-4179.
55. Rachwal, P. A.; Fox, K. R., *Methods* **2007,** 43, (4), 291-301.
56. Brinker, C. J., *J. Non-Cryst. Solids* **1988,** 100, 31-50.
57. Tan, B.; Rankin, S. E., *J. Non-Cryst. Solids* **2006,** 352, (52-54), 5453-5462.
58. A., V. R.; Hararnath, D., *MicroPor. Mesopor. Mat.* **1999,** 20, 267-273.
59. Haranath, D.; Rao, A. V., *Micropor. Mesopor. Mat.* **1999,** 30, 267-273.
60. Schwertfeger, F.; Glaubitt, W.; Schubert, U., *J. Non-Cryst. Solids* **1992,** 145, 85-89.
61. Herskovits, T. T.; Singer, S. J., *Arch. Biochem. Biophys.* **1961,** 94, 99-114.

2.8 APPENDIX

2.8.1 Supplementary Information

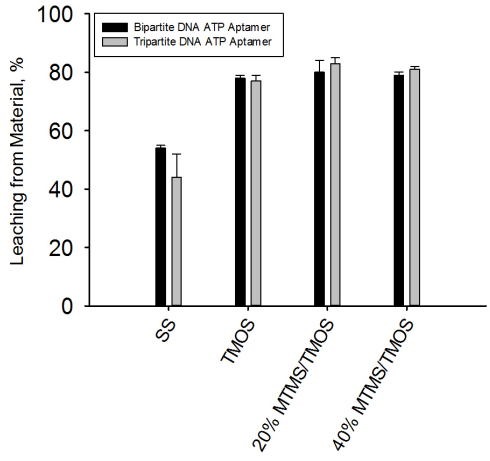

Figure S2-1. Leaching of bipartite and tripartite constructs of ATP-binding DNA aptamers from various sol-gel derived materials.

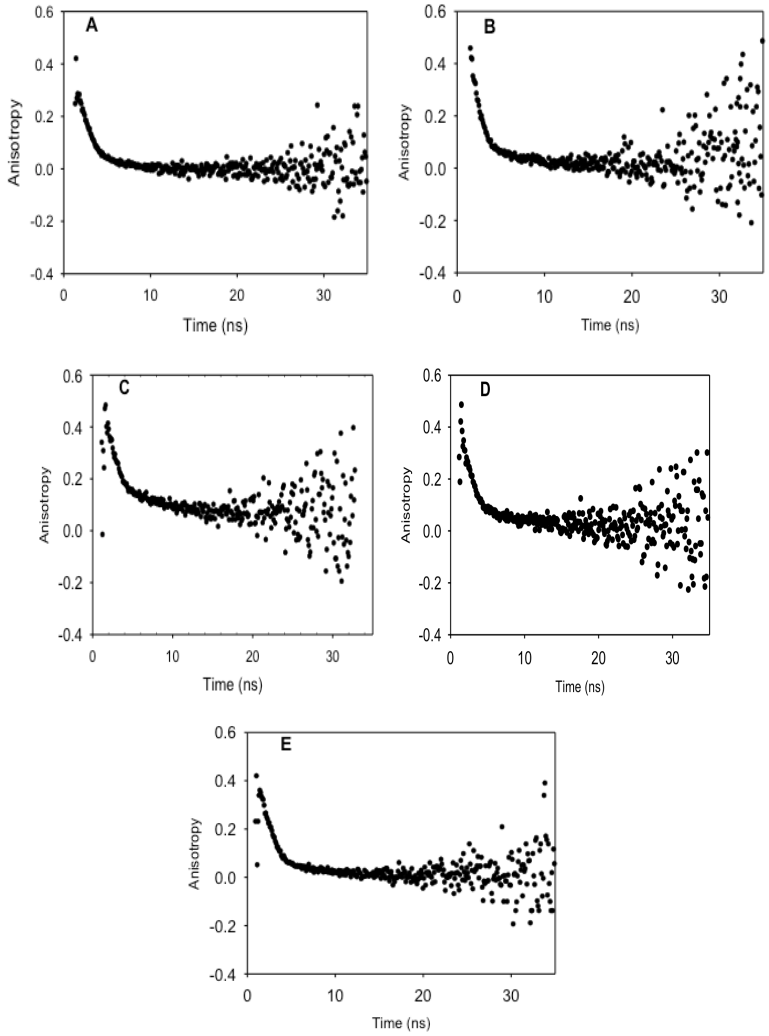

Figure S2-2. Time-resolved anisotropy decays for bipartite construct of ATP-binding DNA aptamer in (A) solution; (B) in SS; (C) in TMOS; (D) in 20% MTMS/TMOS; and (E) in 40% MTMS/TMOS. All samples contained 1 μM aptamer. Excitation: 490 nm; emission: 532 nm; bandwidth: 32 nm for both excitation and emission paths.

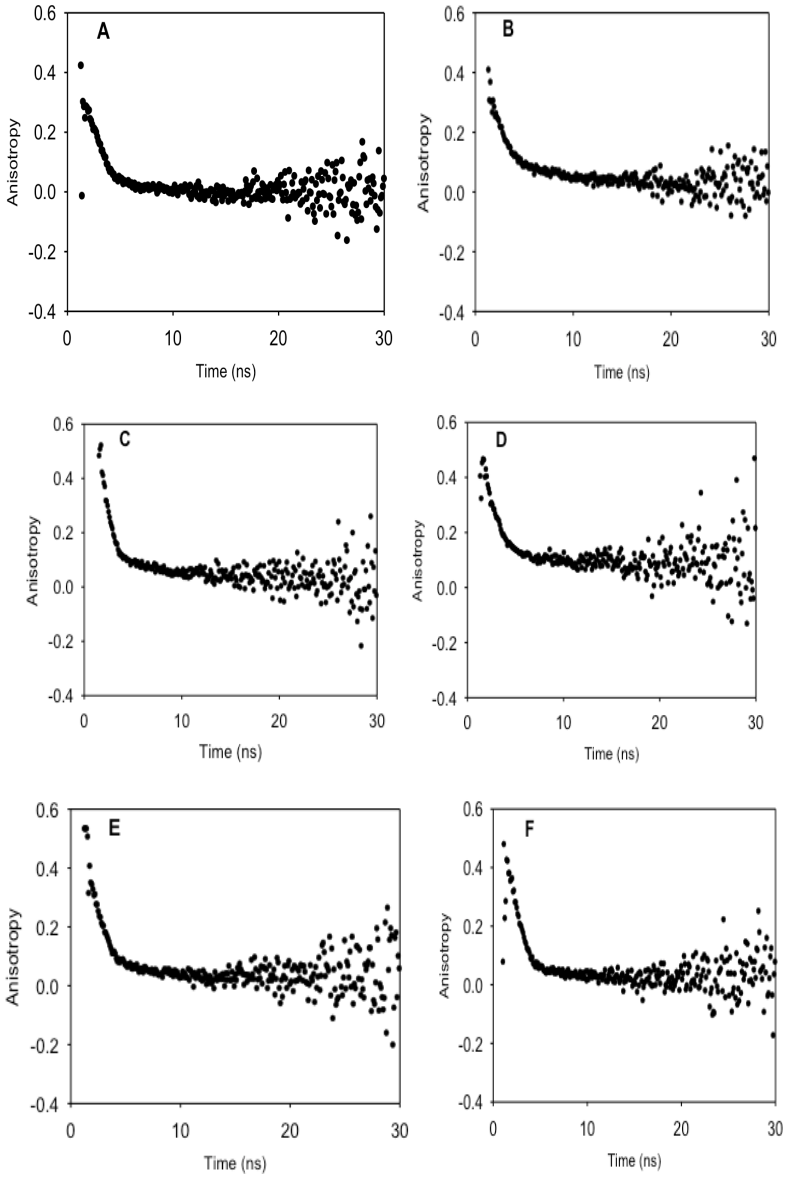

Figure S2-3. Time-resolved anisotropy decays for (A) ***F***-DNA strand only in solution; tripartite construct of ATP-binding DNA aptamer in (B) in solution; (C) in SS; (D) in TMOS; (E) in 20% MTMS/TMOS; and (F) in 40% MTMS/TMOS. All samples contained 1 μM aptamer. Excitation: 490 nm; emission: 532 nm; bandwidth: 32 nm for both excitation and emission paths.

Table S2-1. TRFA decay parameters of bipartite ATP-binding DNA aptamer in solution or entrapped in silica derived from various precursors.

Sample	ϕ_1 /ns	ϕ_2 /ns	f_1 [a]	f_2	g	r_0 [b]	r_∞ [b]	χ^2	r_{ss} [c]
In solution	0.65 ± 0.04	2.94 ± 0.41	0.63	0.38	0.007	0.18	0.001	1.11	0.08
In SS	0.52 ± 0.05	3.59 ± 0.54	0.60	0.32	0.08	0.29	0.02	1.06	0.11
In TMOS	0.66 ± 0.10	5.08 ± 0.88	0.46	0.35	0.19	0.31	0.06	1.02	0.17
In 20% MTMS/TMOS	0.62 ± 0.09	4.51 ± 0.54	0.59	0.32	0.08	0.29	0.02	1.07	0.15
In 40% MTMS/TMOS	0.59 ± 0.08	3.88 ± 0.84	0.68	0.28	0.04	0.27	0.01	1.03	0.12

[a] The typical error in fractional contributions of anisotropy decay times is ± 5% to 10%. [b] Typical errors in r_0 and r_∞ values are ±5%. [c] Typical errors in stead-state anisotropy values are ±0.002. All samples were tested in triplicate.

Table S2-2. TRFA decay parameters of tripartite ATP-binding DNA aptamer in solution or entrapped in silica derived from various precursors.

Sample	ϕ_1 /ns	ϕ_2 /ns	f_1 [a]	f_2	g	r_0 [b]	r_∞ [b]	χ^2	r_{ss} [c]
F-DNA Strand Only	0.43 ± 0.13	2.76± 0.46	0.67	0.31	0.01	0.29	0.004	1.02	0.03
In solution	0.56 ± 0.13	4.89± 0.97	0.49	0.41	0.01	0.26	0.03	1.13	0.15
In SS	0.59 ± 0.17	5.08 ± 0.31	0.70	0.26	0.11	0.32	0.04	1.03	0.22
In TMOS	0.70 ± 0.04	3.76 ± 0.28	0.46	0.25	0.29	0.32	0.09	0.95	0.24
In 20% MTMS/TMOS	0.54 ± 0.04	3.19 ± 0.61	0.65	0.25	0.10	0.31	0.03	1.07	0.21
In 40% MTMS/TMOS	0.59 ± 0.06	3.48 ± 0.61	0.71	0.21	0.08	0.29	0.02	1.05	0.20

[a] The typical error in fractional contributions of anisotropy decay times is ±5% to 10%. [b] Typical errors in r_0 and r_∞ values are ±5%. [c] Typical errors in stead-state anisotropy values are ±0.008. All samples were tested in triplicate.

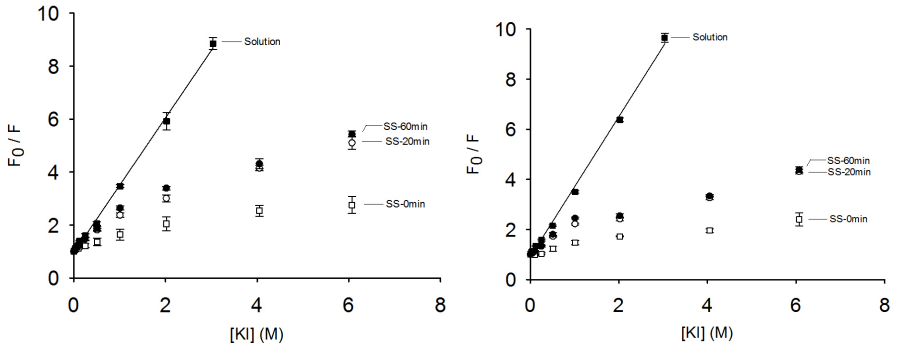

Figure S2-4. Stern-Volmer plot of the quenching of fluorescence for entrapped (A) bipartite aptamer and (B) tripartite aptamer by iodide at different time points upon addition of an anionic quencher: (■) solution, (□) 0-min incubation time, (○) 20-min incubation time, (●) 60-min incubation time.

Table S2-3. Quenching data for bipartite and tripartite constructs of DNA aptamers entrapped in different materials.

		Bipartite construct			Tripartite construct		
Sample	Time	K_a (M^{-1})	k_q ($10^8 M^{-1}$)	τ_0 (ns)	K_a (M^{-1})	k_q ($10^8 M^{-1}$)	τ_0 (ns)
Solution		2.38 ± 0.10	2.52 ± 0.56	4.25 ± 0.02	2.15 ± 0.19	2.58 ± 0.26	4.14 ± 0.02
	0 m	1.37 ± 0.44	0.75 ± 0.27	3.83 ± 0.02	0.93 ± 0.19	0.46 ± 0.10	3.33 ± 0.08
SS	20 m	2.53 ± 0.27	1.69 ± 0.14	3.90 ± 0.03	1.74 ± 0.24	1.25 ± 0.03	3.42 ± 0.01
	60 m	2.35 ± 0.37	1.76 ± 0.18	3.95 ± 0.07	1.93 ± 0.15	1.47 ± 0.05	3.49 ± 0.03
	0 m	2.30 ± 0.58	0.96 ± 0.19	3.64 ± 0.10	1.01 ± 0.17	0.74 ± 0.35	3.27 ± 0.01
TMOS	20 m	2.05 ± 0.13	1.04 ± 0.16	3.59 ± 0.04	0.71 ± 0.38	0.79 ± 0.40	3.22 ± 0.02
	60 m	1.33 ± 0.29	0.76 ± 0.11	3.65 ± 0.06	0.45 ± 0.12	1.67 ± 1.20	3.20 ± 0.01
20%	0 m	0.74 ± 0.36	0.39 ± 0.12	3.76 ± 0.05	0.89 ± 0.09	0.75 ± 0.26	3.42 ± 0.01
MTMS/TMO	20 m	1.48 ± 0.29	1.02 ± 0.04	3.73 ± 0.03	1.11 ± 0.14	1.02 ± 0.06	3.34 ± 0.02
S	60 m	1.82 ± 0.38	1.03 ± 0.05	3.77 ± 0.02	1.20 ± 0.06	0.92 ± 0.06	3.35 ± 0.02
40%	0 m	0.80 ± 0.65	0.29 ± 0.03	3.80 ± 0.04	0.60 ± 0.34	0.30 ± 0.03	3.52 ± 0.03
MTMS/TMO	20 m	1.31 ± 0.29	1.01 ± 0.05	3.84 ± 0.02	0.93 ± 0.03	1.03 ± 0.05	3.57 ± 0.03
S	60 m	1.07 ± 0.05	1.04 ± 0.01	3.84 ± 0.04	0.68 ± 0.34	1.03 ± 0.05	3.59 ± 0.03

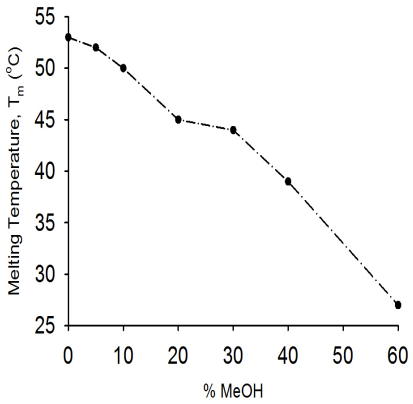

Figure S2-5. Melting temperatures (T_m) of DNA aptamer complex in different concentrations of methanol.

Table S2-4. Summarization of factors that affects aptamers performance upon entrapped in various sol-gel derived silica.

	Parameters						
Materials	Pore Size	Mobility	Accessibility	Leaching	Thermal Stability	Remain hybridized ?	Long term stability
TMOS	Medium	Poor	Poor	High	Poor	No	Poor
SS	Small	Good	Good	Low	Good	Yes	Excellent
MTMS/TMOS hybrids	Large	Good	Good	High	Poor	No	Poor

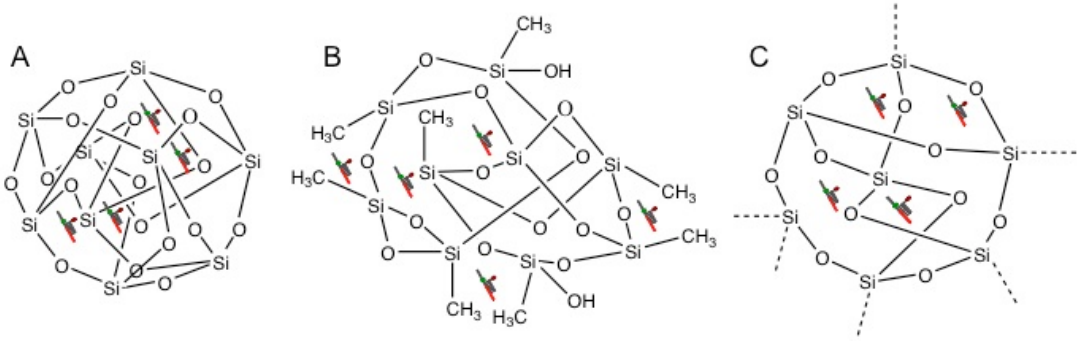

Figure S2-6. Possible configurations of various sol-gel derived silica and microenvironments of entrapped aptamer. (A) TMOS-based material - highly cross-linked material results in dramatic loss in dynamic motion of entrapped aptamer and affects the ability of aptamers to structure-switch. (B) MTMS/TMOS hybrids: some methyl and hydroxyl groups on silica surface creates a more hydrophobic environment that leads to larger pores and increases the mobility of entrapped aptamers and target accessibility. (C) SS-derived material: higher porosity than TMOS-derived material but smaller pores than MTMS/TMOS hybrids allow the entrapped aptamers to retain substantial mobility and with minimum leaching.

CHAPTER 3.

INVESTIGATION OF RNA STRUCTURE-SWITCHING APTAMERS IN TUNABLE SOL-GEL-DERIVED MATERIALS

Author's Preface:

This following chapter was submitted as a full article to the journal, *Journal of Sol-Gel Science and Technology*, under the authorship of Christy Y. Hui, Pui Sai Lau, Yingfu Li, and John D. Brennan. I was responsible for all the experimental protocols, performance of said experiments, data collection, analysis and interpretation. Pui Sai designed the structure-switching RNA-ATP binding aptamer. I wrote the first draft of the manuscript and Dr. Brennan and Dr. Li provided editorial input to generate the final draft.

3.1 ABSTRACT

In recent years RNA aptamers have emerged as potential recognition elements for solid phase assays, including assays that utilize sol-gel based biohybrid materials. However, there is still very little knowledge regarding the behaviour of RNA aptamers when entrapped in sol-gel-derived materials. In this work, we evaluated the performance of an adenosine triphosphate (ATP)-binding structure-switching RNA aptamer in a series of sol-gel derived materials and compared the results to those previously reported for an ATP-binding DNA aptamer. It was observed that the nature of the entrapping material is the key parameter for affecting the functionality of the entrapped ATP-binding RNA aptamer, which mainly impacts the ability to remain fully hybridized to signaling DNA strands upon entrapment. We observed that the materials with a high organic content provided the best performance for entrapped RNA aptamers at early times after entrapment. However, upon aging, materials derived from sodium silicate provided the best performance. Overall, the results suggest that polar materials that do not produce alcohol are optimal for entrapment of both DNA and RNA aptamers that bind ATP.

3.2 INTRODUCTION

The encapsulation of biomolecules in mesoporous silica and organosilicate matrices has been an active area of research for over 25 years.[1-4] Over this time, numerous investigations have reported on the effects of entrapment on the functionality of biomolecules, predominantly focusing on entrapped proteins.[5-10] Overall, the results of such studies have shown that materials that allow proteins to retain conformational

dynamics and accessibly to analytes, while minimizing leaching, are most appropriate for maximizing the performance of entrapped proteins.[11]

An emerging class of biorecognition elements are functional nucleic acids (FNAs), which have become widely used as sensing elements in analytical and diagnostic applications.[12-17] Typical FNAs include structure-switching DNA or RNA aptamers[14, 16, 18-22] and molecular switches that consist of nucleic-acid cleaving DNAzymes[23-26], all of which require substantial conformational changes upon target binding in order to generate adequate signals.[27] Therefore, materials in which such species are entrapped must allow for significant mobility and accessibility without leaching so as to provide optimal performance for sensing applications.

Recently, our group investigated structure-switching DNA aptamers entrapped in various sol-gel derived materials. These species are comprised of the aptamer with an extended 3' primer, with a fluorophorelabelled DNA strand (***F***-DNA) hybridized to the primer, and a quencher-modified DNA strand (***Q***-DNA) hybridized across the region spanning the primer and aptamer such that the ***F*** and ***Q*** moieties are adjacent to each other. Upon target binding, the conformational change in the aptamer causes dissociation of the ***Q***-DNA strand, producing a large increase in the fluorescence signal. Our initial studies found that the key criteria for maintaining the activity of entrapped DNA aptamers was the ability of aptamers to remain fully hybridized to the ***F***-DNA and ***Q***-DNA signaling elements, and that avoidance of alcohol during the production of materials is necessary to achieve this goal.[28] While RNA aptamers, which are more prone to chemical degradation relative to DNA, have also been successfully entrapped in sol-

gel derived materials[29], no studies have been done to assess the factors that affect their performance in different materials. As more and more RNA aptamers are selected for a wide-range of targets and many naturally occurring RNA aptamers are discovered[30-32], it is necessary to understand how RNA aptamers, and in particular structure-switching RNA aptamers, behave when entrapped in sol-gel-derived materials so as to advance the development of solid-phase RNA aptasensors.

In this study, we have used a variety of fluorescence methods to investigate the performance of an ATP binding RNA aptamer in various materials, and compare the results to those reported previously for an ATP binding DNA aptamer.[25] While these species bind the same ATP target, the aptamers have substantially different sequences, secondary structural folds, and ligand-binding stoichiometries[30, 33]. Both the DNA and RNA aptamers were structure-switching aptamers hybridized to ***F***-DNA and ***Q***-DNA strands, which allow for generation of fluorescence upon analyte-triggered dissociation of the **Q**-DNA. The ATP-binding RNA aptamer was entrapped in both polar and non-polar materials using processing methods that either did or did not produce alcohol as a byproduct, and materials were assessed to determine how material properties affected the performance of the RNA aptamer. The data provides insights on how sol-gel derived materials affect RNA aptamers as compared to DNA aptamers, and allows identification of an optimal material for entrapping aptamer species for ATP detection.

3.3 EXPERIMENTAL SECTION

3.3.1 Chemicals

All DNA oligonucleotides were chemically synthesized by Integrated DNA Technologies (Coralville, IA) and purified by HPLC prior to use. Adenosine 5'-triphosphate (ATP) was purchased from Thermo Scientific. Tetramethylorthosilicate (TMOS), methyltrimethoxysilane (MTMS) and Dowex 50 x 8-100 cation-exchange resin were obtained from Sigma (Oakville, ON, Canada). Sodium silicate solution (SS, technical grade, 9% Na2O, 29% silica, 62% water) was purchased from Fisher Scientific (Pittsburgh, PA). Water was purified with a Milli-Q synthesis A10 water purification system. All other chemicals and solvents used were of analytical grade and were used without further purification.

3.3.2 Preparation of RNA ATP aptamers and reporter complex

Polymerase chain reaction (PCR) of the DNA templates for the RNA ATP-binding aptamer and RNA transcription for this aptamer were performed as described elsewhere.[18] The specific DNA template sequences for the RNA aptamer reporter were as follows.

DNA template for PCR: 5'-GAATTCTAATACGACTCACTATA
GGCCTGCCACGCTCCGACGCTATCACTCTATGGGGTTGGGAAGAAACTGTGG
CACTTCGGTGCCAGCAACCC-3'

Forward PCR primer: 5'-GAATTCTAATACGACTCACTATA-3'

Reverse PCR Primer: 5'-GGGTTGCTGGCAC-3'

F-DNA: 5'-FTAGCGTCGGAGCGTGGCAGG-3'

Q-DNA: 5'-CCCCATAGAGTG-dabcyl-3'

The RNA aptamer complex was prepared using a 20-mer ***F***-DNA strand to minimize the potential for dehybridization, and a 12-mer ***Q***-DNA strand, which was obversed to produced the best signaling properties for the RNA aptamer (Figure S1, Appendix). The ***F***-DNA, aptamer and ***Q***-DNA were combined in a 1:2:3 molar ratio (optimization data is shown in Figure S2, Appendix) in 1x RNA assay buffer containing 20 mM Tris buffer (pH 7.60) with 300 mM NaCl and 5 mM $MgCl_2$. This mixture was first heated at 65 °C for 2 min, cooled at room temperature for 10 min, and then stored at 4 °C until analysis as described elsewhere.[29]

3.3.3 Entrapment of RNA Aptamers within Sol-Gel Derived Materials

Precursor sols using sodium silicate (SS), TMOS and MTMS were prepared as described elsewhere.[28, 34] Sodium silicate sols were prepared by diluting 2.59 g of stock sodium silicate in 10 mL of ddH_2O and immediately mixing with 5.5 g of Dowex resin. The mixture was then stirred for 2 minutes and then vacuum filtered through a Buckner funnel. The filtrate was then filtered through a 0.2 μm membrane syringe filter to remove any particulates in the solution. The final pH of the SS solution was ~4. The TMOS sols were prepared by mixing 700 μL of water, 50 μL of HCl (0.1 N) and 2.25 mL of TMOS and then sonicating the mixture in ice-cold water for 20 min.[34] The TMOS/MTMS hybrids were prepared by proportionally diving the 2.25 mL of silane using volume percentages of 20 or 40% MTMS in TMOS, mixing with water and acid and co-

hydrolyzing in a sonicator as above. In all cases, buffered RNA aptamer reporter solutions were mixed in a 1:1 (v/v) ratio with a freshly prepared silica sol at room temperature. The aptamer-sol mixtures were deposited into 96-well microliter plates or polystyrene (PS) fluorimeter cuvettes (1 cm pathlength) and allowed to gel. All samples were aged at room temperature for 3x of the gelation time of each sol (aging time for SS is 30 min; TMOS is 10 min, 20% MTMS/TMOS is 60 min and 40% MTMS/TMOS is 90 min). Microwells containing the various sol-gel derived materials for both aging methods were then incubated with 100 μL of 1x RNA assay buffer for at least 1 h at room temperature. All sol-gel-derived materials were washed with 100 μL of 1x assay buffer three times to remove any leachable aptamers.

3.3.4 Fluorescence Signal Enhancement

All measurements were performed in 96-well microplates at 25 °C using a TECAN M1000 plate reader operated in bottom-read fluorescence mode using the settings as described elsewhere.[24] Initial baseline fluorescence was measured every 15 s for 15 min for samples that had 100 μL of assay buffer overlaying the monolithic materials. Then, a concentrated ATP solution was added to obtain a final concentration of 2 mM, and fluorescence emission was again measured every 15 s for a total of 80 min. Background emission correction was calculated as described elsewhere.[28] All fluorescence measurements are reported as fluorescence enhancement or F/F_0 where F is the end point fluorescence intensity and F_0 is the initial fluorescence intensity prior to target addition. Signal enhancement was obtained at 3x gelation time for each material as

well as for samples aged in buffer at 4 °C over a period of 30 days to assess the effects of aging on signal levels.

3.3.5 Thermal Melt Studies

Fluorescence emission was measured as a function of temperature to generate melting curves and determine melting temperatures (T_m) of RNA aptamers in solution and when entrapped in various materials as described previously[8, 35, 36] using a Cary Eclipse fluorimeter with a computer controlled temperature controller. All samples were prepared in cuvettes. The temperature was raised in ca. 2 °C increments starting at 20 °C and going to 80 °C, with equilibration at each temperature for 10 min prior to measurement of fluorescence intensity. Samples without aptamers present were also tested to perform background correction. Fluorescence intensity of the ***F***-DNA strand alone was also collected to correct for temperature dependent changes in quantum yield. As such, the changes in emission intensity reflect the dehybridization of the ***Q***-DNA strand (which is shorter than the ***F***-DNA strand and should dissociate first). The T_m was determined from the mid-point of a melting curve where the complex is 50% dissociated, and it is determined from the maximum in the first derivative of the melting profile as described elsewhere.[37]

3.3.6 Accessibility Studies

Iodide quenching studies were done for aptamers entrapped in various silanes (SS, TMOS and MTMS/TMOS hybrids) and in solution in the absence of ***Q***-DNA. All studies

were performed in 96-well plates using a TECAN Evolution plate reader operating in bottom-read mode. For solution studies, each sample well in 96-microwell plates contained 50 μL of 200 nM of RNA aptamer and 50 μL of different concentrations of potassium iodide up to 6.0 M were then added to individual sample wells giving a final concentration of aptamer of 100 nM and varying concentrations of quencher up to 3.0 M. The plates were placed on a plate shaker and shaken at 500 rpm for 3 min, after which the fluorescence intensity of each well was collected. For studies of entrapped aptamers, each sample well contained a 50 μL monolith sample which was incubated with 50 μL of varying concentrations of potassium iodide for 60 min. The fluorescence intensity of each well was then collected. The data obtained from different quencher concentrations were combined to yield quenching curves. All quenching data were analyzed using the following equation[8, 38, 39]:

$$\frac{F_0}{\Delta F} = \frac{1}{f_a K_a [Q]} + \frac{1}{f_a} \qquad [5]$$

where F_0 is the fluorescence intensity in the absence of the quencher, ΔF is the difference in fluorescence intensity at a given molar concentration of quencher [Q] relative to F_0, f_a is the fraction of accessible fluorophore, and K_a is the Stern-Volmer quenching constant (M^{-1}) for the accessible fluorophore. A plot of $F_0/\Delta F$ versus 1/[Q] yields $1/f_a$ as the y intercept and $1/f_a K_a$ as the slope.

3.3.7 Target-binding Sensitivity Studies

All measurements were performed in 96-well microplates at 25 °C using a TECAN M1000 plate reader operated in bottom-read fluorescence mode using as described elsewhere[28]. For solution studies, each sample well in 96-microwell plates contained 25 μL of 400 nM of RNA aptamer and 25 μL of various concentrations of ATP from 0 – 12 mM (C_f= 200 nM of RNA aptamer; 0 – 6 mM ATP). The plates were then placed on a plate shaker and shaken at 500 rpm for 3 min, after which the fluorescence intensity of each well was collected. For studies of entrapped aptamers, each sample well contained a 50 μL monolith sample which was incubated with 50 μL of varying concentrations of ATP between 0 – 6 mM for 60 min. The fluorescence intensity of each well was then collected. The fluorescence intensity of undoped materials and solutions without aptamers present were also collected, and the intensity values were subtracted from those of aptamer samples to correct for background emission. All fluorescence measurements are reported as fluorescence enhancement or F/F_0 where F is the end point fluorescence intensity and F_0 is the initial fluorescence intensity prior to target addition.

3.3.8 Steady-State and Time-Resolved Fluorescence Anisotropy

Steady-state fluorescence anisotropy measurements were obtained using a TECAN M1000 plate reader, with instrumental calibration using 1 nM of fluorescein in 0.1 M NaOH. Time-resolved fluorescence intensity and anisotropy decay data were obtained using an IBH 5000U time-correlated single-photon-counting (TCSPC) fluorimeter (Glasgow, UK), as described elsewhere.[8, 10] The measurement settings for

both steady-state and time-resolved fluorescence anisotropy were same as described elsewhere.[28]

In the studies of time-resolved fluorescence anisotropy, 150 μL of RNA aptamer/***F***-DNA duplex was entrapped in various materials at a final concentration of 1 μM fluorophore in microvolume cuvettes (Bio-Rad Laboratories, Inc). Fluorescence anisotropy was collected into 2,048 channels over a range of 200 ns (97.66 ps per channel) until 10,000 counts were obtained in the peak channel, or until the difference in peak intensity between parallel and perpendicularly polarized outputs reached 10,000 counts. The instrument response profile was determined using Rayleigh scattering of the excitation source from a Ludox solution to minimize convolution artifacts.

The anisotropy decays were analyzed using the IBH DAN analysis software package as described elsewhere.[24] The anisotropy decay *r(t)* is defined as

$$r(t)=(D(t))/(S(t))=(I_{VV}(t)-GI_{VH}(t))/(I_{VV}(t)-2GI_{VH}(t)) \quad [1]$$

where *S(t)* is the sum of two decay curves, *D(t)* is the difference of two decay curves, and $I_{VV}(t)$ and $I_{VH}(t)$ are the time dependent intensity values obtained with vertically polarized excitation and vertically or horizontally polarized emission, respectively. All anisotropy values were corrected for the instrumental G-factor to account for polarization bias in the monochromator and PMT. The anisotropy decays were then fit to a two-component hindered rotor model,

$$r(t) = f_1 r_0 \exp(-t/\Phi_1) + f_2 r_0 \exp(-t/\Phi_2) + g r_0 \quad [2]$$

where Φ_1, and Φ_2 are the rapid and progressively slower rotational correlation times, respectively; f_1 (reflects the local motion of fluorophore) and f_2 (reflects global motion of DNA aptamer) are the fractional contributions of Φ_1 and Φ_2 to *r(t)*; *g* is the fraction of fluorescence due to probes that rotate more slowly than can be measured during the probe emission lifetime and r_0 is the limiting anisotropy. The residual anisotropy, r_∞, reflects the anisotropy at times which greatly exceed the lifetime of the fluorescent probe, and is determined by $r_\infty = g r_0$. The fits were considered acceptable when the reduced chi-squared (χ^2) values were close to 1.[8, 10]

3.4 RESULTS AND DISCUSSION

3.4.1 Fluorescence Signal Enhancement

The degree of fluorescence signal enhancement upon target binding was assessed for ATP-binding RNA aptamer reporters in solution and when entrapped in various sol-gel-derived materials. All the sol-gel-derived materials were treated by washing extensively prior to assays to remove all the leachable aptamers and dissociated ***F***-DNA, after which 2 mM ATP was added. Figure 3-1 shows the relative fluorescence enhancement for the RNA aptamer entrapped in various sol-gel-derived materials.

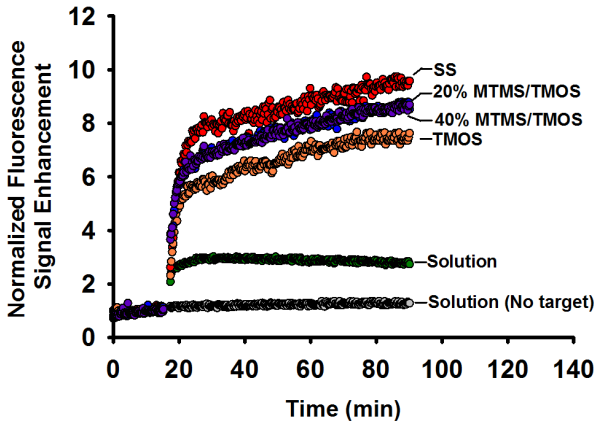

Figure 3-1. Fluorescence signal enhancement of ATP-binding structure-switching RNA aptamers in solution and in various sol-gel-derived materials. The target induced fluorescence signals were normalized to the fluorescence signals obtained from baseline incubation of 15 min. Data were obtained by addition 2 mM of ATP.

Consistent with the previous findings[29, 38], all entrapped samples showed a two-step signal development with a rapid initial rise followed by a slower increase in signal that was due to a subset of aptamers entrapped in a less accessible environment. In general, RNA aptamer reporters entrapped in silica-derived matrices demonstrated a higher fluorescence enhancement than those in solution. These results are most likely related to a reduction in the melt temperature of the ***Q***-DNA for the entrapped species (see below), which would make it easier to dissociate the ***Q***-DNA upon target binding. It is also possible that changes in the local microenvironment of the fluorescein moiety in ***F***-DNA caused changes in the degree of quenching by ***Q***-DNA, which altered the fold-enhancement upon target binding. Importantly, this data suggests that entrapped RNA aptamers may have better sensitivity and detection limits relative to solution, which is discussed in more detail below.

Unlike the previous study utilizing DNA aptamers[28], the fluorescence enhancements observed for entrapped RNA aptamers at early aging times (3× gelation time) were not significantly affected by the material used for entrapment, though it was observed that SS materials produced slightly larger overall enhancements relative to composite materials containing MTMS or TMOS derived materials. It is possible that the extensive washing resulted in similar internal solvent environments and that the materials remained relatively porous owing to the short time allowed for crosslinking, causing the entrapped aptamers to experience relatively similar microenvironments.

3.4.2 Effect of Aging time on Signal Enhancement

It is well known that aging time is one of the key factors that can affect the physical properties of sol-gel-derived materials[35, 40, 41]. As a result, we evaluated the fluorescence signaling of entrapped ATP-binding RNA aptamers relative to those in solution over a period of 1 month, with the materials stored at 4 °C. As shown in Figure 3-2, the RNA aptamer within the SS material retained full signaling ability over a period of 30 days, demonstrating that RNA aptamers were highly stable in such materials. RNA aptamers in TMOS derived materials lost approximately 25% of their initial signaling ability after 1 day (8-fold to 6-fold enhancement) but then remained stable after that. On the other hand, RNA aptamers within composite materials containing MTMS lost 40 – 50% signaling activity over a period of 1 month, suggesting that the presence of the

hydrophobic methyl groups may have caused some dehybridization of ***F***-DNA and/or ***Q***-DNA species, causing lower overall signal enhancements.

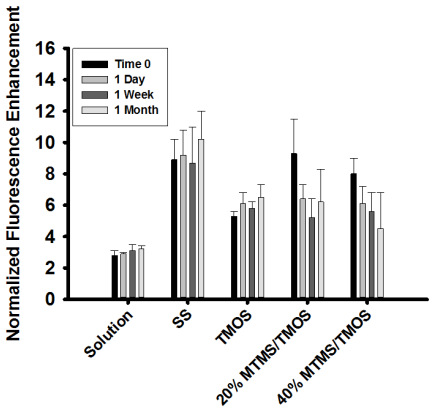

Figure 3-2. Structure-switching and signalling ability of RNA ATP-binding aptamer as a function of storage time. The data were obtained by adding 2 mM ATP to the entrapped aptamer after increasing storage time (up to 1 month) at 4°C.

3.4.3 Dynamics of Entrapped Aptamers

Table 3-1 shows steady-state anisotropy results for ATP-binding RNA aptamers in solution and when entrapped in various sol-gel-derived materials. It was observed that the steady-state anisotropy of the aptamer increased upon entrapment in sol-gel-derived materials when compared to the value in free solution, which agreed with previous studies[8, 10, 28]. The higher anisotropy is primarily due to the higher viscosity of entrapped solvents, which decrease the rotational mobility of the reporter probes. Overall, RNA aptamers showed the same trend as DNA aptamers[28]; materials with smaller mesopores produced higher anisotropy values, signifying lower mobility. Hence, TMOS-derived materials showed the highest anisotropy value as these have the smallest mesopores[29], resulting in restriction of the mobility of entrapped aptamers. This is followed by the SS-

derived materials, which have slightly larger mesopores and finally the MTMS/TMOS composite materials, which have a more open pore structure with increasing concentrations of MTMS[27, 29, 42, 43].

Table 3-1. Steady-state anisotropy data of RNA ATP-binding aptamers in solution and upon entrapped in various sol-gel-derived materials. All samples were excited at 490 nm and emission was collected at 520 nm. All samples were tested in triplicate.

	Anisotropy	
	Average	St. dev.
Solution	0.133	0.003
SS	0.223	0.004
TMOS	0.239	0.001
20% MTMS/TMOS	0.210	0.002
40% MTMS/TMOS	0.200	0.003

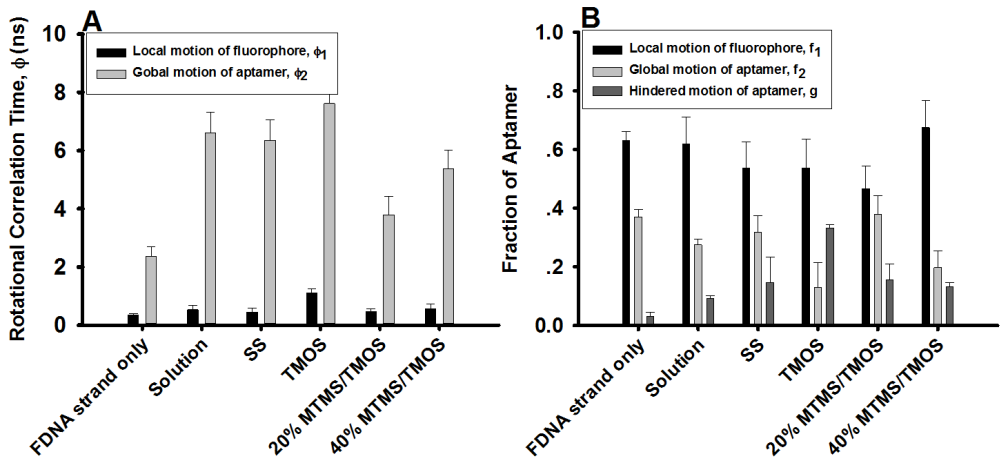

Figure 3-3. Comparison of (A) Rotational correlation times and (B) fractions corresponding to local, global, and hindered motions of RNA ATP-binding aptamerin free solution and entrapped in various sol-gel-derived materials. All samples were excited at 490 nm and emission was collected at 532 nm; 32 nm bandpasses were used in both the excitation and emission paths.

Time-resolved anisotropy data allows us to gain further insight into the factors that affect the mobility of entrapped RNA aptamers. Figure 3-3A shows the comparison of rotational correlation times (Φ_1 and Φ_2) and Figure 3-3B shows the fractional contributions from the local (f_1), global (f_2), and hindered (g) motions of RNA aptamers in solution and when entrapped in various sol-gel-derived materials (Figure S3-3 shows typical anisotropy decay curves). In agreement with the steady-state anisotropy data, the TMOS derived materials showed the slowest correlation times and largest fraction of immobile aptamers (largest g value), consistent with the lowest mobility. Importantly, addition of lower amounts of MTMS (20%) produced a significant increase in mobility (shorter correlation times and lower fraction of immobile aptamers), while higher MTMS levels (40%) caused a significant increase in the fraction of fluorophores with rapid motion, potentially indicating significant dissociation of ***F***-DNA from the RNA aptamer in the very hydrophobic material[28].

3.4.4 Accessibility of Entrapped Aptamers.

The overall fluorescence signal enhancement is also affected by the ability of analyte to reach the entrapped aptamer and cause structure-switching. Figure 3-4 shows the fraction of aptamers that are accessible to anioinic species for both the free and entrapped aptamers at various times over 1 month of storage (Figure S3-4 shows typical Stern-Volmer plots for entrapped RNA aptamers). Iodide was chosen as the quencher since ATP is a trianion, and hence both substances should be electrostatically repelled from the anionic silica matrix. In agreement with the previous studies[28, 29] and the

dynamics data, the fraction of accessible entrapped aptamers decreased with increased storage time due to the continuous evolution of the silica-derived materials, which resulted in pore shrinkage and decreased accessibility. In addition, the fractional accessibility increased with increasing amounts of MTMS present in the materials, suggesting that the larger pore size produced a higher fraction of accessible aptamer. It is possible that the hydrophobic silane precursors reduced the negative charge on the matrix and allowed the iodide anion to better penetrate into the material and access a higher amount of entrapped aptamer[28].

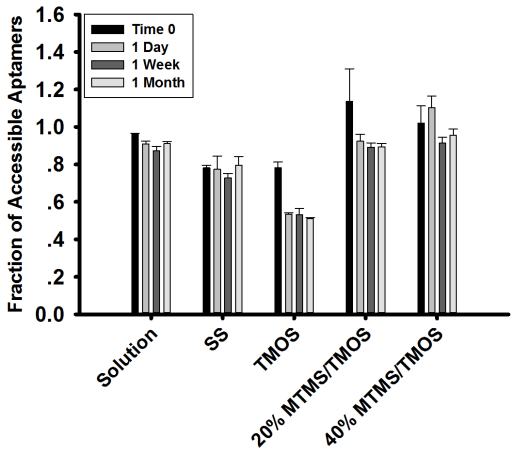

Figure 3-4. Fractional accessibilities of the entrapped ATP-binding RNA aptamers in free solution and entrapped in various sol-gel derived materials as a function of storage time. The data were obtained by adding iodide anion solution to the entrapped aptamer after increasing storage time (up to 1 month) at 4°C and taken after 60 min incubation with iodide anion solution.

3.4.5 Thermal Stability

The melting temperatures (T_m) for dissociation of the ***Q***-DNA strand from the RNA aptamer was determined in solution and for aptamers entrapped in various silica materials to examine how entrapment affected the stability and potentially signaling ability of the structure-switching aptamer construct. Figure 3-5 shows the temperature-dependent increases in fluorescence intensity of the free and entrapped ATP-binding RNA aptamer resulting from loss of the ***Q***-DNA strand. It was observed that RNA aptamer entrapped in SS exhibited a similar melting temperature to the aptamer in free solution, while the melting temperature in all alcohol producing materials was substantially lower, demonstrating that the materials that liberated methanol during formation caused significant destabilization of the RNA-DNA hybridization[28]. This was not likely a direct result of alcohol present in the pore solvent, as all materials were washed extensively prior to performing the melting studies.

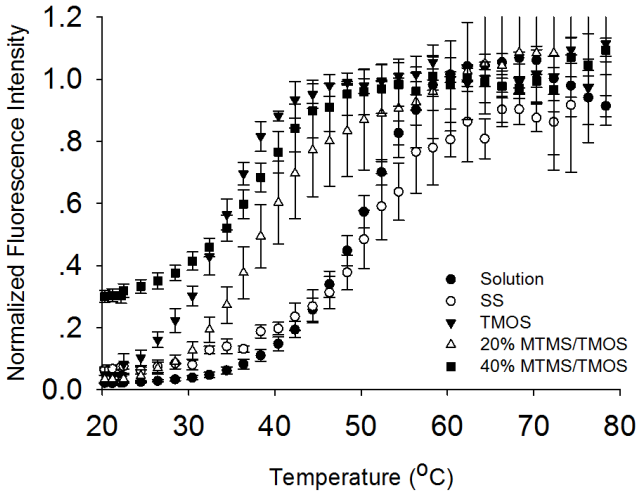

Figure 3-5. **Fluorescence signal enhancement cased by dehybridization of the quencher strand of the RNA ATP aptamer complex as a function of temperature.** The quencher strand is considered to be dehybridized at a temperature corresponding to 50% of the maximum enhancement. The quencher strand dehybridized at: solution: 52.1°C ± 0.5 °C; SS: 59.4°C ± 2.7°C; TMOS: 34.9°C ± 2.8°C; 76.8°C ± 2.0°C; 20% MTMS/TMOS: 37.0°C ± 1.2°C; 58.4°C ± 1.3°C; 40% MTMS/TMOS: 38.1°C ± 0.5 °C; 63.4°C ± 2.4°C.

Of the alcohol-producing materials, the material formed with 20% MTMS in TMOS showed the highest melting temperature, while TMOS and 40% MTMS/TMOS showed the lowest melt temperatures. The 40% MTMS material also showed a much higher initial fluorescence signal, suggesting that some ***F***-DNA or ***Q***-DNA was already dissociated, which is consistent with the much higher fraction of rapidly rotating species in 40% MTMS/TMOS materials (Figure 3-3B). These data suggest that the hybridization of the ***Q***-DNA (and possibly the ***F***-DNA) to the aptamer are significantly affected by the nature of the pore wall – it would be expected that all alcohol producing materials would still have substantial numbers of methoxy groups remaining bound to the silica matrix, as

suggested by previous solid-state nuclear magnetic resonance studies describing the hydrolysis and condensation reactions of such species[44]. Hence, the overall more hydrophobic environment likely destabilizes the hybridization of the signaling strands.

The results obtained for the ATP-binding RNA aptamer are similar to those obtained for the ATP-binding DNA aptamer reporter, where both aptamers performed best when entrapped in polar silica materials derived from sodium silicate[24]. Most importantly, RNA aptamer complexes remain hybridized to signaling DNA strands and thus are able to generate signals when entrapped in non-alcohol based materials such as SS. However, the RNA aptamers do appear to be more tolerant of hydrophobic and alcohol-producing materials relative to DNA aptamers, though long-term stability in such materials is not as great as in SS derived materials.

3.4.6 Analyte Response and Detection Limits for Entrapped RNA Aptamers

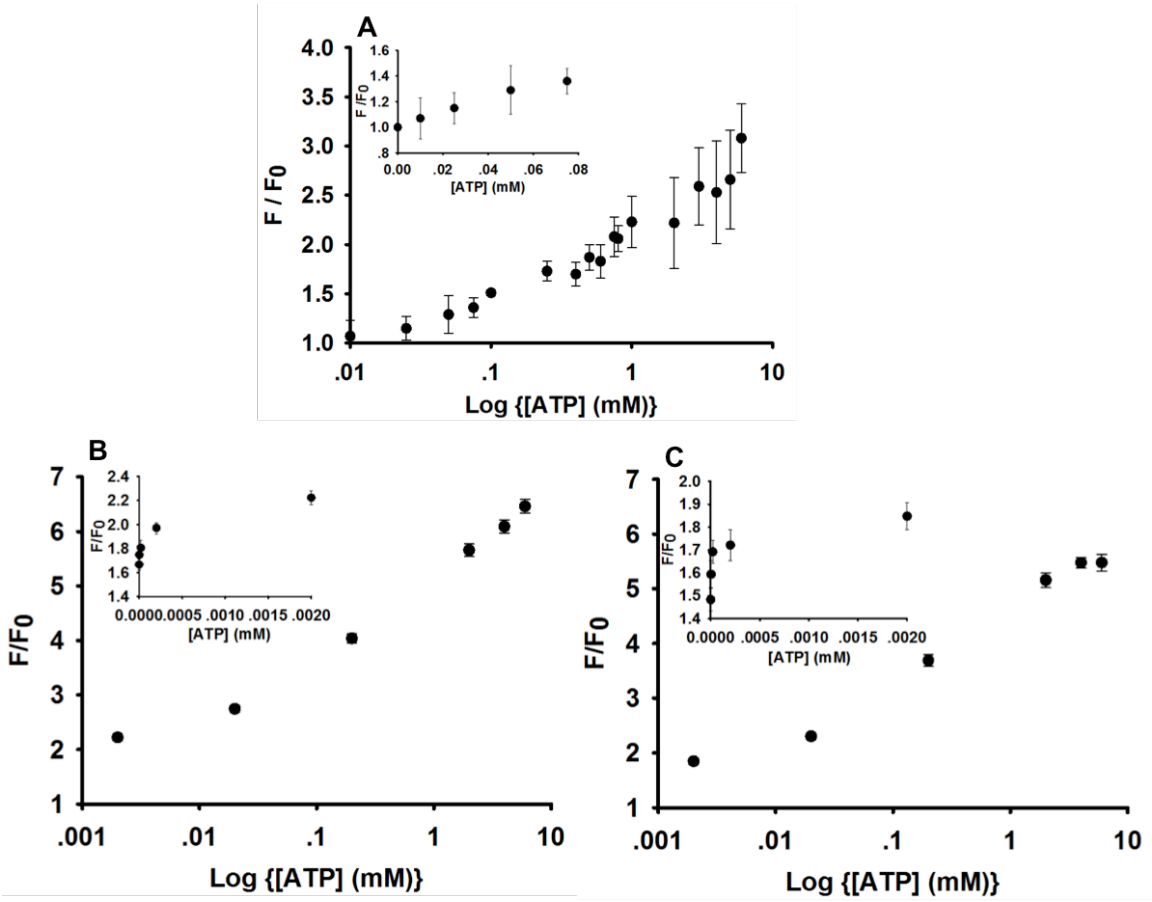

Figure 3-6. Concentration-response curves of RNA ATP-binding aptamer in (A) solution and when entrapped in (B) polar – SS-derived and non-polor – (C) 40% MTMS/TMOS-derived silica materials at 25 °C with different concentrations of ATP (0 – 4 mM). The data are reported as F/F_0 ratios, where F is the fluorescence intensity upon addition of a given concentration of ATP and F_0 is the initial reading for the aptamer reporter in the absence of ATP. All samples were tested in triplicate. The detection limit is determined to be 100 μM in solution, 1 μM in sodium silicate-derived and 2 μM upon entrapped in 40% MTMS/TMOS-derived materials.

As a final test of the performance of entrapped RNA aptamers, we evaluated the fluorescence response of ATP-binding RNA aptamers in SS (representative polar material) and 40% MTMS (representative non-polar material) relative to solution. Figure 6 shows the responses in solution (Fig. 6A), SS (Fig. 6B) and 40% MTMS (Fig.

6C) after 1 day of aging and clearly demonstrates that the entrapped aptamers have substantially greater sensitivity and also much better detection limits relative to the aptamers in solution regardless of the material used. In solution, the RNA aptamers have a limit of detection (LOD) of ca. 100 μM, while RNA aptamers in SS demonstrated a LOD of below 1 μM and those in 40% MTMS showed a LOD of 2 μM, consistent with the much steeper initial slope of the response for the entrapped RNA aptamers. These results demonstrate that RNA aptamers not only show greater overall signal enhancements (Fig. 1), but also respond at much lower levels of analyte, consistent with a more facile removal of the ***Q***-DNA strand for entrapped aptamers.

3.4.7 Significant Findings

According to the results outlined above, the highly cross-linked and alcohol-producing TMOS-based material was the least suitable for RNA aptamer entrapment. RNA aptamers entrapped in this material resulted in a dramatic loss in dynamic motion, likely caused dissociation of the ***Q***-DNA signaling strand, and reduced the ability of aptamers to undergo structure-switching, decreasing the overall signal enhancement. Aptamers entrapped in TMOS-derived materials also demonstrated the least accessibility and lowest thermal stability. Therefore, this material was deemed to be unsuitable for entrapments of RNA aptamers.

MTMS/TMOS-based hybrid materials have larger pores compared to TMOS-derived materials due to a lower degree of crosslinking, and also have fewer residual hydroxyl groups on their surfaces; therefore, the aptamers likely have fewer biomolecule-

surface interactions, leading to an increase in mobility of entrapped aptamers. Larger pore sizes also allow the entrapped RNA aptamers to be more accessible, and thus, the fraction of aptamers that were able to undergo structure-switching increased, resulting in a higher signal enhancement. However, the hydrophobic internal environment also reduced accessibility to anionic species, which likely was manifested in a reduction in the amount of ATP that could access the entrapped aptamer, ultimately leading to a decrease in signaling ability. In addition, the reduction in thermal stability of ***Q***-DNA hybridization in such materials likely led to partial dehybridiztaion of the ***Q***-DNA strand, which would also cause a reduction in signaling ability, particularly at longer aging times.

RNA aptamers entrapped in SS-derived materials produced the highest signal enhancement, highest fractional accessibility, best thermal and long-term stability, and a better LOD value compared to aptamers in solution or in other sol-gel derived materials. Overall, sodium silicate-derived material was identified to be the optimal material for entrapping structure-switching RNA aptamers that detect anioinic species such as ATP, since it allows entrapped RNA aptamers to retain mobility and structure-switching activity, and to generate large signals.

We note that the studies outlined above demonstrate that both aptamers for ATP function best in sodium silicate derived materials. However, previous studies using aptamers for other analytes (theophylline or thiamine pyrophosphate)[25] suggested that such aptamers functioned optimally in more hydrophobic materials derived from 40% MTMS/TMOS, suggesting that the optimal material for entrapping a given aptamer is determined at least in part by the ability of the analyte to enter the matrix and access the

aptamer, and may also depend on the specific structure of the aptamer itself. Studies on the role of these properties on entrapped aptamer performance will be reported in future work.

3.5 CONCLUSIONS

We show that the properties of sol-gel-derived materials play an important role in altering the performance and stability of entrapped ATP-binding RNA aptamers. Our key findings show that non-alcohol producing materials provide the best environment for both initial and long-term stabilization of aptamers, while also allowing entrapped aptamers to produce significantly larger fluorescence responses upon target binding relative to the RNA aptamer in solution. Our findings suggest that the improved signaling properties likely relate to a combination of factors that ultimately produce an enhanced ability of the ***Q***-DNA strand to dissociate from the RNA aptamer upon ligand binding, though secondary effects such as specific photophysical effects related to the emission of the fluorescein probe may also play a role. Interestingly, the RNA aptamer initially retained high activity in hydrophobic materials, showing that such materials do not dramatically alter the ability of the RNA aptamer to fold into an active structure, unlike the case for many proteins. However, upon aging, such materials are not optimal for retaining the performance of aptamer that interact with charged analytes. Overall, these studies show that significant optimization of material properties is needed to maximize aptamer performance, and that the optimal material may depend on both the specific sequence/structure of the aptamer and also on the nature of the analyte.

3.6 ACKNOWLEDGMENT

We thank the Natural Sciences and Engineering Research Council of Canada (NSERC) and Pro-Lab Diagnostics Inc. for funding this work. We also thank the Canada Foundation for Innovation and the Ministry of Research and Innovation (Ontario) for support of this work. Y.L. holds the Canada Research Chair in Directed Evolution of Nucleic Acids. J.D.B holds the Canada Research Chair in Bioanalytical Chemistry and Biointerfaces.

3.7 REFERENCES

1. Braun S, Rappoport S, Zusman R, Avnir D, Ottolenghi M (1990) Mater Lett 10: 1-2
2. Braun S, Shtelzer S, Rappoport S, Avnir D, Ottolenghi M (1992) J Non-Cryst Solids 147-148: 739-743
3. Avnir D, Braun S, Lev O, Ottolenghi M (1994) Chem Mater 6: 1605-1614
4. Avnir D, Coradin T, Lev O, Livage J (2006) J Mater Chem 16: 1013
5. Brennan JD (1999) Applied Spectroscopy 53: 106A-121A
6. Jin W, Brennan JD (2002) Analtica Chinica Acta 461:1-36
7. Goring GLG, Brennan, JD (2002) J Mater Chem 12: 3400-3406
8. Siu X, Cruz-Aguado JA, Chen Y, Zhang Z, Brook MA, Brennan JD (2005) Chem Mater 17: 1174-1182.
9. Besanger TR, Brennan JD (2006) J Sol-Gel Sci Tech 40: 209-225
10. Eleftheriou NM, Brennan JD (2009) J Sol-Gel Sci Tech 50: 184-193
11. Jin W, Brennan JD (2002) Anal Chim Acta 461: 1-36
12. Tombelli S, Minunni M, Mascini M (2005) Biosensors and Bioelectronics 20: 2424-2434
13. Banerjee J, Nilsen-Hamilton M (2013) J Mol Med 91: 1333-1342
14. Clark SL, Remcho VT (2002) Electrophoresis 23: 1335-1340
15. de Aguiar Ferreira C, de Barros ALB (2013) J Mol Pharm Org Process Res 1: 1000105
16. Famulok M, Mayer G (2011) Acc Chem Res 44: 1349-1359
17. Iliuk AB, Hu L, Tao WA (2011) Anal Chem 83: 4440-4452
18. Lau PS, Coombes BK, Li Y (2010) Angew Chem Int Ed 49: 7938-7942

19. Sassanfar M, Szostak JW (1993) Nature 364: 550-553
20. Huizenga DE, Szostak JW (1995) Biochemistry 34: 656-665
21. Nutiu R, Li Y (2003) J Am Chem Soc 125: 4771-4778
22. Nutiu R, Li Y (2005) Angew Chem Int Ed 44: 1061-1065
23. Nutiu R, Mei S, Liu Z, Li Y (2004) Pure Appl Chem 76: 1547-1561
24. Schlosser K, Li Y (2009) Chem Biol 16: 311-322
25. Silverman SK (2016) Trends Biochem Sci 41: 595-609
26. Liu M, Chang D, Li Y (2017) Acc Chem Res 50: 2273-2283
27. Haranath D, Rao AV (1999) Micropor Mesopor Mat 30: 267-273
28. Hui CY, Li Y, Brennan JD (2014) Chem Mater 26: 1896-1904
29. Carrasquilla C, Lau PS, Li Y, Brennan JD (2012) J Am Chem Soc 134: 10998-11005
30. Tucker BJ, Breaker RR (2005) Curr Opin Struct Biol 15: 342-348
31. McCown PJ, Corbino KA, Stav S, Sherlock ME, Breaker RR (2017) RNA 23: 995-1011
32. Carrasquilla C, Kapteyn E, Li Y, Brennan JD (2017) Angew Chem Int Ed 56: 10686-10690
33. Lin CH, Patel DJ (1997) Chem Biol 4: 817-832
34. Shen Y, Mackey G, Rupcich N, Gloster D, Chiuman W, Li Y, Brennan JD (2007) Anal Chem 79: 3494-3503
35. Zheng L, Brennan JD (1998) Analyst 123: 1735-1744
36. Flora KK, Brennan JD (2001) Chem Mater 13: 4170-4179
37. Rachwal PA, Fox KR (2007) Methods 43: 291-301
38. Rupcich N, Nutiu R, Li, Y, Brennan JD (2005) Anal Chem 77: 4300-4307
39. Rupcich N, Chiuman W, Razvan N, Mei S, Flora KK, Li Y, Brennan JD (2006) J Am Chem Soc 128: 780-790
40. Gupta R, Chaudhury NK (2007) Biosens Bioelectron 22: 2387-2399
41. Zheng L, Reid WR, Brennan JD (1997) Anal Chem 69: 3940-3949
42. Brinker CJ (1988) J Non-Cryst Solids 100: 31-50
43. Tan B, Rankin SE (2006) J Non-Cryst Solids 352: 5453-5462
44. Brennan JD, Hartman JS, Ilnicki EI, Rakic M (1999) Chem Mater 11: 1853-1864

3.8 APPENDIX

3.8.1 Supplementary Information

A

FDNA: 5' F - TAGCGTCGGAGCGTGGCAGG 3' (20 nt)
QDNA16: 5' CCAACCCCATAGAGTG-Q 3' (16 nt)
QDNA14: 5' AACCCCATAGAGTG-Q 3' (14 nt)
QDNA12: 5' CCCCATAGAGTG-Q3' (12 nt)

ATPa: 5' **GG**CCUGCCACGCUCCGACGCUA**U**CACUCUAUG

GGGUUGGGAAGAAACUGUGGCACUUCGGUGCCAGC
AACCC 3'

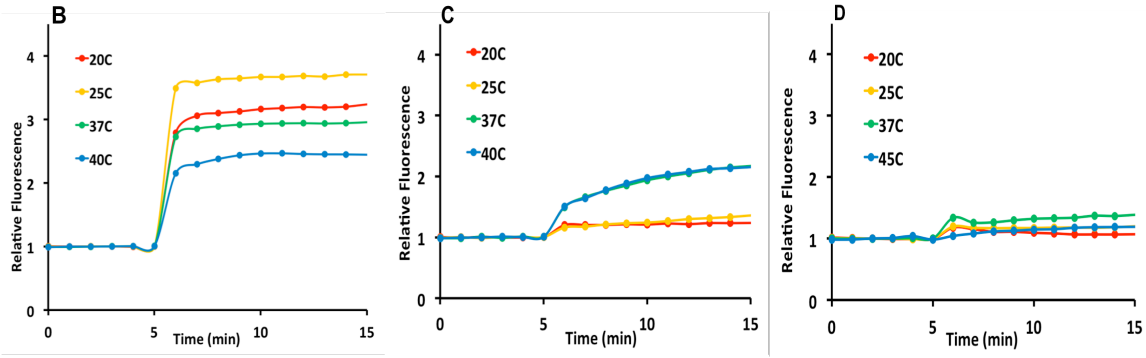

Figure S3-1. The design of structure-switching RNA ATP aptamer. (A) The sequences of F-DNA, Q-DNAs, and RNA aptamer. (B-D) Structure-switching activity of duplex made from F-DNA, ATPa, along with Q-DNA12 (B), Q-DNA14 (C), and Q-DNA16 (D) upon the addition of 1 mM ATP at different temperatures. Each duplex was incubated for 5 min followed by the addition of 1mM ATP.

The design of the ATP RNA aptamer reporter the identical strategy that was used to produce structure-switching reporters from DNA aptamers. We examined three Q-DNA sequences with different lengths and discovered that Q-DNA sequences more than 12 nt could not be effectively dehybridized from the duplex upon target addition. In addition, we have examined the signalling ability of Q-DNAs with different lengths at different temperatures. It was observed that duplex of RNA aptamer and F-DNA hybridized with 12 nt Q-DNA at 25 °C generated the highest fluorescence enhancement upon addition of target.

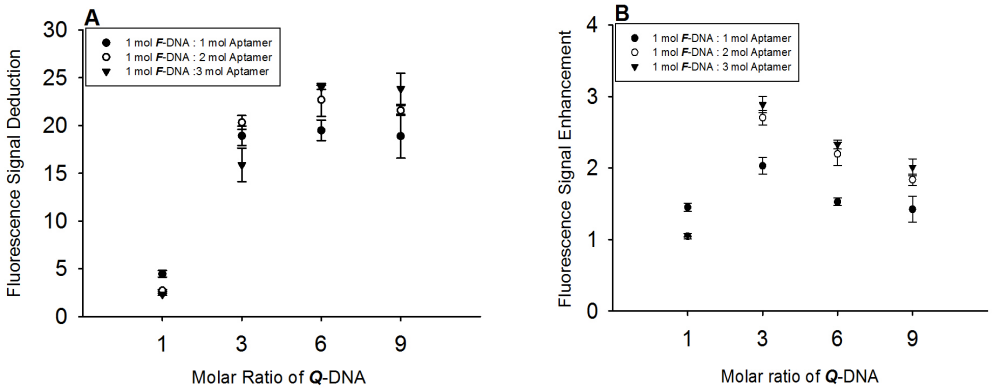

Figure S3-2. Optimization of Ratio of RNA aptamer with F-DNA and Q-DNA complementary strands. (A) Fluorescence signal deduction of 1 mole of F-DNA strand with 1-3 moles of RNA aptamer and 1-9 moles Q-DNA strands. (B) Fluorescence signal enhancement of 1 mole of F-DNA strand with 1-3 moles of RNA aptamer and 1-9 moles of Q-DNA strands upon addition of 2 mM of ATP. Each duplex was incubated for 5 minutes before fluorescence signal measurements were taken, followed by addition of 2 mM of ATP, incubated for 5 minutes again and took another fluorescence signal measurement.

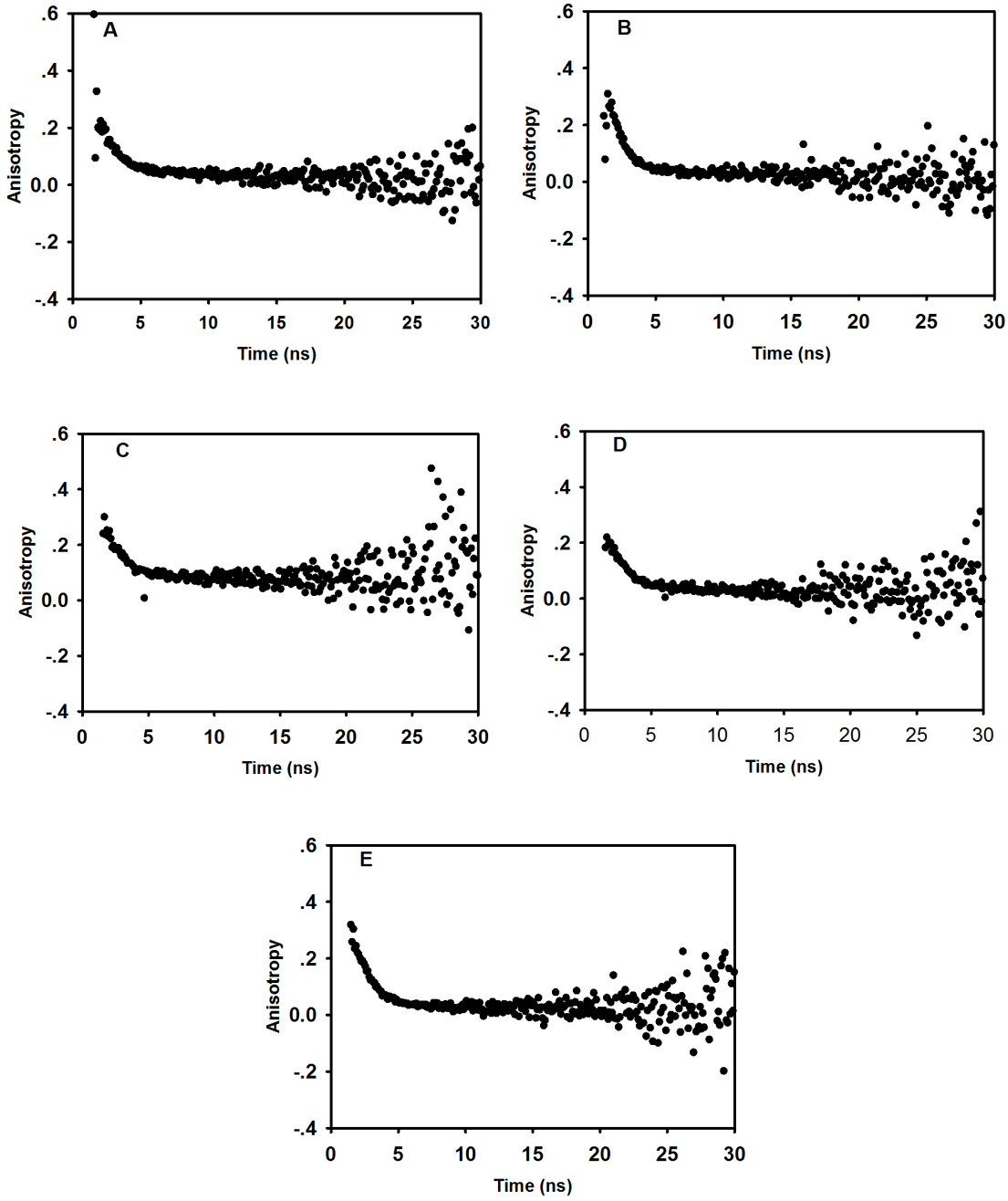

Figure S3-3. Time-resolved anisotropy decays for RNA ATP-binding aptamer in (A) solution; (B) in SS; (C) in TMOS; (D) in 20% MTMS/TMOS; and (E) in 40% MTMS/TMOS. All samples contained 1 μM aptamer. Excitation: 490 nm; emission: 532 nm; bandwidth: 32 nm for both excitation and emission paths

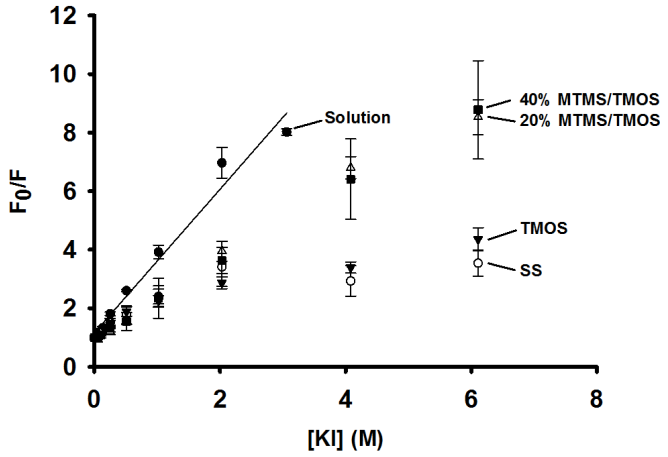

Figure S3-4. Stern-Volmer plot of quenching of fluorescence for entrapped RNA aptamer by iodide upon addition of anionic quencher: (●) solution, (○) SS,(▲) TMOS, (Δ) 20% MTMS/TMOS, (■)40% MTMS/TMOS

Table S3-1. TRFA decay parameters of ATP-binding RNA aptamer in solution or entrapped in silica derived from various precursors.

Sample	ϕ_1 /ns	ϕ_2 /ns	f_1 [a]	f_2	g	r_0 [b]	r_∞ [b]	χ^2	r_{ss} [c]
F-DNA Strand Only	0.43 ± 0.13	2.76 ± 0.46	0.67	0.31	0.01	0.29	0.004	1.02	0.03
In solution	0.56 ± 0.13	4.89 ± 0.97	0.49	0.41	0.01	0.26	0.03	1.13	0.15
In SS	0.59 ± 0.17	5.08 ± 0.31	0.70	0.26	0.11	0.32	0.04	1.03	0.22
In TMOS	0.70 ± 0.04	3.76 ± 0.28	0.46	0.25	0.29	0.32	0.09	0.95	0.24
In 20% MTMS/TMOS	0.54 ± 0.04	3.19 ± 0.61	0.65	0.25	0.10	0.31	0.03	1.07	0.21
In 40% MTMS/TMOS	0.59 ± 0.06	3.48 ± 0.61	0.71	0.21	0.08	0.29	0.02	1.05	0.20

[a] The typical error in fractional contributions of anisotropy decay times is ±5% to 10%. [b] Typical errors in r_0 and r_∞ values are ±5%. [c] Typical errors in stead-state anisotropy values are ±0.008. All samples were tested in triplicate.

CHAPTER 4.

A PAPER SENSOR PRINTED WITH MULTIFUNCTINOAL BIO/NANO MATERIALS

Author's Preface:

This following chapter is submitted as a full article to the journal, *Angewandte Chemie International Edition*, under the authorship of Christy Y. Hui, Meng Liu, Yingfu Li, and John D. Brennan. I was responsible for all the experimental protocols, performance of said experiments, data collection, analysis and interpretation. Dr. Meng Liu helped with experimental design. I wrote the first draft of the manuscript and Dr. Brennan and Dr. Li provided editorial input to generate the final draft.

4.1 ABSTRACT

We report a dual-response paper aptasensor platform that uses two reaction zones and a connecting bridge along with printed multifunctional bio/nano materials to achieve molecular recognition and signal amplification. Upon addition of analyte to the first zone, a fluorescently labelled DNA or RNA aptamer is desorbed from printed graphene oxide, producing an initial fluorescence signal. The released aptamer then flows to the second zone where it reacts with printed reagents to initiate rolling circle amplification, generating DNA amplicons containing a peroxidase-mimicking DNAzyme, which produces a colorimetric readout as a secondary response. The sensor was demonstrated using an RNA aptamer for adenosine triphosphate (a bacterial marker) and a DNA aptamer for glutamate dehydrogenase (*Clostridium difficile* marker) with excellent sensitivity and specifcity. These targets could be detected in spiked serum or feacal samples, demonstrating the potential for testing clinical samples.

4.2 INTRODUCTION

Paper based analytical devices have been increasingly utilized as low cost and user-friendly point-of-care (POC) diagnostic tools.[1] Given the availability of high throughput printers, such devices are also amenable to rapid and scaleable manufacturing,[2] and can be produced using minute amounts of reagents for tests that require microliter sample volumes. Until now, the vast majority of paper-based sensors have relied on protein-based assays utilizing well-known enzyme[3] or antibody-based[4] reactions, or used nucleic acids to detect complementary DNA.[5] In the case of nucleic

acid detection, isothermal amplification methods such as recombinase polymerase amplification (RPA),[6] loop-mediated isothermal amplification (LAMP),[7] helicase dependent amplification (HDA),[8] strand displacement amplification (SDA)[5c,9] and rolling circle amplification (RCA)[10] can all be performed on paper devices, resulting in extremely low detection limits.

Our group and others have recently reported on simple paper sensors that utilize either DNA aptamers[11] or DNAzymes[12] to generate colorimetric or fluorescence outputs upon introduction of target. While these were capable of detecting analytes with good sensitivity, none of these paper-based sensors has incorporated molecular amplification directly on the device to improve detection limits for non-nucleic acid targets.

Our groups have also reported a number of different methods by which DNA aptamers or DNAzymes can be linked to RCA.[13] Among these was a method whereby DNA aptamers were first desorbed from reduced graphene oxide upon target-induced structure switching, with the released aptamer then acting as a primer for RCA.[13d] The RCA reaction generated repetitive sequence units that could easily be detected using colorimetric or fluorimetric readouts. While these assays have been demonstrated in the solution phase, their integration into paper-based devices has not been demonstrated.

Herein, we report on the first paper-based analytical device to incorporate an aptamer for molecular recognition and rolling circle amplification for on-device isothermal signal amplification. The paper device is configured as a physically detachable sensor that allows for effective generation of two different signal outputs, a

prompt fluorescence output that can be read by an instrument and a delayed colorimetric output that can be detected using the naked eye. The detachable bridge design also prevents both unwanted forward flow during the sample incubation period and back flow when the sensing solution is transferred to a different location for signal amplification. We demonstrate the potential of the paper sensor for detection of infectious organisms using an RNA aptamer for ATP (a general bacterial marker)[14] and a DNA aptamer for glutamate dehydrogenase (GDH, a marker for *Clostridium difficile*).[15]

4.3 RESULTS AND DISCUSSION

The design of the paper sensor is illustrated in Figure 4-1. It consists of two pieces of paper on a backing card. The first piece is configured to be a molecular recognition-fluorescence readout zone (Zone 1), and the second piece contains a DNA amplification-colorimetric readout zone (Zone 2), with a bridge that can be used to transfer the reaction mixture from Zone 1 to Zone 2. The two reaction zones and the bridge are demarcated on a nitrocellulose surface using wax barriers.

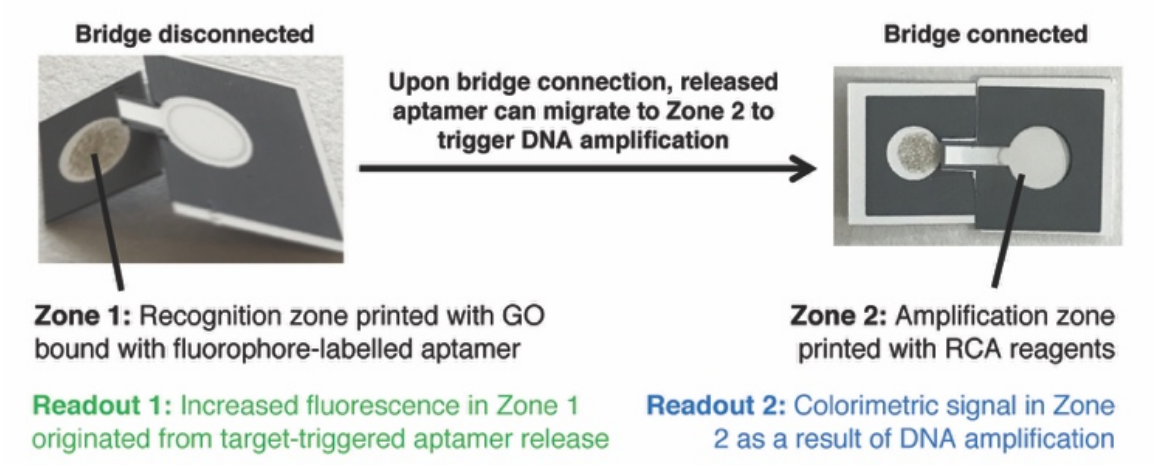

Figure 4-1. The design of dual output paper-based aptasensor. Zone 1 is printed with aptamer (Apt):GO complex and Zone is printed with a pullulan solution with RCA reagents. Upon addition of a test sample to Zone 1 and incubation for 30 minutes, the fluorescence intensity is read. The bridge is then connected to allow the solution mixture to migrate to Zone 2. After 1 minute, the bridge is disconnected. The RCA reaction is then conducted for 60 minutes, followed by addition of the colorimetric assay reagents. Colour appears in Zone 2 in about 5 minutes; a photo is then taken using a smartphone.

To produce a sensor, a fluorescently labeled RNA or DNA aptamer-graphene oxide (GO) mixture is first printed onto Zone 1. Figure S4-1 shows that the printed GO is strongly adsorbed to the nitrocellulose membrane, providing a useful platform to immobilize aptamers. Zone 2 contains a printed mixture of RCA reagents, including a circular DNA template (CDT), phi29 DNA polymerase (ϕ29DP), dNTPs and hemin, in a 10% (w/v) pullulan solution. The test sample is initially added to Zone 1 of the sensor in the "disconnected bridge" configuration, whereupon aptamer reporters that bind to the targets will "switch-off" from GO, causing dequenching of fluorescence from the fluorescent aptamer and producing an initial fluorescence signal. A sufficient reaction time is allowed in this configuration to provide high levels of desorbed aptamer (determined to be 30 min, see Figure S4-2), which can then migrate to Zone 2 in the

"connected bridge" configuration over a period of 30 sec (see Figure S4-3) and undergo RCA using either a fluorophore-labeled DNA strand (named FDNA) hybridized to the RNA aptamer (Figure S4-4, panel A) or a fluorophore-labelled DNA aptamer itself (Figure S4-4, panel B) as a primer for RCA (Figure S4-4, panels C and D).[13d] The RCA products (RP) contain repetitive units of a peroxidase-mimicking DNAzyme, PW17,[16] which generate a colourimetric signal in the presence of H_2O_2 and chromogenic compounds such as 3,3',5,5'-tetramethylbenzidine (TMB) and 2,2'-anizo-bis(3-ethylbenzithiazoline-6-sulfonic acid) (ABTS).

Optimization experiments indicated that 600 nM of both the RNA aptamer (Figure S4-5) and DNA aptamer (Figure S4-6) on GO gave the best response in both fluorescence and colorimetric modes, as higher levels led to excess unadsorbed aptamer. Note that ABTS and TMB were used in combination to generate a colorimetric readout based on our observation that even though the colour development time for ABTS was fast (a few seconds), it disappeared relatively quickly (~5 minutes). In contrast, the combination of TMB and ABTS made both color development time (5 minutes) and color loss time (~10 minutes) more manageable (Figure S4-7).

Initial studies indicated very strong binding between the RNA and DNA aptamers and the GO. In the case of the DNA aptamer for GDH, we had previously determined that addition of the CDT allowed for facile target-induced desorption of the aptamer from GO.[13d,16] For the RNA aptamer, we examined the use of a "helper DNA (HDNA) strand" complementary to the aptamer, as a modulator to control the target-induced release of the RNA aptamer from GO.[17] Given that GO has greater affinity for single-stranded (ss)

DNA relative to double-stranded DNA and that the size of single-stranded DNA can affect its affinity for GO,[18] we examined varying lengths of HDNA to fine-tune the aptamer/GO affinity. Consistent with a previous findings,[17] hybridization of a 12-nucleotide HDNA to the RNA aptamer caused a weakening of the RNA/GO interaction, which in turn allowed a much higher amount of the RNA aptamer to desorb upon addition of target (Figure S4-8). Importantly, inclusion of the HDNA on the RNA aptamer did not affect the ability of the released aptamer to initiate RCA (Figure S4-8), likely owing to the use of the FDNA as the RCA primer.

Figure 4-2 shows the fluorescence and colorimetric outputs from both the ATP and GDH sensors along with control experiments to confirm the mechanism of action of each sensor when tested separately. For the ATP system (Figure 4-2A), addition of 2 mM ATP alone (lane 2) or with CDT (lane 4) resulted in an increase in fluorescence intensity, due to the release of the aptamer (revealed by agarose gel analysis; bottom gel). On the contrary, adding the buffer only (lane 1) or the buffer containing CDT did not cause release of the aptamer (lane 3). For the GDH system (Figure 4-2B), only the simultaneous addition of GDH and CDT (lane 4) resulted in substantial release of the GDH aptamer. Addition of GDH alone (lane 2) only resulted in a small fluorescence signal, corresponding to minimal release of the labelled GDH aptamer. In this case, the CDT binds to the primer region that extends from the aptamer, causing weakening of the aptamer/GO complex and facilitating target-induced desorption, as described previously.[13d]

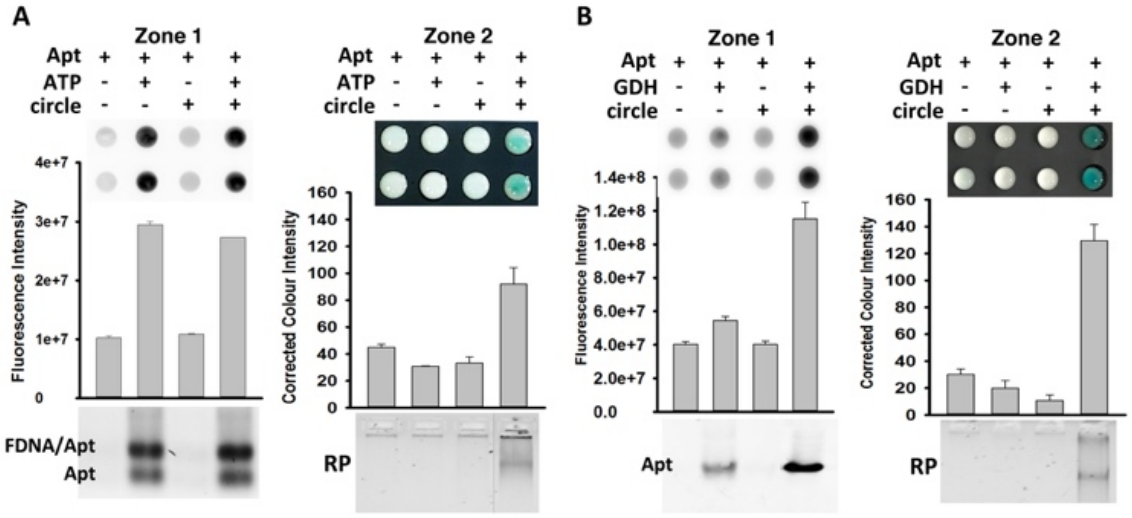

Figure 4-2. Examination of functionality of aptamer/GO paper sensors. (**A**) ATP sensor. (**B**) GDH sensor. Left panel: Fluorescence image (top), fluorescence intensity (middle) and agarose analysis of **(A)** ATP and **(B)** GDH system upon addition of: lane 1 – buffer; lane 2 – target (ATP or GDH) only; lane 3 – circular DNA template only; lane 4 – target (ATP or GDH) and circular DNA template. Right panel: Colorimetric image (top), color intensity (middle) and agarose gel analysis (bottom) of RCA reaction mixtures produced with the same samples taken from the left panel. After 60-minute RCA reaction, 1 µL H_2O_2, 1 µL TMB and 1 µL ABTS were added to initiate the colorimetric reaction. The image was captured by an iPhone at 5 minutes after all components were added. Note that for the ATP sensor, FDNA:Apt = 1:3.

Attempts to perform the RCA directly on Zone 1 were unsuccessful as the desorbed aptamer readsorbed on the GO surface over time and led to no RCA products (data not shown). As a result, the reaction mixtures were transferred to separate microzones containing the printed RCA reagents. The right panel of Figure 4-2A (ATP sensor) and 4-2B (GDH sensor) shows that only the microzones that contained both targets and CDT generated a colorimetric signal. Taken together, these results demonstrate that both the ATP-binding RNA aptamer and GDH-binding DNA aptamer can ”switch-off” from GO upon target addition, and the released aptamers can successfully initiate RCA.

We then assembled the paper-based aptasensor as shown in Figure 4-1 and examined the migration of released aptamer from Zone 1 to Zone 2 through the connecting bridge upon paper folding. Initial studies (Figure S4-9A) demonstrated that the fluorescence signal was enhanced in Zone 1 upon target addition, indicating release of the fluorescent aptamer from the GO, and that upon connecting the bridge, the fluorescence intensity in Zone 2 increased while the fluorescence intensity in Zone 1 decreased (Figure S4-9B), indicating that the aptamers traveled from Zone 1 to Zone 2. Furthermore, it was determined that the RCA reaction and colorimetric assay in Zone 2 was initiated in the presence of target (Fig. S4-9C), as indicated by the presence of the colour output. Taken together, these results show that the dual-response sensor can produce analyte-triggered fluorescence and amplified colorimetric responses on a single device.

The sensitivity of each response mode of the paper-based aptasensors was then analyzed for both GDH (Figure 4-3) and ATP (Figure S4-10). It was observed that both the fluorescence (Panel A) and colour intensity (Panel B) generated were proportional to the concentrations of GDH (Figure 4-3) and ATP (Figure S4-10).

The sensor provided a detection limit (LOD) (3σ/slope) of ~10 μM for both the fluorescence readout and colorimetric readout in the case of the ATP aptasensor, and LOD values of ~3 nM for both the fluorescence and colorimetric readouts for the GDH aptasensor, demonstrating that the inclusion of a 60 min amplification step allowed the color based readout to match the fluorescence readout. Both of the LOD values (ATP and GDH) were similar to or better than the values obtained in solution-based fluorescence

assays (LOD of the ATP-binding RNA aptamer = 100 μM; GDH-binding DNA aptamer = ~1 nM[15]). The sensor also exhibited excellent selectivity for its cognate targets (Figure S4-11). No fluorescence or colour-based signal was generated when GTP, UTP or CTP were added to the ATP sensor, or when Tcd A (Toxin A) or Tcd B (Toxin B) from *C. difficile*, or BSA were added to the GDH sensor.

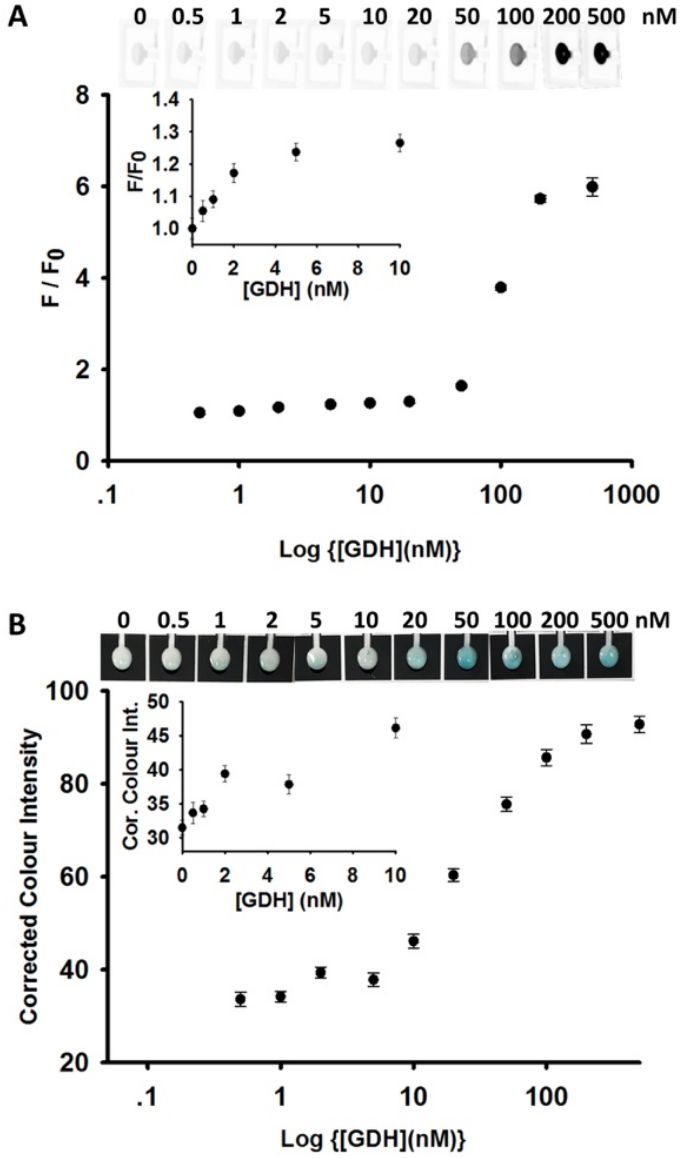

Figure 4-3. Detection of GDH using the printed GDH sensor. Concentration-response curves for **(A)** fluorescence readout and **(B)** colorimetric readout for GDH detection using the DNA aptamer. Different concentrations of GDH were introduced to Zone 1, then incubated for 30 minutes followed by fluorescence imaging. The solution was then migrated to Zone 2 by closing the bridge; RCA was performed for 1 min, after which H_2O_2, TMB and ABTS were added to initiate the colorimetric reaction. The image was captured by an iPhone 5 minutes after all components were added and analyzed by ImageJ to produce a color intensity value.

We next evaluated the utility of the paper-based aptasensors as potential point-of-care devices for testing of clinical samples. Analyte (ATP or GDH) was spiked into 50%

human serum and/or patient stool samples to examine if the aptasensors could operate in the presence of interfering compounds and in samples containing nucleases that could degrade the RNA or DNA aptamers.

Figure 4-4 shows that ATP and GDH targets spiked into human serum or stool samples generated the expected fluorescence and colorimetric signals, while both signals remained low in the presence of negative control samples containing no targets. This is particularly noteworthy in the case of the RNA aptamer, which can be easily degraded by nucleases in solution. Even direct addition of RNase A or H to the RNA aptamer/GO complex on paper (Figure S4-12) produced minimal degradation of the aptamer, showing that the GO effectively protects the RNA aptamer from degradation.[19] Similar results were obtained for the GDH aptamer/GO complex, where DNase I produced minimal degradation or either the fluorescence or colorimetric signals (Figure S4-12).

Finally, we evaluated the long-term stability of both aptamers on the paper sensor. The aptasensors were stored at 4 °C after assembly and tested periodically over 30 days. As shown in Fig. S4-13, the aptasensors were able to generate both a fluorimetric and colorimetric signal upon storage for at least one month (signal on Day 30 was about ~75% of Day 1 for the ATP sensor and ~79% for the GDH sensor). Interestingly, all of the loss in activity occurred in the first 10 days for both sensors, suggesting that a fraction of the adsorbed aptamers may have been degraded, or that a fraction of the adsorbed enzyme (ϕ29), perhaps at the surface of the pullulan film, was in an environment that was susceptible to denaturation. Given the concordance between fluorescence and colorimetric data, it is most likely that instability occurs in Zone 1 owing to degradation

of aptamers rather than instability of RCA reagents. Overall, this study demonstrates that the biomolecules (DNA and RNA aptamers as well as RCA reagents) can be effectively protected from degradation upon adsorption onto GO (RNA/DNA aptamers) or encapsulation in pullulan, in agreement with previous reports.[20]

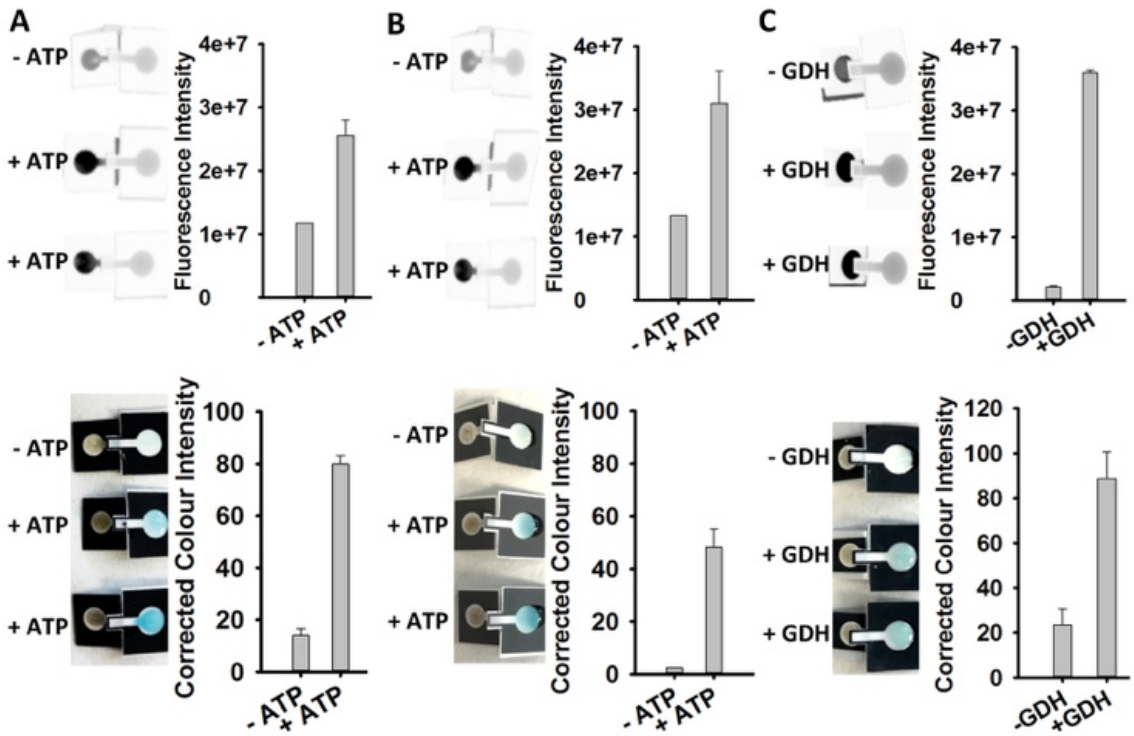

Figure 4-4. Robustness of dual-response paper sensors. (A) The ATP sensor with 1:1 ratio of human blood serum spiked with 2 mM ATP. (B) The ATP sensor with 1:1 ratio of stool sample spiked with 2 mM ATP. (C) The GDH sensor with 1:1 ratio of stool sample spiked with 500 nM GDH.

4.4 CONCLUSIONS

In conclusion, this work demonstrates that dual-response detection of targets is possible using aptamers printed onto paper devices with a connecting bridge design, wherein an initial fluorescence response based on aptamer desorption from GO can be followed by an amplified colorimetric response using RCA. Such a system allows for both a prompt instrument-based fluorescence readout and a delayed colorimetric readout after an amplification step. The sensor can utilize either RNA or DNA aptamers as recognition elements to detect both small molecules and proteins. Inclusion of an isothermal amplification step can significantly improve LOD values for colorimetric assays to equal those of fluorescence assays. Finally, the paper sensor is amenable to direct analysis of clinical samples (serum or stool), demonstrating the versatility of the sensor. This low-cost and highly functional paper-based biosensor should provide a useful platform for point-of-care and in-field applications.

4.5 ACKNOWLEDGMENTS

We thank the Natural Sciences and Engineering Research Council of Canada (NSERC), Ministry of Research and Inovation (Ontario Research Fund) and Pro-Lab Developments for funding this work. We also thank the Canada Foundation for Innovation for support of this work. J.D.B. holds the Canada Research Chair in Bioanalytical Chemistry and Biointerfaces.

4.6 REFERENCES

[1] a) R. Pelton, *Trends Anal. Chem.* **2009**, *28*, 925; b) A. W. Martinez, S. T. Philips,G. M. Whitesides, *Anal. Chem.* **2010,** *82*, 3; c) X. Li, D. R. Ballerini, W. Shen, *Biiomicrofluidics* **2012,** *6*, 011301; d) V. Gubala, L. F. Harris, A. J. Ricco, M. X. Tan, D. E. Williams, *Anal. Chem.* **2012,** *84*, 487; e) A. K. Yetisen, M. S. Akram, C. R. Lowe, *Lab Chip* **2013,** *13*, 2210; f) C. Parolo, A. Merkoci, *Chem. Soc. Rev.* **2013,** *42*, 450; g) N. Komuro, S, Takaki, K. Suzuki, D. Citterio, *Anal. Bioanal. Chem.* **2013,** *405*, 5785; h) J. Hu, S. Wang, L. Wang, F. Li, B. Pingguan-Murphy, T. J. Lu, F. Xu, *Biosens. Bioelectron.* **2014,** *54*, 585; i) S. F. Cheung, S. K. L. Cheng, D. T. Kamei, *JALA* **2015,** *20*, 316; j) R. Derda, et al., *PLOS Negl. Trop. Dis.* **2015,** *9*, e0003676.

[2] C. R. Mace, R.N. Deraney, *Microfluid. Nanofluidics* **2014,** *16*, 801.

[3] a) A. W. Martinez, S. T. Phillips, M. J. Butte, G. M. Whitesides, *Angew. Chem. Int. Ed.* **2007**, *46*, 1318; c) W. Zhao, M. M. Ali, S. D. Aguirre, M. A. Brook, Y. Li, *Anal. Chem.* **2008**, *80*, 8431; c) S. M. Z. Hossain, R. E. Luckham, M. J. McFadden, J. D. Brennan, *Anal. Chem*. **2009**, *81*, 9055; c) Z. Zhang *et al.*, *Analyst* **2014,** *139*, 4775.

[4] a) C.-M. Cheng, A. W. Martinez, J. Gong, C.R. Mace, S. T. Phillips, E. Carrilho, K. A. Mirica, G. M. Whitesides, *Angew. Chem. Int. Ed.* **2010,** 49, 4771; b) M. S. Verma, M.-N. Tsaloglou, T. Sisley, D. Christodouleas, A. Chen, J. Milette, G. M. Whitesides, *Biosens. Bioelectron.* **2018**, *99*, 77; c) G. E. Fridley, L. Huy, P. Yager, *Anal. Chem.* **2014**, *86*, 6447.

[5] a) M. M. Ali, S. D. Aguirre, Y. Xu, C. D. Filipe, R. Pelton, Y. Li, *Chem Comm.* **2009**, *43*, 6640; b) K. Scida, B. Li, A. D. Ellington, R. M. Crooks, *Anal. Chem.* **2013,** *85*, 9713; c) X. Li, K. Scida, R. M. Crooks, *Anal. Chem*. **2015**, *87*, 9009; c) J. Li, J. Macdonald, *Lab Chip* **2016**, *16*, 242; d) L. K. Lafleur, et al., *Lab Chip* **2016,** *16*, 3777; e) L. Magro, *et al.*, *Lab Chip* **2017**, *17*, 2347; f) L. Rivas, A. de la Escosura Muñiz, L. Serrano, L. Altet, O. Francino, A. Sánchez, A. Merkoçi, *Nano Res*. **2015**, *8*, 3704.

[6] L. Magro, B. Jacquelin, C. Escadafal, P. Garneret, A. Kwasiborski, J.-C. Manuguerra, F. Monti, A. Sakuntabhai, J. Vanhomwegen, P. Lafaye, P. Tabeling, *Sci. Rep.* **2017**, *7*, 1347.

[7] a) C. Liu, E. Geva, M. Mauk, X. Qiu, W. Abrams, D. Malamud, K. Curti, S. Owen, H. Bau, *Analyst* **2011**, *136*, 2069; b) J. Linnes, N. Rodriguez, L. Liu, C. Klapperich, *Biomed. Microdevices*, **2016**, 18.

[8] S. Prasad, G. Dipayan, S. Minakshi, T. Aparna, P. Dabjani, *RSC Adv*. **2016**, 56205.

[9] B.J. Toley, *et. al.*, *Analyst* **2015,** *140*, 7540.

[10] M. Liu, C.Y. Hui, Q. Zhang, J. Gu, B. Kannan, S. Jahanshahi-Anbuhi, C.D.M. Filipe, J.D. Brennan, Y. Li, *Angew. Chem. Int. Ed* **2016,** *55*, 2709.

[11] a) J. Liu, Y. Lu, *Angew. Chem. Int. Ed* **2006,** *45*, 90; b) J. Liu, D. Mazumdar, Y. Lu, *Angew. Chem. Int. Ed* **2006,** 45, 7955-7959; c) S. Su, R. Nutiu, C. D. Filipe Y. Li, R. Pelton, *Langmuir* **2007**, *23*,1300; d) S. Su, M. M. Ali, C. D. Filipe, Y. Li, R. Pelton, *Biomacromolecules* **2008**, 9, 935; e) C. Carrasquilla, J. R. Little, Y. Li, J. D. Brennan, *Chem. Eur. J.* **2015,** *21*, 7369.

[12] a) J. C. Cunningham, N.J . Brenes, R. M. Crooks, *Anal. Chem.* **2014**, *86*, 6166; b) Y. Zhang, D. Gao, J. Fan, J. Nie, S. Le, W. Zhu, J. Yang, J. Li, *Biosens. Bioelectron.* **2016**, *78*, 538.

[13] a) M. M. Ali, Y. Li, *Angew. Chem. Int. Ed.* **2009**, *48*, 3512; b) S. A. McManus, Y. Li, *J. Am. Chem. Soc.* **2013**, *135*, 7181; c) L. Wang, K. Tram, M. M. Ali, B. J. Salena, J. Li, Y. Li, *Chem. Eur. J.* **2014**, 20, 2420; d) M. Liu, J. Song, S. Shuang, C. Dong, J. D. Brennan, Y. Li, *ACS Nano* **2014,** 8, 5564; e) M. Liu, Q. Zhang, Z. Li, J. Gu, J. D. Brennan, Y. Li, *Nat. Commun*. **2016**, *7*, 12074; f) M. Liu, Q. Zhang, D. Chang, J. Gu, J. D. Brennan, Y. Li, *Angew. Chem. Int. Ed.* **2017**, *56*, 6142.

[14] M. Sassanfar, J. W. Szostak, *Nature* **1993**, *364*, 550.

[15] M. Liu, Q. Yin, J. D. Brennan, Y. Li, *Biochimie* **2017,** pii: S0300-9084(17)30224-9. doi: 10.1016/j.biochi.2017.08.015

[16] a) P. Travascio, Y. Li, D. Sen, *Chem. Biol.* **1998**, *5*, 505 –517; b) P. Travascio, P. K. Witting, A. G. Mauk, D. Sen, *J. Am. Chem. Soc.* **2001**, *123*, 1337–1348; c) Z. Cheglakov, Y. Weizmann, B. Basnar, I. Willner, *Org. Biomol. Chem.* **2007**, *5*, 223–225; d) D. Chang, S. Zakaria, M. Deng, N. Allen, K. Tram, Y. Li, *Sensors*. **2016**, *16*, 2061.

[17] J. Song, P. S. Lau, M. Liu, S. Shuang, C. Dong, Y. Li, *ACS Appl. Mater. Interfaces* **2014,** 6, 21806-21812.

[18] a) M. Wu, R. Kempaiah, P.-J. Huang, V. Maheshwari, J. Liu, *Langmuir* **2011,** 27, 2731; b) Liu, B.; Sun, Z.; Zhang, X.; Liu, J., *Anal. Chem.* **2013,** 85, 7987; c) L. Gao, C. Lian, Y. Zhou, L. Yan, Q. Li, C. Zhang, et al., *Biosens. Bioelectron.* **2014**, *60*, 22; d) M. Liu, W. Zhang, D. Chang, Q. Zhang, J. D. Brennan, Y. Li, *Trends Anal. Chem.* **2015,** 74, 120-129; e) J. Lee, Y. Yim, S. Kim, M.-H. Choi, B.-S. Choi, Y. Lee, D.-H. Min, *Carbon* **2016,** 97, 92.

[19] L. Cui, Z. Chen, Z. Zhu, X. Lin, X. Chen, C. J. Yang, *Anal. Chem.* **2013,** 85, 2269.

[20] a) S. Jahanshahi-Anbuhi, K. Pennings, V. Leung, M. Liu, C. Carrasquilla, B. Kannan, Y. Li, R. Pelton, J. D. Brennan, C. D. M. Filipe, *Angew. Chem. Int. Ed.* **2014,** 53, 6155; b) P.-Y. Hsieh, M. M. Ali, K. Tram, S. Jahanshahi-Anbuhi, C. L. Brown, J. D. Brennan, C. D. M. Filipe, Y. Li, *ChemBioChem* **2017,** 18, 502-505.

4.7 APPENDIX

4.7.1 Supplementary Information

A. Experimental Details

Oligonucleotides and Other Materials
All DNA oligonucleotides were obtained from Integrated DNA Technologies (IDT), and purified by high-performance liquid chromatography (HPLC). All oligonucleotide sequences are listed in Table S1. T4 polynucleotide kinase (PNK), T4 DNA ligase and phi 29 DNA polymerase (ϕ29DP) were purchased from Thermo Scientific. Glutamate dehydrogenase (GDH) was obtained from List Biological Laboratories Inc. (Campbell, California, US). Sybr Gold (10,000x concentrated stock in DMSO) was purchased from Life Technologies (Burlington, ON, Canada). Pullulan (molecular weight of ~200,000 Daltons) was obtained from Polyscience Inc. Nitrocellulose membranes with a plastic backing (HF 180 4XSS) were obtained from Millipore. All other chemicals, including graphene oxide (GO), hydrogen peroxide, 3,3′,5,5′-tetramethylbenzidine (TMB) and 2,2′-anizo-bis(3-ethylbenzithiazoline-6-sulfonic acid) (ABTS) were purchased from Sigma-Aldrich (Oakville, Canada) and used without further purification.

Preparation of Circular DNA Templates
Circular DNA templates were synthesized from 5′-phosphorylated linear DNA oligonucleotides through template-assisted ligation using T4 DNA ligase. The protocol for phosphorylation of DNA is described elsewhere.[1] 200 pmol of circular template was first mixed with 10 U PNK and 1 mM ATP in 100 μL of 1x PNK buffer A (final concentration: 50 mM Tris-HCl, pH 7.6, 10 mM $MgCl_2$, 5 mM DTT, 0.1 mM spermidine). The mixture was then incubated at 37 °C for 40 minutes, followed by heating at 90 °C for 5 minutes. Then, 300 pmol of ligation template was added, heated at 90 °C for 5 minutes, and cooled at room temperature for 15 minutes. Next, 15 μL of 10x T4 DNA ligase buffer (400 mM Tris-HCl, 100 mM $MgCl_2$, 100 mM DTT, 5 mM ATP, pH 7.8 at 25 °C) and 1 μL of 10 U T4 DNA ligase was added to the above mixture (total 150 μL). The resultant mixture was then incubated at room temperature for 2 h before heating at 90 °C for 5 minutes to deactivate the ligase. The ligated circular DNA products were concentrated by standard ethanol precipitation and purified by 10% dPAGE.

Preparation of Aptamer reporters
In case of RNA aptamer reporters, polymerase chain reaction (PCR) of the DNA templates for the ATP-binding RNA aptamer and RNA transcription for this aptamer were performed as described elsewhere.[2] A tripartite aptamer complex (in a 1:2:3 F′DNA/RNA/HDNA molar ratio) was prepared at double the concentration of typical solutions in 20 mM Tris buffer (pH 7.60) with 50 mM NaCl and 5 mM $MgCl_2$. This mixture was first heated at 65 °C for 2 minutes, cooled at room temperature for 10 minutes, and then stored at 4 °C for at least 1 h before mixing with a 1:1 volume ratio of graphene oxide (C_f = 0.1 mg/mL). In case of the GDH aptamer, the aptamer was

prepared at double the concentration in 2x PBS (100 mM, pH 7.6) containing 300 mM NaCl and 0.04% Tween-20.

Preparation of Aptamer:GO mixtures

To prepare aptamer:GO mixtures, the ATP- or GDH-binding aptamer (C_f = 600 nM) was mixed in a 1:1 volume ratio with graphene oxide (C_f = 0.1 mg/mL) and incubated at room temperature for 30 minutes. The aptamer:GO mixture was then blocked with 1% BSA and incubated at room temperature for 30 minutes. The mixture was then spun down at 14, 000 rpm for 5 minutes at 4 °C. The supernatant was then removed and the aptamer:GO complex was resuspended to the original 600 nM concentration in the appropriate buffer for the RNA or DNA aptamer. The resulting mixture was then ready to be printed.

Fabrication of aptamer µPAD sensor

To facilitate the immobilization of the aptamer:GO assembly, we first printed outlines of the sample loading and fluorescence signaling zone (Zone 1) and the amplification and colorimetric readout zone (Zone 2), along with a connecting channel, on a nitrocellulose membrane using a wax printer (Xerox ColourQube 8570N), followed by heating at 120 °C for 2 min to melt the wax through the membrane to form hydrophobic barriers. Next, the RNA or DNA aptamer:GO assembly was printed onto Zone 1 using a Canon MX280P inkjet printer (30 layers). Fig. S1 shows that the printed GO was strongly adsorbed to the NC membrane, providing a useful platform to immobilize the aptamers. The mixture of RCA reagents containing 1 pmol of ligated circular DNA, 1 µL of 10 mM dNTPs, 0.3 µL of 10 U ϕ29DP, 1 µL of 100 µM hemin and 5 µL of 10% (w/v) pullulan solution was then printed onto Zone 2 using a BioDot XYZ3060 automated lateral flow dispenser (~5 µL total volume printed). In all cases the printed zones were allowed to dry at RT for 1 h, after which Zones 1 and 2 were assembled together by putting both zones on a backing card, as shown in Figure 1. The fully integrated aptamer sensor was stored at 4 °C until use.

Evaluation of Dual-Response Paper Sensor Performance

In a typical experiment, 20 µL of sample solution was added to Zone 1 and incubated for 30 minutes. Fluorescence measurements (first response) of the released aptamer reporter were then obtained using a Biorad Chemidoc Imaging system. The fluidic channel was then connected and 20 µL of 1x RCA reaction buffer was added to Zone 1 to allow the released aptamer to flow to Zone 2 to initiate amplification. After 0.5 min the µPAD was then unfolded to break the fluidic channel in order to prevent back flow of the reaction mixture (see Fig. S3). RCA reactions were allowed to proceed at room temperature for 1 hour, after which the colourimetric assay was performed by introducing 3 µL of a mixture of a 1:1:1 volume ratio of 40 mM H_2O_2, 20 mM TMB and 50 mM of ABTS. After 5 min, images were obtained using an iPhone and processed using ImageJ (second response). To evaluate detection limits, 20 µL of various concentrations of ATP (0 - 2000 µM) or 1 pmol DNA circular template (CT) with GDH (0 – 500 nM) were added to Zone 1 and assays were performed as described above. Selectivity was evaluated by introducing 20

μL of 2 mM UTP, CTP or GTP to the ATP sensor, or 1 pmol CT with 500 nM of Toxin A or Toxin B or 1% (w/v) of BSA to the GDH sensor and performing assays as described above. The stability of the sensors was evaluated over a period of 30 days by introducing 2 mM of ATP to RNA aptamer sensors or 500 nM of GDH with 1 pmol CT to GDH sensors and assaying as above. Storage was done at 4 °C in the dark.

Nuclease resistance and signal recovery assay

20 μL of RNase A or RNase H (3 Units) was added to Zone 1 for RNA aptasensors while 20 μL of DNase I (3 Units) was added to Zone 1 for DNA aptasensors. Sensors were incubated for 30 minutes followed by fluorescence imaging as above. The nuclease solution was then removed and Zone 1 was then treated with 20 μL of Ribolock RNase Inhibitor (80U) for RNA aptasensors and 20 μL of DNase Inactivation Reagent (5 μL) for DNA aptasensors 3 times followed by 3 more washes with 20 μL of 1x RNA or DNA aptamer buffer to remove or inhibit any remaining nucleases. Next, 20 μL of 2 mM of ATP was added to Zone 1 for RNA aptasensors while 20 μL of 500 nM of GDH was added to Zone 1 for DNA aptasensors and incubated for 30 minutes followed by fluorescence imaging. The fluidic channel was then connected and 20 μL of 1x RCA reaction buffer was added to elute the aptamer to Zone 2, followed by the RCA reaction, colorimetric assay and data acquisition, as described above. Aptasensors that were not treated with nucleases were tested as outlined above and used as positive controls to establish a 100% signal level. The fluorescence or colour intensity of nuclease treated sensors was compared to that of positive control sensors to calculate a percent signal recovery, which wsa indicative of the amount of RNA or DNA aptamer that survived the nuclease treatment.

Evaluation of ATP and GDH in Serum and Feacal Samples

10 μL of 2 mM ATP or 1 pmol CT with 500 nM GDH was spiked into human serum or stool samples in a 1:1 volume ratio and mixed thoroughly. These samples were then assayed as described above. Samples consisting of a 1:1 volume ratio of 1x aptamer buffer solution to human serum or stool sample were used as negative controls. Fluorescence and colourimetric assays were performed using a 20 μL total sample volume, as outlined above.

B. Supporting Tables

Table S4-1. Sequence of DNA oligonucleotides used in this work

Name of oligonucleotides	Sequence (5'-3')
ATP DNA template for PCR	GAATT CTAAT ACGAC TCACT ATAGG CCTGC CACGC TCCGA CGCTA TCACT CTATG GGGTT GGGAA GAAAC TGTGG CACTT CGGTG CCAGC AACCC
Forward PCR primer	GAATT CTAAT ACGAC TCACT ATA
Reverse PCR primer	GGGTT GCTGG CAC
F´DNA	TAGCG TCGGA GCGTG GCAGG CTCAC TTCAA TTCAT CTGAC
HDNA	CCCCA TAGAG TG
Circular DNA template (for both RNA and GDH aptamers)	TTGAA GTGAG AAAAC CCAAC CCGCC CTACC CAAAA GTCAG ATGAA
Circular DNA ligation template	CTCAC TTCAA TTCAT CTGAC
DNA GDH aptamer-primer	TAGGA GGAGG TATTT AGTGC CAAGC CATCT CAAAC GACGT CTGAG TCGCA CTGCT CCTGC TCACT TCAAT TCATC TGAC
Fluorescently labeled F´DNA	F – TAGCG TCGGA GCGTG GCAGG CTCAC TTCAA TTCAT CTGAC
Fluorescently labeled GDH aptamer	F- TAGGA GGAGG TATTT AGTGC CAAGC CATCT CAAAC GACGT CTGAG TCGCA CTGCT CCTGC TCACT TCAAT TCATC TGAC

C. Supporting Figures

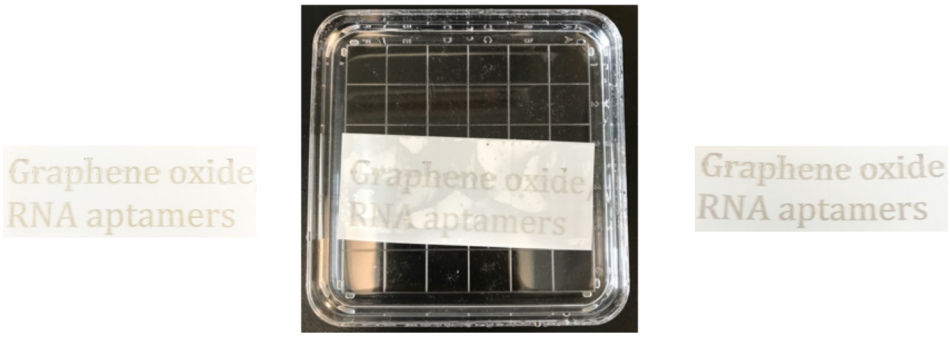

Figure S4-1. Printing of graphene oxide (GO). Left image: 30 layers of GO (0.1 mg/mL) was printed onto nitrocellulose paper using a Canon inkjet printer. Middle image: the printed paper was immersed in reaction buffer and was shaken for 30 minutes. Right image: the printed text after drying of the paper.

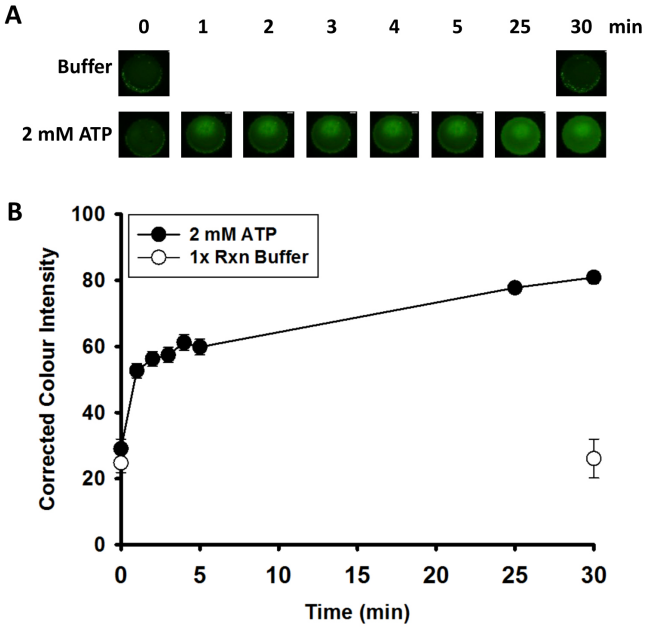

Figure S4-2. Optimization of signal development on paper. (A) Fluorescence images of the ATP sensor treated with reaction buffer only or with buffer containing 2 mM of ATP for increasing reaction times. (B) Signal intensity vs. reaction time.

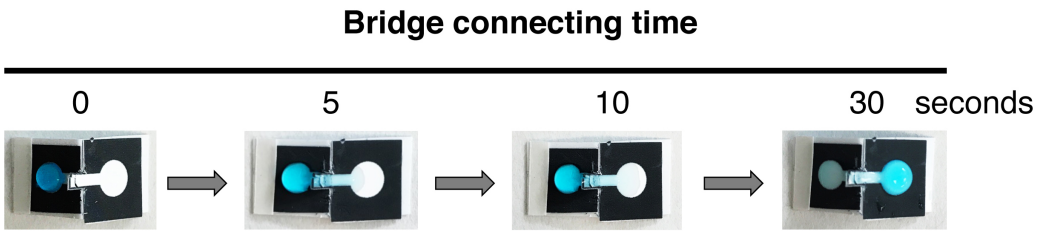

Figure S4-3. Connecting the bridge between Zone 1 (left zone) and Zone 2 (right zone) to allow for migration of solution from Zone 1 to Zone 2.

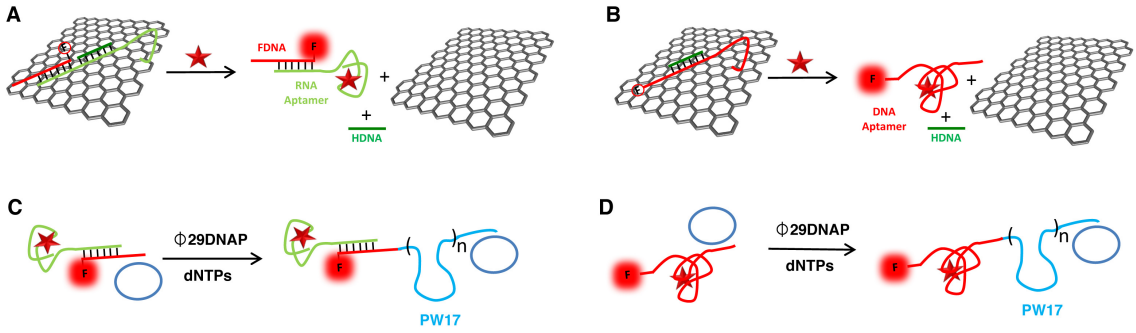

Figure S4-4. Graphic illustration of signaling mechanisms. Target-induced desorption of **(A)** FDNA-labeled RNA aptamer and **(B)** fluorescent DNA aptamer occurs first in Zone 1, followed by the RCA reaction with **(C)** the RNA aptamer and **(D)** the DNA aptamer migrated to Zone 2 from Zone 1 upon bridge connection. HDNA stands for "helper DNA", which is used to facilitate the aptamer desorption.

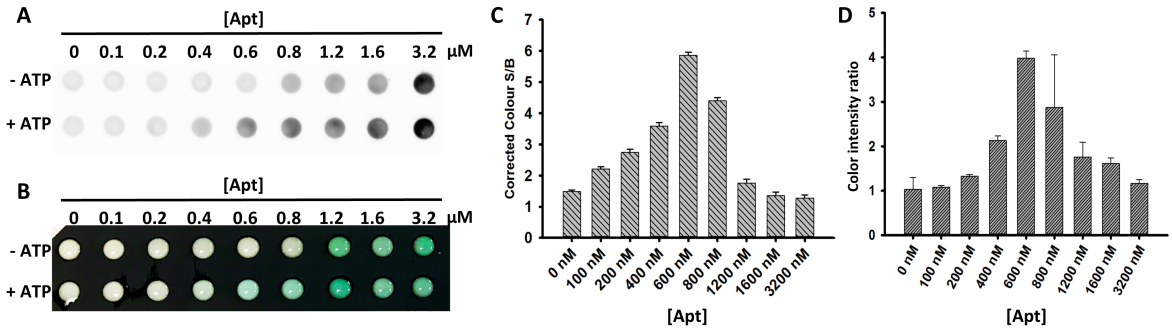

Figure S4-5. Optimization of the ATP sensor. **(A)** Fluorescence images of GO/aptamer complex upon incubation with reaction buffer ± 2 mM ATP for 30 minutes. GO was used at 0.1 mg/µl. **(B)** Colorimetric assay following RCA using mixtures taken from panel A. (C) Fluorescence ratio of +ATP/-ATP samples vs. aptamer concentration. (C) Color intensity ratio of +ATP/-ATP samples vs. aptamer concentration.

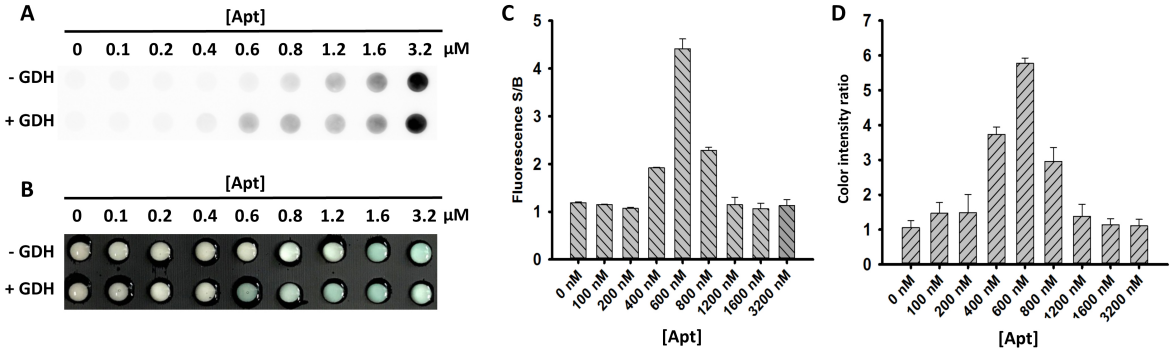

Figure S4-6. Optimization of the GDH sensor. **(A)** Fluorescence images of GO/aptamer complex upon incubation with reaction buffer ± 500 nM GDH for 30 minutes. GO was used at 0.1 mg/mL. **(B)** Colorimetric assay following RCA using mixtures taken from panel A. (C) Fluorescence ratio of +GDH/-GDH samples vs. aptamer concentration. (C) Color intensity ratio of +GDH/-GDH samples vs. aptamer concentration.

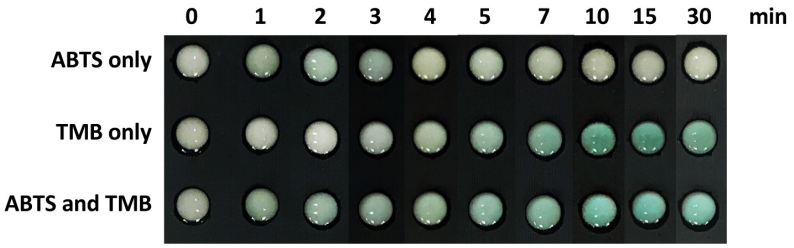

Figure S4-7. Evaluation of the use of 3,3',5,5'-tetramethylbenzidine (TMB) and 2,2'-anizo-bis(3-ethylbenzithiazoline-6-sulfonic acid) (ABTS) as chromogenic agents. The combination of TMB and ABTS offered a quicker color change (than TMB alone) that lasted much longer (than ABTS alone).

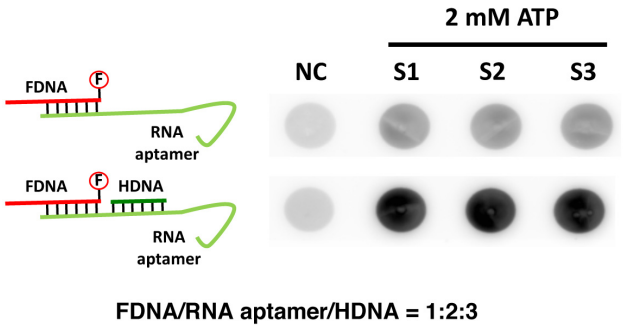

Figure S4-8. Ability of the ATP sensor to "switch-off" from GO with and without HDNA. HDNA is used as a modulator in this design. The fluorescence intensity of the FDNA/RNA aptamer duplex remained low upon addition of target (Top), indicating that without the HDNA strand, the release of the aptamer duplex was minimal. The fluorescence intensity of the FDNA/RNA aptamer/HDNA complex increased significantly upon target addition (bottom), revealing that the HDNA strand helped the release of the aptamer complex from GO upon target addition.

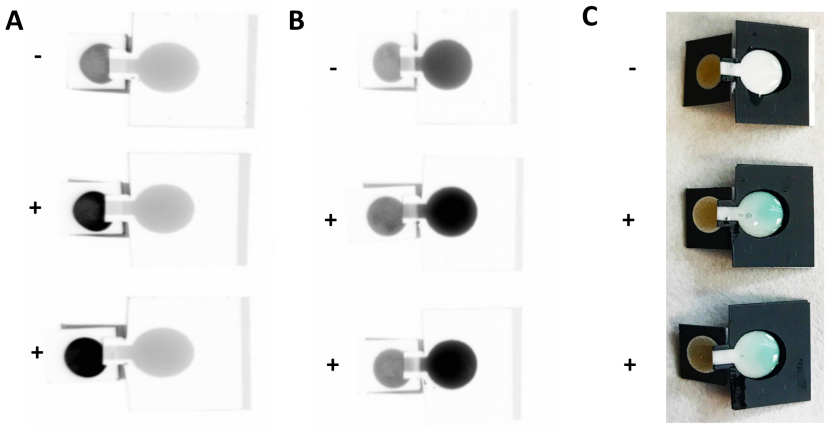

Figure S4-9. Dual-Response readouts of the ATP sensor. (A) Fluorescence readout of Zone 1 upon the addition of buffer or 2 mM ATP target in "open bridge" configuration. **(B)** Upon closing the bridge, the released aptamer travelled from Zone 1 to Zone 2, decreasing fluorescence in Zone 1 and increasing fluorescence in Zone 2. **(C)** Colorimetric readout in Zone 2 following RCA, which produces a peroxidase-mimicking DNAzyme that can oxidize TMB and reduce ABTS in the presence of hemin and H_2O_2. The bottom two sensors are replicates. 600 nM RNA aptamer complex was incubated with 0.1 mg/mL GO, and then deposited on Zone 1. 2 mM of ATP was added to Zone 1 and incubated for 30 minutes. Upon closing the bridge, the sample mixture was then flowed to Zone 2 by capillary action of paper. The RCA reaction was then performed for 1 hour.

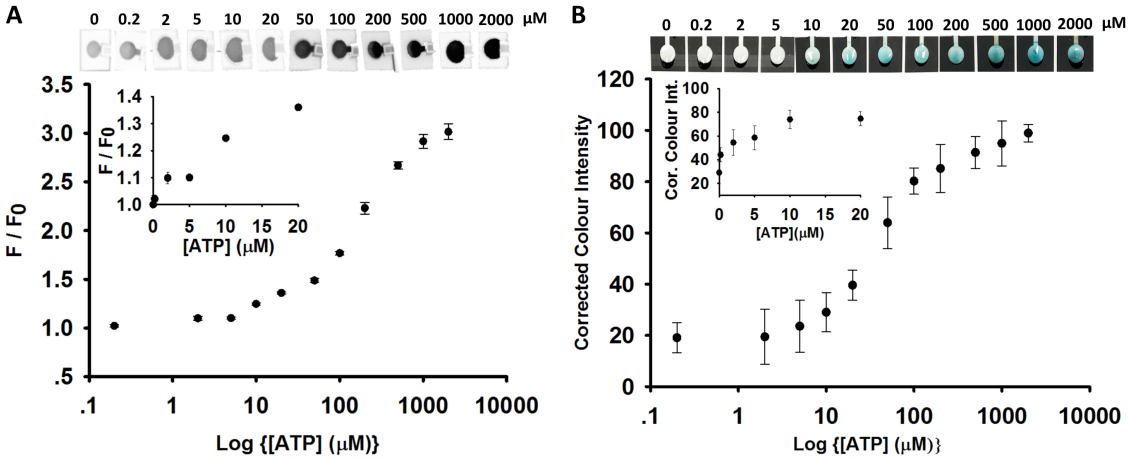

Figure S4-10. Detection of ATP Using the ATP Sensor. Concentration-response curves for **(A)** fluorescence readout and **(B)** colorimetric readout. Different concentrations of ATP were introduced to Zone 1, then incubated for 30 minutes followed by fluorescence imaging. The solution was then migrated to Zone 2 by closing the bridge; RCA was performed for 1 min, after which H_2O_2, TMB and ABTS were added to initiate the colorimetric reaction. The image was captured by an iPhone, 5 minutes after all components were added, and analyzed by ImageJ to produce a color intensity value

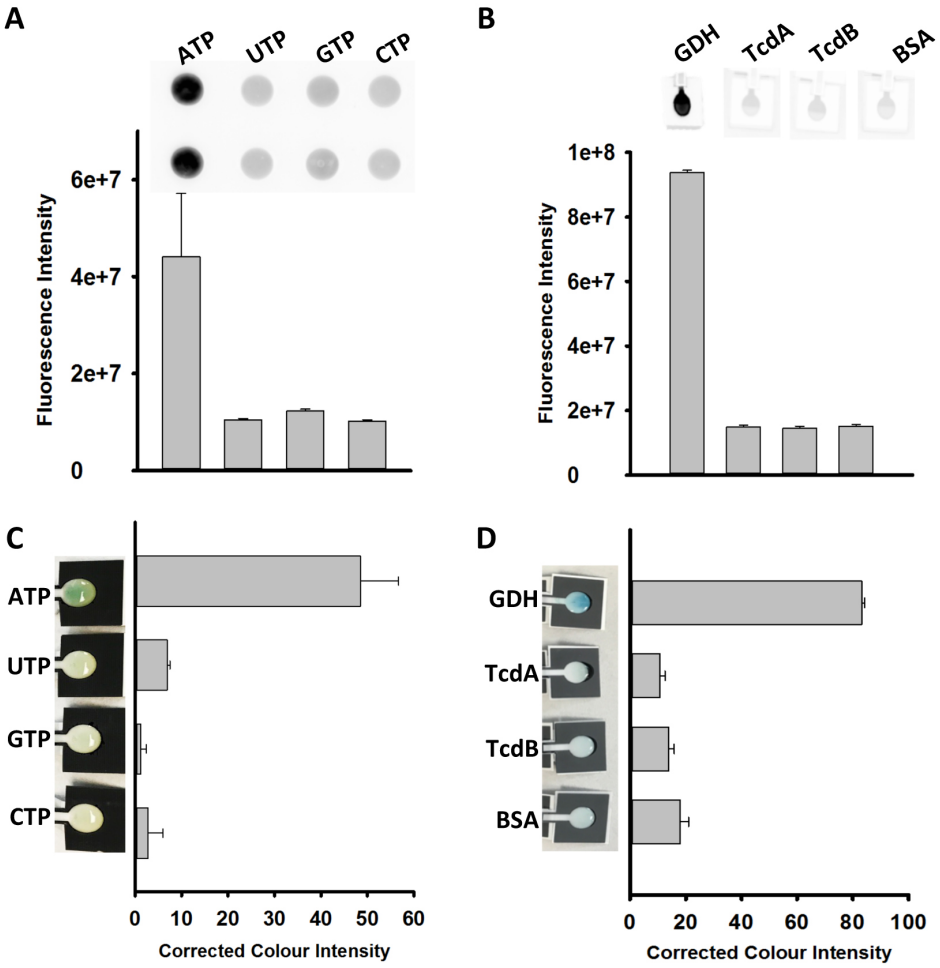

Figure S4-11. Selectivity of the paper sensors. Fluorescence images and measured emission intensity of (A) the ATP sensor upon addition of ATP, UTP, CTP, and GTP, and (B) the GDH sensor upon addition of GDH, TcdA, TcdB and BSA. Colourimetric images and quantitative assays of the RCA reaction for (C) the ATP sensor and (D) the GDH sensor.

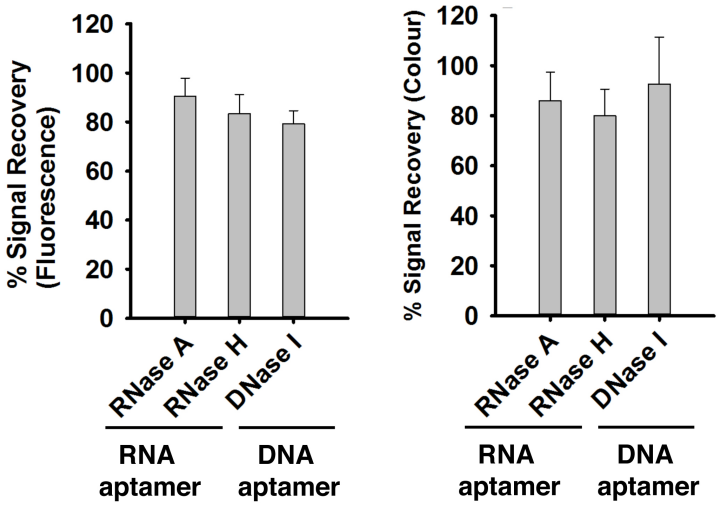

Figure S4-12. % Signal Recovery using (A) fluorescence readout in Zone 1 and (B) colorimetric readout in Zone 2 for the ATP sensor and GDH sensor. 3 units of RNase A and RNase H were added to Zone 1 of ATP sensor while 3 units of DNase I was added to Zone 1 of the GDH sensor, followed by a 30-minute incubation. Zone 1 of both sensors were then treated with nucleases inhibitor cocktails described in the experimental section to remove and/or inhibit the nucleases. Analyte (2 mM ATP or 500 nM GDH) was then added to Zone 1 followed by a 30-minute incubation. Fluorescence images were then taken and the intensity was compared to that for a sample that was not treated with nucleases. The fluidic channel was then connected and aptamer was then eluted to Zone 2 for the RCA reaction. The percent signal recovery was determined by comparison to samples not treated with nucleases.

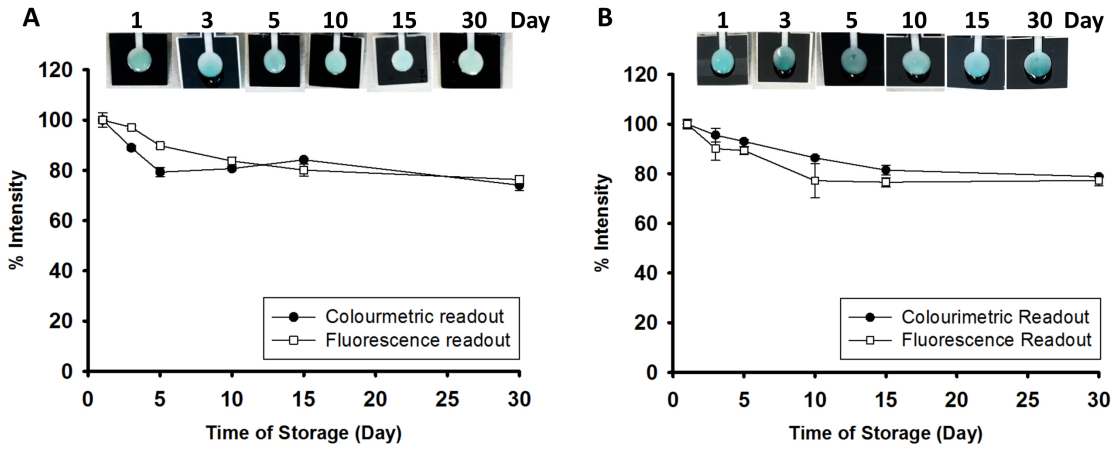

Figure S4-13. Storage stability of (A) the ATP sensor and (B) the GDH sensor. Both the fluorimetric and colorimetric assays were used to determine the stability of paper sensor over 30 days of storage at 4 °C. The concordance between fluorescence and colorimetric results suggest that the loss of signal is related to degradation of aptamers in Zone 1 rather than poor stability of RCA reagents in Zone 2.

CHAPTER 5.

CONCLUSION

5.1 SUMMARY AND FUTURE OUTLOOK

The key goals of this thesis were to undertake a fundamental study of the properties of aptamers entrapped in sol-gel materials, and to explore immobilized aptamers as components of paper-based biosensors. In Chapters 2 and 3, both DNA and RNA aptamer reporters were examined after entrapment in a variety of sol-gel-derived materials. Using a series of steady-state and time-resolved fluorescence methods, it was found that the ability of the entrapped aptamer reporters to remain fully hybridized to signalling sequences was the most important factor in terms of signalling capability for both DNA and RNA aptamer reporters. It was also observed that more polar materials derived from sodium silicate are optimal for both aptamer reporters. A key finding from this work was that aging of entrapped aptamers produces losses in performance, with sodium silicate derived materials being the most appropriate matrix to retain aptamer stability. While these studies provided useful insights into methods to achieve optimal aptamer performance, their utility is severely limited as they can only be used to detect small molecule analytes (owing to the small pore sizes of the sol-gel derived materials) and are very difficult to print, making their use for paper-based sensors challenging.

In Chapter 4, a novel immobilization method was used to produce a new type of paper-based sensor that could utilize both RNA and DNA aptamer reporters as biorecognition elements. Using an “all printed” system, a dual-response (fluorescence

and colorimetric) point-of-care paper-based biosensing device was developed. Desorption from graphene oxide produced an initial fluorescence signal, with the desorbed aptamer being able to initiate RCA in a separate zone to produce an amplified colorimetric output. The sensor could be used to detect bacterial markers such as ATP and GDH, and could function in clinically relevant matrixes such as blood serum and stool.

The paper-based platform could potential be further enhanced by examining alternative species such as reduced graphene oxide[1, 2], to further modulate the affinity of aptamers, the use of DNA enzymes as recognition elements coupled the use of fluorescence[3] or RCA methods[4], and the use of exponential RCA methods such as hyperbranched rolling circle amplification ((HRCA)[5] or DNAzyme feedback modulated RCA[6] to further increase the sensitivity. Furthermore, such sensors could potentially be multiplexed to allow for several anlaytes and appropriate controls to be present on a single paper-based sensor device.[7] As more and more functional nucleic acids are developed to diverse targets, the potential of the paper-based sensor for rapid testing of a wide range of targets in various clinical or environmental matrices will increase. It is expected that the sensors described in this thesis could be further developed to produce a versatile platform for rapid sensing of analytes in resource-limited settings.

5.2 REFERENCES

1. Liu, M.; Zhang, W.; Chang, D.; Zhang, Q.; Brennan, J. D.; Li, Y., *Trends in Analytical Chemistry* **2015,** 74, 120-129.
2. Liu, M.; Yin, Q.; Brennan, J. D.; Li, Y., *Biochimie* **2017,** In press.
3. Zhao, X.-H.; Kong, R.-M.; Zhang, X.-B.; Meng, H.-M.; Liu, W.-N.; Tan, W.; Shen, G.-L.; Yu, R.-Q., *Anal. Chem.* **2011,** 2011, (83), 13.
4. Ali, M. M.; Li, Y., *Angew. Chem. Int. Edit.* **2009,** 48, (19), 3512-3515.
5. Liu, M.; Zhang, W.; Zhang, Q.; Brennan, J. D.; Li, Y., *Angew. Chem. Int. Edit.* **2015,** 54, (33), 9637-9641.
6. Liu, M.; Zhang, Q.; Chang, D.; Gu, J.; Brennan, J. D.; Li, Y., *Angew. Chem. Int. Edit.* **2017,** 56, (22), 6142-6146.
7. Hu, R.; Liu, T.; Zhang, X.-B.; Huan, S.-Y.; Wu, C.; Fu, T.; Tan, W., *Anal. Chem.* **2014,** 86, (10), 5009-5016.